FACULTY OF
BIOSCIENCE ENGINEERING

COMPARISON OF DATA CLEAN-UP TECHNIQUES FOR NOISY FISH POSITIONING DATA

Thomas Vanwyck
Student ID: 01308715

Promotor: Prof. Dr. Ir. Ingmar Nopens
Tutor(s): Ir. Jenna Vergeynst

Master thesis submitted for obtaining the degree: master in Bio-ingenieurswetenschappen.
Academic year: 2017 - 2018

GHENT
UNIVERSITY

Gent, June 4, 2018

The promotor,	The author,
Prof. Dr. Ir. Ingmar Nopens	Thomas Vanwyck

DANKWOORD

Deze thesis was een erg leerrijke ervaring, zowel op academisch als persoonlijk vlak. Het is een mooie afsluiter van mijn opleiding als bio-ingenieur. De verwezenlijking van dit werk zou niet mogelijk zijn geweest zonder de hulp en steun van heel wat mensen, die een persoonlijk bedankje verdienen.

Eerst en vooral wil ik mijn tutor, Jenna Vergeynst bedanken. Ze gaf mij de vrijheid om alle methoden te testen die ik relevant achtte. Tegelijkertijd stuurde ze me duidelijk bij waar nodig, waardoor de kwaliteit van dit werkstuk sterk verbeterde. Haar begeleiding in het schrijven heeft me veel bijgeleerd, niet alleen in de context van deze thesis, maar ook voor mijn verdere (academische) carrière. Haar flexibiliteit qua deadlines maakte zowel mijn Erasmus als thesis-ervaring een stuk aangenamer. Daarnaast bedank ik mijn promotor, Ingmar Nopens, om diezelfde flexibiliteit te tonen, maar tegelijk nuttige feedback en suggesties te voorzien om de kwaliteit van het werk te verhogen.

Verder wil ik iedereen van de vakgroep BIOMATH bedanken. Het grootste deel van deze thesis is geschreven aan een bureau van hun afdeling, en hun gezelschap en interesse motiveerde me om verder te werken. Vooral mijn thesis-kompaan, Ruben Ingels, verdient een vermelding. Zijn dagelijkse gezelschap en onze praatjes zorgde voor de broodnodige dosis afleiding en relativering. Ik ben blij dat ik een vriend zoals hem aan mijn opleiding overhoud.

Furthermore, I want to thank Henrik Baktoft and James Campbell. Henrik's approachability and genuine interest in this project were a humbling experience. His efforts to optimize his algorithm for our case study and him granting us early access to his R-package tremendously helped me in my research. James Campbell's feedback gave me a deeper understanding of the YAPS algorithm, and his adaptations were the inspiration for my own improvements.

As part of this thesis was written during my exchange, I have some international friends to thank as well. Sitting inside to write while you are in a beautiful country with beautiful people was not always easy, but thanks to their genuine interest and support I was able to succeed. A special thanks goes out to Daisy, who kept me motivated to save the salmon, even from the other side of the world.

Ten laatste bedank ik mijn familie en vrienden om me steeds de kans te geven om me uit te laten over het verloop van de thesis, ook al stond dit vaak erg ver van hun leefwereld. Bedankt om steeds een luisterend oor te bieden. Ik beloof dat ik in de toekomst minder over de positionering van vissen zal praten.

Thomas Vanwyck

1 juni 2018

CONTENTS

SUMMARY

Migrating fish populations are heavily hindered by the man-made structures present in most river ecosystems. Reducing the impact of these structures on the migration of these species is key to their survival. This requires knowledge of fish behaviour in the vicinity of such structures. The first step in creating this knowledge, is obtaining accurate and reliable fish tracks. Unfortunately, concrete canal walls create a highly reflective environment, which results in heavily distorted tracks. Therefore, a pre-processing step is crucial to obtain usable tracks. A wide variety of clean-up methods is available in the literature, but most studies do not rigorously test and compare the performance of these methods under different circumstances. There is no clearly superior method, nor guideline to select one. This thesis aims to provide a comprehensive and in-depth comparison of the most relevant clean-up techniques to obtain the best method for this case-specific problem.

Two radically different approaches to the problem were implemented and compared. Firstly, we implemented the traditional system, which performs positioning, outlier filtering," and noise removal via Kalman filtering in separate, subsequent steps. Secondly, we tested a new approach: the YAPS-algorithm of Baktoft et al. (2017). This method implements the positioning and data clean-up as one big minimization problem. All techniques were optimized individually to assure the comparison was as fair as possible.

This thesis focusses on the applicability to real life situations in highly reflective areas, with random burst intervals transmitters and a high probability of missing detections. Therefore, the results are based on three test tracks, combined with realistic simulated data and a qualitative analysis of actual fish tracks. Through this evaluation, this study highlights the strengths and weaknesses of all possibilities, and defines which method provides the best solution to our problem.

This extensive comparison proves YAPS is superior to all clean-up systems that follow the traditional approach. It provides more accurate tracks, it is more reliable and consistent and its error measure is more relevant. Thanks to its different approach, it can calculate more positions and works further from the array, revealing track features

that go unnoticed in traditional systems. Additionally, it is a completely transparent method that enables users to customize the model's core structure to their needs.

Next, we showed the performance of YAPS can be further enhanced by combining the old and new approach. Applying the traditional Kalman filter to the YAPS results further reduces the impact of noise and errors, and results in a small, yet consistent increase in accuracy. Additionally, we show for the first time that Kalman filtering improves the correlation between the calculated and true error. The combination of YAPS and Kalman filtering is the most accurate and reliable positioning system in noisy, highly reflective environments.

Despite its distinct advantages over other clean-up methods, YAPS is still a new method. Meanwhile, the traditional algorithms underwent many stages of performance evaluation. Therefore, we suggest some improvements to the algorithm, based on lessons learned from the traditional approach. This fine-tuning can further cement the value of YAPS in the future.

SAMENVATTING

Migrerende vissen worden sterk gehinderd door menselijke interventies in het natuurlijke verloop van aquatische ecosystemen. De impact van zulke constructies moet gereduceerd worden om het voortbestaan van deze soorten te verzekeren. Om dit te verwezenlijken is er meer informatie nodig over het gedrag van de vissen nabij deze constructies. Het produceren van accurate en betrouwbare vispaden is een belangrijke eerste stap om deze kennis te verwerven. Dit is echter geen gemakkelijke opgave: de betonnen wanden veroorzaken reflecties van signalen, waardoor de trajecten sterk verstoord worden. In de literatuur is een brede waaier aan technieken beschikbaar voor de opzuivering van zulke data, maar de methoden worden zelden diepgaand geÃńvalueerd of vergeleken met andere technieken. Hierdoor is er geen duidelijke optimale techniek, noch een richtlijn om er een te selecteren. Deze thesis geeft een uitgebreid, gedetailleerd overzicht van de meest relevante opzuiveringstecknieken op dit moment, zodat de optimale methode voor dit specifiek probleem bekomen wordt.

Twee totaal verschillende benaderingen werden geÃńvalueerd en vergeleken. Ten eerste implementeerden we het traditionele systeem, dat positionering, verwijdering van uitschieters, en ruis minimalisatie via de Kalman filter uitvoert in verschillende, opeenvolgende stappen. Ten tweede testte we een nieuw, radicaal ander systeem: het YAPS-algoritme van Baktoft et al. (2017). Deze methode implementeert de positionering en data opzuivering als één grote minimalisatie. Om te verzekeren dat de vergelijking zo eerlijk mogelijk verloopt, werden alle technieken apart geoptimaliseerd.

Deze thesis focust op de praktische toepasbaarheid in realistische omstandigheden, met veel reflecties, random tijdsintervallen tussen transmissies en een grote kans op gemiste detecties. Daarom zijn de resultaten gebaseerd op een combinatie van een testtraject, een simulatiestudie en een kwalitatieve analyse van echte visposities. Dankzij deze benadering legt deze thesis de sterktes en zwaktes van alle technieken bloot, en kan de beste oplossing voor ons probleem geselecteerd worden.

Deze diepgaande vergelijking geeft aan dat YAPS beter presteert dan alle alternatieven die de klassieke benadering volgen. YAPS produceert meer accurate trajecten, is meer consistent en betrouwbaar, en de meegeleverde onzekerheid is rel-

evanter. Dankzij de andere benadering kan het meer posities bepalen, en werkt de positionering verder weg van de site. Dit produceert nieuwe secties in de vispaden die niet opgemerkt worden via de traditionele benadering. Daarnaast is deze methode volledig transparant, en laat het gebruikers toe het model aan te passen aan hun specifieke vereisten.

Verder tonen we aan dat de prestaties van YAPS verder verbeterd kunnen worden door de oude en nieuwe benadering te combineren. Door de traditionele Kalman filter op de resultaten toe te passen, wordt de impact van fouten en ruis verder beperkt. Het zorgt voor een kleine, maar consistente verbetering in de nauwkeurigheid van de posities. Daarnaast tonen we voor het eerst dat de Kalman filter de correlatie tussen de berekende en werkelijke fout verbetert. De combinatie van YAPS en de Kalman filter is dus het meest accurate, betrouwbare positioneringssysteem in omgevingen met veel ruis en reflecties.

Hoewel YAPS duidelijk superieur is ten opzichte van de alternatieven, is het nog een erg nieuwe techniek, in tegenstelling tot de traditionele algoritmen. Deze traditionele methoden ondergingen reeds verschillende cycli van evaluatie en verbeteringen. Daarom eindigen we deze thesis met een aantal suggesties voor verdere verbeteringen van het YAPS-algoritme, op basis van de lessen die getrokken kunnen worden uit de traditionele benadering. Deze verbeteringen kunnen het belang van YAPS verder funderen in de toekomst.

GLOSSARY

Symbols

$\boldsymbol{A}_k$	Transition matrix of the process model
c	Speed of sound
C	Covariance beteen the speed and sound for the CTCTW model
$\boldsymbol{D}_c$	Diffusivity of the speed of sound (YAPS)
$\boldsymbol{D}_{RW}$	Diffusivity of a RW model
$\boldsymbol{D}_{CRW}$	Diffusivity of a CRW model
$\boldsymbol{D}_{xy}$	Diffusivity of the fish movement (YAPS)
$\boldsymbol{h}_i$	Coordinates of hydrophone i: $(h_{i,1}, h_{i,2})^T$
$h_{i,j}$	Position of hydrophone i in dimension j
$\boldsymbol{H}_k$	Transition matrix of the measurement model
i	Subscript used for the receiver number
j	Subscript used for the dimension
J_{TDOA}	Cost function for hyperbolic positioning
k	Subscript used for the time step
$\boldsymbol{K}_k$	Kalman gain factor
$\boldsymbol{M}$	Weight matrix for the Ehrenberg error
$\boldsymbol{m}_k$	Mean of the Gaussian distribution of the system state
$\boldsymbol{m}_k^*$	Predicted mean of the system state
$\boldsymbol{m}_k^*$	Smoothed mean of the system state
N	Number of detecting hydrophones
$\boldsymbol{p}$	Coordinates of the transmitter, in two dimensions: $(p_1, p_2)^T$
$\boldsymbol{p}*$	Predicted coordinates of the transmitter
Δp	Total location error in Ehrenberg error
Δp_j	Location error in direction j

$\boldsymbol{P}_k$	Total error covariance matrix
$\boldsymbol{P}_k^*$	Predicted error covariance matrix
$\boldsymbol{P}_k^S$	Smoothed error covariance matrix
$\boldsymbol{q}_k$	Process noise
$\boldsymbol{Q}_k$	Covariance matrix of the process noise
$\boldsymbol{r}_k$	Measurement noise
$\boldsymbol{R}_k$	Covariance matrix of the measurement noise
S	Salinity
$\overline{s_k}$	Average swimming speed, from McConnel speed filter
s_j	Swimming speed in direction j
$\boldsymbol{S}_k$	Innovation of the state covariance matrix in the KF
T	Final time step
T_w	Water temperature
Δt_k	Time difference between time step $k-1$ and k
$t_{i,k}$	Measured TOA at hydrophone i, at time step k
$t_{i,k}^*$	Predicted TOA
$t_{P,k}$	Transmission time at time step k (= time of ping)
$\boldsymbol{v}_k$	Offset between measured and predicted state in the KF
V_{pos}	Variance of the position for the CTCRW model
V_{speed}	Variance of the speed for the CTCRW model
$\boldsymbol{x}_k$	State of the system
$\boldsymbol{y}_k$	Measured state of the system
$\boldsymbol{y}_k^m$	Actual measurement
z	Depth
β	Autocorrelation parameter in the CTCRW model
$\epsilon_{i,k}$	Residual between measured and predicted TOA (YAPS)
$\boldsymbol{\theta}$	Vector of parameters that have to be estimated
θ_{mix}	Mixture ratio (YAPS)
θ_{scale}	Scaling factor (YAPS)
μ_{bi}	Mean of the burst interval (YAPS)
σ	Overall variability of the velocity in the CTCRW model
σ_{bi}	Standard deviation of the burst interval (YAPS)

σ_ϵ	Standard deviation of the residual (YAPS)
ϕ	Turning angle
φ_k	Energy function

Abbreviations

CRW	Correlated random walk
CTCRW	Continuous-time correlated random walk
HPE	Horizontal Position Error
HPEm	Measured error
KF	Kalman filter
LS	Least squares
p(NA)	Probability of missing detections (simulation study)
p(MP)	Probability of multipath errors (simulation study)
RTSS	Rauch-Tung-Striebel smoother
RW	Random walk
TOA	Time of arrival
TDOA	Time difference of arrival
VPS	VEMCO Positioning System
YAPS	Yet Another Positioning Solver
YAPS-SS	YAPS version using the calculated sound speed
YAPS-BI	YAPS version using the calculated sound speed and mean burst interval

CHAPTER 1

INTRODUCTION

Due to the introduction of man-made structures in waterways, migrating fish face challenges that threaten their existence. Constructions such as sluices, hydropower plants, and pumping stations intervene with the natural flow of water and, consequently, with fish migration. Continental aquatic ecosystems are in worse condition overall than any other ecosystem type. Worldwide, more than 40 % of the river systems have been fragmented due to the construction of dams or other hydraulic structures (Hassan et al., 2005). In Belgium, two-thirds of all pumping stations are located on crucial migration routes of the European Eel (Stevens et al., 2011). The Albert Canal is one of these heavily fragmented waterways. To overcome the height difference between Antwerp and Liège, six navigation lock complexes were built (nv De Scheepvaart, 2017). At one of these complexes (Kwaadmechelen) a pumping station has already been constructed, and there are plans to do the same at the other five sites. These could generate renewable energy during high flow conditions by passing the water through hydropower turbines. Nevertheless, they would form an additional obstacle in the path of migrating fish, possibly causing damage to fish passing through the turbines.

Belgium is native to two fish species that have an obligatory migration phase through these waterways: the European eel (*Anguilla anguilla*) and the Atlantic salmon (*Salmo salar*). The European eels belong to the catadromous fish species; they spawn in the Sargasso Sea (in the Northern Atlantic). Their larvae then drift with the ocean currents towards the European continent. Subsequently the glass eels swim up the rivers, maturing and undergoing several transformations along the way. After spending most of their lives in fresh water, the partially matured adults travel back to the ocean to reproduce. Although the entire reproduction process is not yet fully understood, it is clear that migration through continental river systems forms a crucial step (van Ginneken and Maes, 2005). Atlantic salmon, on the other hand, is an anadromous fish, migrating upstream to spawn in fresh water. After spawning they spend the first part of their lives in fresh water, undergoing several transformations. Following a metamorphosis into smolts, they begin their downstream journey towards the ocean. They then spend most of their lives in the ocean and return only to the rivers

to reproduce, after which they mostly die (McCormick et al., 1998). The smolt stage is a critical step in the life cycle that involves morphological changes to adapt to the new environment and several dangers such as diseases, parasites, and predators (McCormick et al., 1998). The flow conditions seem to control the start of the smolt migration (Allen, 1944; Hesthagen and Garnås, 1986). Juvenile salmon also seem less capable of bypassing hydraulic structures through fish ladders (Goodwin et al., 2014). Thus the investigation of smolt behaviour can provide some important insights in the vulnerability of salmon populations.

The extensive hydraulic modifications of aquatic ecosystems mentioned above have had a detrimental impact on the populations of these species. Virtually all migrating species experienced population declines, reaching all time lows in the most recent observations. Many of them are now listed as threatened or endangered (Limburg and Waldman, 2009). European eel populations in Belgium steeply decreased, with a drop of over 90 % from 1996 to 2011 (Belpaire et al., 2013). It is now considered a critically endangered species in Belgium (Verreycken et al., 2014; Jacoby and Gollock, 2014). Wild Atlantic salmon was affected to degree of extinction in Belgium, with the last caught specimen in 1942. Since 1987, scientists attempt to re-establish the population through reintroduction programs and restoration of migration routes (Røed et al., 2001). Thanks to these efforts, the status has recently been upgraded to critically endangered in Flanders, but it remains on the IUNC Red List (Verreycken et al., 2014; Freyhof, 2014).

Gaining more knowledge on how these species interact with man-made obstructions is a crucial step in the recovery of these native populations. Several institutions are aware of this issue and are taking action to resolve it. Regulations by the European Commission require that in the future at least 40% of the adult European Eels must succeed in reaching the ocean (European Council, 2007). The Benelux set the objective to remove all obstructions for fish migration by 2027 (Benelux Committee of Ministers, 2009). In order to achieve these goals, current hydraulic structures will need to be altered or removed. At the same time, complete removal is not always possible, since these constructions often have an important function. Predicting the influence of local hydraulic conditions on the movement of the considered fish species can be useful to select the most fish-friendly option without spending money and resources on pilot sites. Goodwin et al. (2014) used a Computational Fluid Dynamics (CFD) model to link local water velocity and pressure to the behaviour of Pacific Salmon smolts. Despite its simplifications, the model captured some important features of the animals' behaviour and led to new insights. The authors argue that further research into this topic is necessary so that design decisions can take these biological factors into account. To our knowledge such a model has not been developed yet for

Atlantic salmon or European eels. Furthermore, most research so far has focussed on dams and not sluices. In addition, there is a clear and urgent need to accurately define the influences of man-made structures on migrating fish, as some authors are starting to doubt their impact (Hilborn, 2013).

INBO and the BIOMATH department of Ghent University are working on a model to predict the effects of hydraulic infrastructures on Atlantic salmon and European eel. As a part of this, Jenna Vergeynst will use CFD to link local hydraulic conditions to fish behaviour. This model will be developed for one of the navigation lock complexes on the Albert Canal mentioned above. A first step in creating such a model is obtaining reliable, high quality fish tracks. To achieve this, she tagged and released smolts and eels with an acoustic tag near the navigation lock, which is equipped with hydrophones. Via the VEMCO positioning system, a time series of the fish positions can then be obtained.

Before these positioning data can be used in the model, the data need to be preprocessed and a relevant clean-up technique must be selected. Near hydraulic structures there is a high level of interference, such as reflections, and background noise from boats and pumps. These interferences cause artefacts in the data, which results in unrealistic or even biased fish tracks (Alós et al., 2016). Some form of data clean-up is thus required. The VEMCO company provides tools to achieve this, but these are often insufficient. Current literature offers a wide range of potential solutions for this processing. However, these are often limited to ideal cases with simulated data or little background noise. As acoustic conditions near hydraulic structures are harsher, these methods may perform differently in realistic situations. Furthermore, the cleaned track is often only compared to the raw, uncleaned tracks, but not to the results of other methods. Thus, a comparison of the best methods under these circumstances is lacking.

To fill up this knowledge gap, we tested and evaluated some of the most relevant data clean-up techniques. These methods range from the basic tools provided by the positioning company to more advanced filtering techniques, such as the Kalman filter. We then compared these traditional methods to a new technique that performs positioning and clean-up simultaneously: the YAPS algorithm, developed by Baktoft et al. (2017). The emphasis of this thesis is on the performance of these methods on real data obtained near a navigation lock, containing high levels of noise, missing detections and multipath errors.

This thesis is organised as follows. The second chapter summarizes all current literature to give an overview of the basic principles and shortcomings of the currently most relevant techniques. Subsequently, the third chapter outlines how all the considered

methods were implemented. The performance of these systems is then assessed in the fourth chapter. First, this chapter selects the best configuration for the traditional and new approach separately, then it compares the two, and finally, it evaluates the effects of combining both methods. This assessment is based on test tracks with known true positions, a simulation study, and a qualitative analysis of actual fish tracks. Finally, general conclusions and ideas for future research are presented in chapter five and six respectively.

CHAPTER 2

LITERATURE REVIEW

2.1 The VEMCO Positioning System and its error sensitivity measure

Cleaning up positioning data requires an error measure that approaches the true error as closely and unambiguously as possible. VEMCO, the company that provides the acoustic telemetry positioning system, includes a measure of positioning error sensitivity with the location data: the Horizontal Position Error (HPE). To explore the potential of this measure, a basic understanding of the positioning system and the calculation of the error measure are essential. These are described in Section 2.1.1 and 2.1.2 respectively. In Section 2.1.3, some of the drawbacks of this error measure are mentioned. Because of these shortcomings, the HPE cannot be used directly to clean up the tracks. However, the Kalman filter, presented in Section 2.2, still requires an error sensitivity measure for the calculated positions. Therefore, we discuss some possible alternatives to the HPE in Section 2.1.4.

2.1.1 Hyperbolic positioning

VEMCO Positioning System (VPS) has been used in several studies of the behaviour, habitat use and movement patterns of aquatic animals (Espinoza et al., 2011a; Coates et al., 2013; Furey et al., 2013; Piraino and Szedlmayer, 2014; Roy et al., 2014). It uses hyperbolic positioning algorithms to determine the location of the animal tags. The basics of this system are outlined in this section.

Hyperbolic positioning systems calculate positions using simple physical and mathematical properties. The transmitters implanted in the fish continuously emit acoustic signals. These signals are then detected by stationary receivers with a known location. When a signal is detected by two receivers, the difference between the detection times (time of arrival, TOA) can be determined (time difference of arrivals, TDOA). Ideal signal propagation is assumed, meaning that the signal from the transmitter travels at the same speed in all directions. Therefore, the time until detection

is proportional to the distance between receiver and transmitter. The time difference can thus also be expressed as a distance, called the range difference. This range difference reflects how much closer the transmitter was to one of the two receivers. In two dimensions, this represents a range of possible positions that are located along a hyperbola. In order to obtain a single solution, the signal has to be detected by a third receiver. Then, two hyperbolas can be constructed and the intersection is the calculated position. In three dimensions, these range differences will result in intersecting hyperboloids leading to an infinite amount of possible positions. To obtain a three dimensional position, the depth of the transmitter is required. This depth is used to draw a horizontal plane in which a two-dimensional hyperbolic positioning can be performed as outlined previously. VPS thus needs 3 inputs to calculate a position of the animal tag: the range differences, transmitter depth and three dimensional positions of the receivers (Smith, 2013).

The hyperbolic positioning algorithm is susceptible to various sources of error. It entails strict requirements to work properly: time synchronization of all receivers, determination of the speed of sound, a receiver array of sufficient quality and an accurate knowledge of the receivers' positions. Any deviation from these requirements can cause positioning errors (Andrews et al., 2011; Biesinger et al., 2013). Furthermore, the speed of sound is a function of the temperature, salinity and depth. This dependence can result in deviations from the assumption of ideal propagation. Salinity and temperature are assumed to be uniform in space and can only vary through time (Smith, 2013). The study site of this thesis is located at a navigation lock complex, so local conditions can change rapidly when a navigation lock opens. This spatial variation in temperature or salinity can be a source of error. Finally, the actual time of arrival is discretized to some extent to allow digital processing, which may result in a quantization error (Ehrenberg and Steig, 2002).

Abstractions of reality caused by the assumptions lead to varying degrees of positioning error. Because of the simplifications, the real position will not be on the hyperbolas exactly. The magnitude of the deviation depends on how the receivers are positioned, and thus how the hyperbolas intersect (Smith, 2013). If the intersection of the hyperbolas is almost perpendicular, a mistake will have a relatively small influence. If the legs of the hyperbolas almost coincide, a deviation from the ideal scenario will lead to a much larger error (Figure 2.1). Thus, the shape of the receiver triangles and the location of the transmitter relative to these triangles is an important parameter that determines the error sensitivity (Ehrenberg and Steig, 2002; Smith, 2013; Biesinger et al., 2013). As a consequence, the precision of readings outside the receiver array will be significantly less reliable (O'Dor et al., 1998; Espinoza et al., 2011b; Smith, 2013).

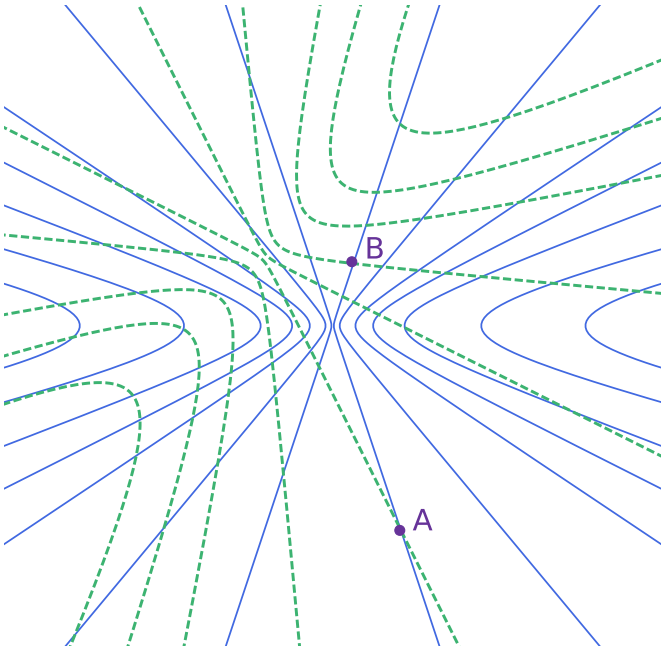

Figure 2.1: Illustration of how the location of transmission can influence the reliability of hyperbolic positioning. The figure shows a few possible hyperboles between two different receiver pairs. Location A will have a smaller certainty than location B.

In this thesis, we implemented a basic hyperbolic positioning system. The VPS system performs well and has no downsides besides its back box approach. Our own hyperbolic positioning will be mainly used on simulated data, where VPS results are not available.

2.1.2 Determination of the Horizontal Position Error

The HPE is a unitless measure of error sensitivity. It is calculated by VEMCO based on the raw data and included with the calculated positions. This section outlines the main concept of its determination based on a guide by the director of data analysis at VEMCO, Frank Smith (2013).

First, the synthesized error sensitivity is calculated. From each triangle of receivers that picked up a signal, a position can be calculated as outlined before. These are called basic positions. VPS approximates the error sensitivity of every basic position by estimating the level of uncertainty in the range difference and depth determination. VEMCO claims this calculation is based on dataset-specific information about the temperature range, potential depth range and distance between transmitters and receivers, but no elaboration or formulae are provided. The result is a measure expressed in meters, but it cannot be interpreted as a distance since the obtained error values are not calibrated. If more than three receivers pick up the same signal, mul-

tiple basic positions are obtained. All of them represent the same real position. For each tag transmission, a weighted average of the basic positions can be calculated. This location is the synthesized position and is the one provided by VEMCO. The weight given to each basic position is the previously described error sensitivity. These error sensitivities are also used to obtain an overall error sensitivity for the synthesized position.

The HPE is then derived from the synthesized position error to obtain a more realistic error measure, calibrated on site-specific conditions by use of stationary transmitters (synctags) installed in the test site. The positions of these transmitters are calculated through VPS in the same way as the transmitters implanted in the fish. Since the synctags are stationary, their real position can be determined with GPS. This actual position can be used to calculate the real horizontal position error for the synctags, expressed in meters, called the measured error (HPEm). A linear weighted regression model of the measured errors and their calculated error sensitivities is constructed using all basic positions of the synctags. The calculated error sensitivities of the mobile transmitters attached to the animals are then fed to this regression model to obtain the HPE. As the HPE is still based on the basic error sensitivities, which are not calibrated through time, the calibration is only partial. Therefore, the result should be treated as unitless (Smith, 2013).

2.1.3 The shortcomings of HPE

The HPE has been used in many studies as a measure of error sensitivity. This can be achieved by linking HPE to the HPEm of the synctags (Scheel and Bisson, 2012; Roy et al., 2014). This method assumes that the HPE characteristics of the stationary receivers are similar to those of the animal tags. The error on fish positions is then estimated based on a statistical comparison of HPE and HPEm by binning the data into HPE ranges and calculating measures such as twice the distance root mean square or percentiles (Smith, 2013). The HPE can also be used to filter data by setting a cut-off value above which data points are rejected. This threshold is often chosen arbitrarily by testing different values and looking for a balance between the reliability and loss of data points (Espinoza et al., 2011a; Coates et al., 2013; McMahan et al., 2013). This cut-off can also be defined using multiple accuracy targets, which are linked to HPE values through the methods mentioned above (Meckley et al., 2014). However, the HPE has several shortcomings that should be kept in mind when using this value as an error measure.

The HPE cannot be directly used as an error measure expressed in meters. Instead, it needs to be treated as a unitless approximation of the relative error sensitivity of

different data points. The absolute value bears no direct physical meaning and only serves as a rough estimate of how sensitive the position is to errors. It can significantly over - or under-estimate the real error, so its use is restricted to informal preliminary assessment of data quality and filtering out data points of low quality (Smith, 2013). This forms an issue for its application in the Kalman filter, as the filter requires an error measure with the same unit as the position (see Section 2.2). Therefore, direct HPE usage is impossible in our study and a relationship with the HPEm is needed. For the dataset used in this thesis, however, the correlation between HPE and HPEm was of insufficient strength to result in a reliable error measure (see Figure 2.2 for an example of the weak relationship).

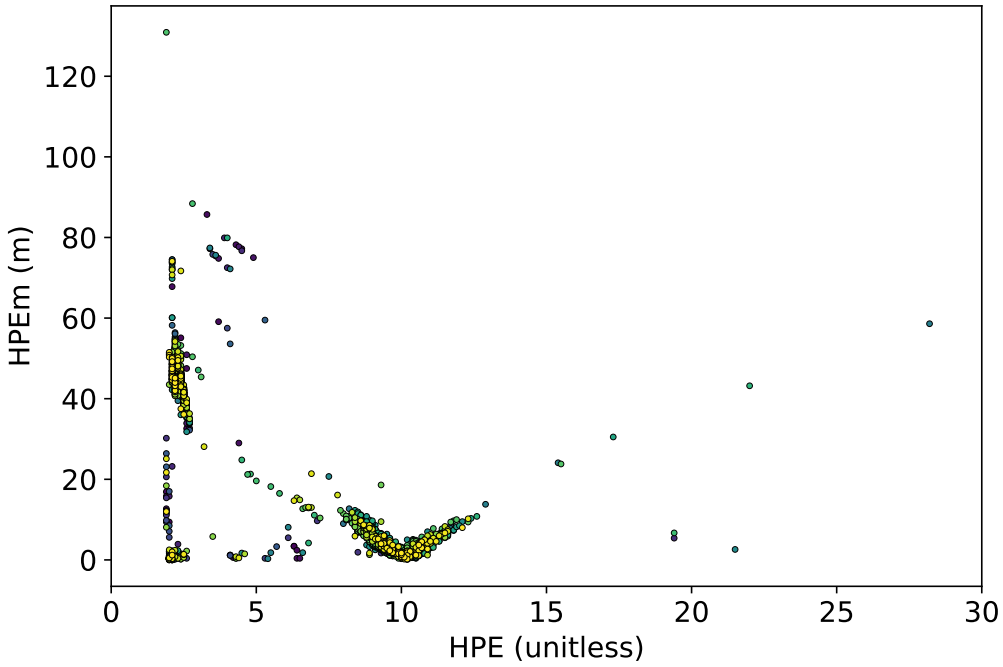

Figure 2.2: Example of the relation between the calculated error (HPE) and true error (HPEm) for a synctag. In this case, for calculated positions of one month for synctag 'S7'. The colour represents the time of the transmission from 15/12/2015 (purple) to 15/01/2016 (yellow). The most recent yellow V-shape is the clearest, but below it, green and blue ones from earlier dates appear.

Furthermore, the HPE cannot be interpreted unambiguously. As its calculation is based on the location specific properties of the calculated position instead of the actual position, the estimated error can be far from the true value. This results in typical V-shaped patterns on plots of the HPEm versus the HPE of synctags (see Figure 2.2, with a V-shape at HPE 10). At the tip of the V, the HPEm is zero, so the position is calculated correctly. However, the HPE is still 10 here, while for some other correct points it is smaller. This may be caused by unfavourable conditions (i.e. temperature and salinity) that are incorporated in the HPE calculation. If now a position is determined incorrectly (i.e. with a higher HPEm) right after this one (i.e. under the same

conditions), two things can happen. Firstly, the wrongly calculated position may lie in a more reliable zone than the actual transmitter position. Since the HPE determination uses this calculated position, it will assume that this data point is highly reliable. This wrong position will be appointed a lower HPE than the real location (left leg of V-shape). Secondly, some calculated positions will fall in a less reliable zone than the true one, leading to a larger HPE value (right leg of V shape). Here, the HPE will increase as the wrong position ventures further into unreliable zones (Smith, 2013). So, in the right leg, HPE is a relevant error measure as it positively correlates to the real error. For points from the left leg, however, incorrect positions will be assigned a disproportionally high confidence. This phenomenon prevents the straight-forward interpretation of the HPE.

In addition, the HPE does not account for one of the main error sources: the multipath errors. Reflection of the acoustic signals is not considered in the HPE calculation (Welsh et al., 2012). Multipath interferences, where the reflected signals are used to calculate new positions, can thus go unnoticed (Ehrenberg and Steig, 2002). This false position has no connection to the actual path of the fish and can heavily distort fish tracks. Since our study site is located at a navigation lock complex in a canal, surrounded by concrete walls, reflections can have a substantial impact. Boat traffic can also influence the reflection characteristics by creating surface roughness and air bubbles (Trevorrow, 1998). As the HPE neglects this process, a data point that is the result of a multipath error can still have a low HPE. Therefore, it is impossible to remove these false positions based on HPE alone.

Reflected signals of the actual fish tag, background noise (i.e. noise from boat engines or pumps), and transmissions from other fish tags, can collide and interfere with the correct signal. Usually this will prevent the signal from being detected, so it does not cause a false detection (Simpfendorfer et al., 2008; Welsh et al., 2012; Binder et al., 2016). However, VEMCO uses the same frequency on all transmitters to increase the robustness and flexibility of its system. Therefore, if transmissions of two tags collide, this can create a new, false signal that can still be detected by the receivers (Pincock, 2012). This signal will have a new tag ID, so it will not interfere with the track of the original transmitting tag. This new tag ID will usually create a new track with only erroneous positions. This can be easily dealt with by only considering known ID's. However, this new tag ID can also be identical to that of another fish present in the study. The track of this second fish will then be heavily distorted by these false detections. Even though these errors are unlikely, they remain possible (Simpfendorfer et al., 2015). In this study, up to 50 fish were released in a short time span, so many signals were transmitted in a small area and signal collision is likely to occur. Even though VPS incorporates a system to detect these false tag ID's based on

the expected ping times, some errors can still slip through (Pincock, 2012). As with reflected signals, the HPE has no way of recognising these false detections.

Finally, HPE usage makes the comparison between different studies difficult. The HPE is designed and used by VEMCO only. Data from other companies will report a different error parameter (e.g. Lotek Wireless Inc. uses the condition number (Hanson et al., 2007) and reliability index (Niezgoda et al., 2002)). As the HPE determination of the basic positions is not fully explained and thus not reproducible, the resulting error values cannot be quantitatively compared to other measures. Even if all animals are tracked via VPS, the HPE values are not comparable between different studies (Smith, 2013). This is again a result of the lack of calibration. Furthermore, there is little consistency and communication between researchers when selecting HPE cut-off criteria. This results from the lack of a general guideline for HPE usage. With this in mind, Meckley et al. (2014) designed a generalised procedure. However, this does not solve the other issues outlined above.

2.1.4 Alternative error measures

In summary, there are two main disadvantages of the HPE: it lacks physical relevance (cannot be expressed in meters) and it fails to recognise multipath errors. This section will mention some alternatives and how they cope with these issues.

To evaluate the temporal variation in accuracy, the data from the synctags can be used. The calculated positions of a stationary transmitter with a known position can be used as indication of the average positioning accuracy at that time. It reflects the effects of the environmental conditions on the reliability of the results (Biesinger et al., 2013). So by using the HPEm data recorded at the time of transmission, we can estimate the error present because of temporal variations. The calculation of such a measure is further discussed in Section 3.3. Binder et al. (2016) illustrated that a relationship between the variability of positioning results and the environmental conditions is too complex to be modelled robustly. Therefore, this simplified approach is currently the only available way to account for environmental temporal variations. However, this does not cover the location specific error (i.e. distance from hydrophones) or the quality of the detecting hydrophones.

Incorporating spatial variation is less straightforward. This source of error depends on many factors which may be difficult to quantify. As an approximation, the reliability of a position can be determined based on the receiver cluster used for its calculation (Vergeynst, 2017). The average HPEm of stationary tags positioned by this cluster can then serve as a measure of its reliability. Some receivers may be in unfavourable

positions with bad lines of sight or areas with many reflections. The receiver clusters can also have a poor geometric shape (i.e. 3 receivers lay in one line instead of an isosceles triangle). If a transmitter signal is picked up by such a bad receiver cluster, the resulting position will inherently be less reliable. Despite their heavy simplification, the two error measures mentioned above will be used in this study to examine the effects of environmental conditions and receiver cluster quality respectively.

Ehrenberg and Steig (2002) developed an alternative measure that can be calculated using the calculated positions. It is based on the positions of the detecting hydrophones relative to the transmitter, on the variability of the TOA, and on the uncertainty of the sound speed due to temperature variations. Thus this measure incorporates both spatial and environmental error causes. In addition, its calculation is independent of the used positioning system, so it could serve as a unifying error measure that can be used in all studies. However, its calculation requires several parameters: temperature, salinity, signal-to-noise ratio, signal bandwidth and the sampling interval. If one of these parameters is unknown, as is the case in our study, it has to be guessed. In that case, the equations lose their physical relevance and the corresponding error value can no longer serve as a true error measure expressed in meters. As with HPE, the error is also based on the calculated position, resulting in strong over -or underestimations of the error for wrong positions. Furthermore, this error measure is unable to cope with multipath errors or external noise, so additional filtering steps are still required to remove these.

The error measure developed by Wahlberg et al. (2001) is based on the same principles. The main difference is that it uses the uncertainty of the TDOA between two hydrophones instead of the TOA at each hydrophone. Furthermore, it takes a more empirical approach: the standard deviation of the sound speed is estimated based on data and the TDOA uncertainty is guessed based on expert knowledge. Thus, it shares the same pros and cons as the previous measure.

In conclusion, none of the available error measures capture the effects of multipath errors, and undefined sources of noise remain. Thus, removing positions with high error values is not an effective clean-up strategy. Therefore, we introduce the Kalman filter in the next section to remove noise and increase the reliability of the data. To deal with the multipath errors, we implemented an additional outlier filter, preceding the Kalman filter.

The usage of error measures cannot be omitted completely, as the Kalman filter still requires an indication of the reliability of the positions. In this context, the values are strictly used as a measure of relative error sensitivity, and not for noise or error characterisation. The HPE and Ehrenberg error both show potential for this purpose.

The HPE includes the same error-inducing factors as the last two alternatives mentioned, but adds information about the environmental conditions by calibrating the error using the synctags. The Ehrenberg error will be tested as a possible alternative. Even though it takes a more simplified approach, it has the added advantages of transparency and universal applicability.

2.2 The classic approach: the Kalman filter

To deal with noise from undefined sources, we applied a well established technique used in a wide range of applications: the Kalman filter (KF). The KF is part of the bigger group of Bayesian filtering algorithms (also referred to as state-space models). All algorithms in this group combine a model that captures how the measurements are related to the system and a mechanistic model that predicts the behaviour of the system. Thereby, they allow validation of observations based on previous information and minimize the impact of impossible or unlikely observations (Patterson et al., 2008). Most non-Bayesian filtering methods simply remove noisy data-points based on one or multiple parameters (Espinoza et al., 2011a; Coates et al., 2013; McMahan et al., 2013; Meckley et al., 2014). Although these points are noisy, they still contain some information about the animal's movement, especially if ping intervals are large and removing points can lead to long periods without information. The main advantage of Bayesian filtering algorithms is that all information from the noisy dataset is used (Jonsen et al., 2005), preventing huge amounts of data loss.

Bayesian filtering techniques have been used in a wide range of applications, such as navigation, telecommunication, brain imaging, robotics, process control etc. (Sarkka, 2013). In ecology, these techniques are used for population modelling (Sullivan, 1992; Ennola et al., 1998; Clark and Bjørnstad, 2004), ocean floor analysis (Ellis et al., 2007), forecasting algal blooms (Mao et al., 2009), and determination of environmental conditions (Sengupta et al., 2012). However, they find their main uses in tracking applications (Morales et al., 2004; Royer et al., 2005; Jonsen et al., 2006; Pedersen et al., 2008). The Kalman filter specifically, has been successfully used to track animals in terrestrial (Anderson-Sprecher and Ledolter, 1991; Anderson-Sprecher, 1994; Nations and Anderson-Sprecher, 2006; Forester et al., 2007), and aquatic environments (Sibert et al., 2003; Royer et al., 2005; Sibert et al., 2006; Nielsen et al., 2006; Lam et al., 2008; Johnson et al., 2008; Jensen and Chen, 2013; Lopez et al., 2014). Argos, a GPS tracking company for ecological applications, even includes the Kalman filter as an optional post-processing step (Lopez et al., 2014; Lowther et al., 2015), although its reception has been mixed (Boyd and Brightsmith, 2013).

This part of the literature review explains which combination of filter components we selected for our case-specific tracking problem. Section 2.2.1 explains the basic principles of Bayesian filters. Section 2.2.2 clarifies why the standard KF was used in this study. Section 2.2.3 introduces an extension to improve its performance: the RTS-smoother. Section 2.2.4 presents the movement models necessary for the filter. As this method mainly deals with noise and not other interferences, Section 2.2.5 proposes an additional filtering step that will precede the KF.

2.2.1 Basics of Bayesian filters

The explanation of the basic principles of Bayesian filtering in this section is based on Chapter 4 of the book 'Bayesian Filtering and Smoothing' by Sarkka (2013), which gives a concise and updated overview of the available techniques.

All Bayesian filters estimate the true state of the system at time step k, x_k, based on two probability distributions:

$$\begin{aligned} x_k &\sim p(x_k \mid x_{k-1}), \\ y_k &\sim p(y_k \mid x_k), \end{aligned} \tag{2.1}$$

with y_k the measured state at time step k.

The first probability distribution is calculated by the process model that predicts the current state (at time k), based on the filter output of the last time step ($k-1$). In our case, this is a movement model that describes the basics of fish behaviour (Section 2.2.4). The second distribution is calculated by a measurement model that describes how the measured variable relates to the system state under interest. In our case, this system state is the longitudinal and latitudinal position of the fish.

A Bayesian filter then uses these two models to calculate the optimal estimate of the current state based on all previous measurements: $p(x_k \mid y_{1:k})$. This is done recursively for every observed position. First, the current state is predicted using the process model:

$$p(x_k \mid y_{1:k-1}) = \int p(x_k \mid x_{k-1})\, p(x_{k-1} \mid y_{1:k-1})\, dx_{k-1},$$

where $p(x_{k-1} \mid y_{1:k-1})$ is the previously filtered point.

Then, this predicted current state is combined with the measured state to determine the optimal estimate of the true state using Bayes' rule:

$$p(x_k \mid y_{1:k}) = \frac{p(y_k \mid x_k)\, p(x_k \mid y_{1:k-1})}{\int p(y_k \mid x_k)\, p(x_k \mid y_{1:k-1})\, dx_k}.$$

The prediction step and update step are illustrated in Figure 2.3.

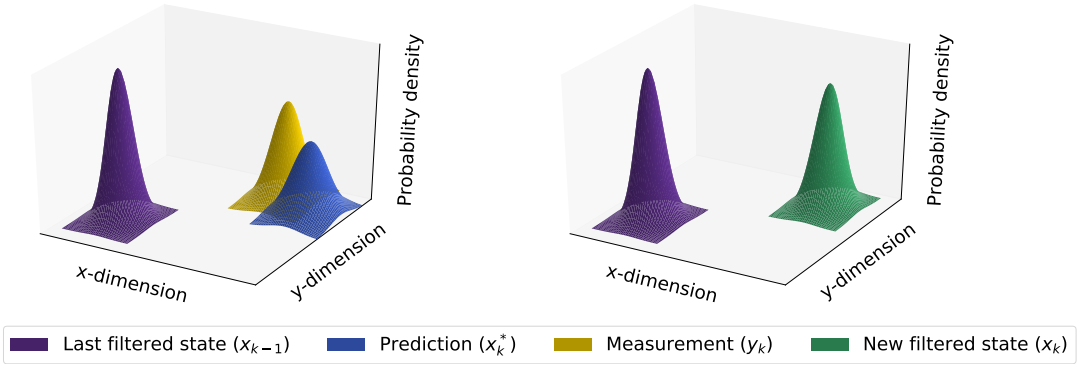

Figure 2.3: Illustration of the principle of the KF. The first plot shows the result of the prediction step. The process model predicts the position at the next time step based on the last filtered state (purple). The second plot shows the result of the update step, which combines this predicted state (blue) with the measured state (yellow) to determine the optimal estimate of the current state (green).

These general Bayesian filtering equations are then translated into usable formulae by the different filters. The choice of the filter depends on the properties of the used models and the measurement noise. The KF solves these equations using simple matrix algebra by calculating the closed form solution. Chapter 3 describes this recursive process in detail.

2.2.2 Selection of the appropriate filter

Of the Bayesian filters, the KF is one of the simplest and computationally lightest algorithms. Its main downsides are its stringent assumptions. It can only be used if the measurement noise is approximated by a Gaussian distribution, and the measurement and process model are linear. Most other state-space models serve as extensions or alternatives for cases where these assumptions do not hold (Sarkka, 2013).

In the field of ecology, this basic approach is often regarded as too constraining. The assumption of linearity severely limits the options for the movement model. Linear models are often unable to capture the complex processes that define actual animal movement. They do not allow for different behavioural modes or the incorporation

of external influences, such as water temperature (Jonsen et al., 2003; Royer et al., 2005; Patterson et al., 2008; Lam et al., 2008).

Despite its stringent assumptions, we found the standard KF to be the best choice for this study. The main reason is the strict need for unbiased fish tracks. Most of the studies mentioned in the introduction above draw their conclusions directly from the resulting tracks (i.e. statistical hypotheses testing using a parameter derived from the tracks) or from the parameters that are estimated in the movement model of the filter. The assumptions made by the model will not bias the conclusion as they are clearly mentioned and accounted for. In our case, however, the resulting dataset will be used as an input for another study that will attempt to explain the movement patterns of the fish. Thus, using complex models with assumptions about the preferred travelling direction or the presence of different behavioural modes may impact the resulting fish tracks and bias the subsequent study. Therefore, the model was kept as simple as possible so only the most general and verifiable assumptions are made (see Section 2.2.4). Since the used model has to be simple anyway, using the standard KF is the best option: it is still the fastest and simplest Bayesian filter (Sarkka, 2013). It is the best linear unbiased estimator if all assumptions are met, and it solves the equations continuously. Other algorithms, like the Unscented Kalman filter or the Particle Filter, sample the probability distributions and only approximate the filtering distributions. The latter two algorithms are useful when not all assumptions are met, but otherwise they unnecessarily discretize and complicate the calculation (Royer et al., 2005).

2.2.3 Bayesian smoothers

Bayesian smoothing can be applied during or after the filtering step to maximise the information used and increase the reliability. The filtering algorithms so far only used the available measurements until the current time-step. In our case, however, an extra form of information is available. All positions of the fish are provided at once, so measurements after the current time-step are also available. A Bayesian smoother incorporates information of all measurements into every state estimation:

$$p(x_k \mid y_{1:T}),$$

with $y_{1:T}$ all available measurements and T, the time-step of the last availably measurement. The theoretical explanation of the Bayesian smoothers is based on Chapter 8 of the book by Sarkka (2013).

Since all measurements are given in our case, Bayesian fixed interval equations can be used to calculate this probability distribution. First, the distribution of the next

state x_{k+1} is predicted using the filtering distribution of the current state $p(x_k \mid y_{1:k})$ and the process model:

$$p(x_{k+1} \mid y_{1:k}) = \int p(x_{k+1} \mid x_k)\, p(x_k \mid y_{1:k})\, dx_k\,.$$

Then the current state is recalculated based on Bayes' rule using the predicted future state and the measured future state:

$$p(x_k \mid y_{1:T}) = p(x_k \mid y_{1:k}) \int \left[\frac{p(x_{k+1} \mid x_k)\, p(x_{k+1} \mid y_{1:T})}{p(x_{k+1} \mid y_{1:k})} \right] dx_{k+1}\,.$$

In this thesis, the Rauch-Tung-Striebel smoother (RTSS, also called the Kalman smoother) is used to test the effect of smoothers. From these theoretical equations, the strong similarities with Bayesian filtering is clear. The RTSS captures this similarity by using the same analytical updating procedures as used in the KF. Therefore, when using the KF for the filtering recursion, the RTSS is the most intuitive and logical choice for the smoothing recursion. It smooths the data after the filtering step is complete, allowing a comparison between results before and after smoothing. This is an advantage compared to the two-filter smoother, the main alternative, which runs in between the filtering steps, so that no purely filtered solution can be obtained without implementing it in a separate algorithm.

Due to the extra information incorporated in the smoother, the filter-smoother combination will increase the reliability of position estimates of these positions (Anderson-Sprecher and Ledolter, 1991; Anderson-Sprecher, 1994). However, if the process and measurement models and their noise are not accurately defined, the smoother may deviate from the true track as it is based on false information (Sengupta et al., 2012). Thus, the filter and smoother construction steps are crucial and will be further discussed in Chapter 3.

2.2.4 State prediction: fish movement models

As outlined in Section 2.2.1, the KF requires a process model to evaluate the validity of the measurements. In our case, this is a model that describes the movement of fish. Due to the specific requirements of this study, assumptions made by such a model have to be kept to a minimum. Therefore, this section suggests a few basic models that only make plausible assumptions.

A first option is a standard Gaussian random walk model (RW). These models and their extensions are the most widely used models in biology (Codling et al., 2004; Alós et al., 2016). In its simplest form, the isotropic RW, every movement is completely

random and independent of the last one. Thus, the probability distribution of the current state x_k is a Gaussian distribution with mean x_{k-1}. Due to its simplicity and omnipresence, basic RW models have frequently been used as the process model in Bayesian filters (Anderson-Sprecher, 1994; Pedersen et al., 2008; Sengupta et al., 2012), especially in filters that switch between behaviour modes, where it is used as the stationary mode (Jonsen et al., 2005; Lopez et al., 2014). Despite its simplicity, the regular random walk model lacks biological relevance (Royer et al., 2005; Alós et al., 2016).

A popular extension of the RW is adding a bias or drift to the model; the biased random walk models (BRW). These incorporate how fish are drawn more strongly in a certain direction. This way, currents or the effects of food and danger can be implemented (Codling et al., 2004). Such BRWs have been successfully used in Bayesian filters (Sibert et al., 2003; Jonsen et al., 2003; Nations and Anderson-Sprecher, 2006; Alós et al., 2016). However, BRWs are not relevant in this thesis as they will incorporate directional bias in the path, which may interfere with the subsequent study.

A more useful extension of the RW is the correlated random walk model (CRW). Here, the random walk component does not apply to positions themselves, but to the speed and direction of travel between subsequent positions (Jonsen et al., 2005). In this way, CRWs allow some correlation between subsequent locations and modelled fish are likely to maintain their current trajectory (Codling et al., 2004). As this may describe actual fish movement more accurately, it has been incorporated in several Bayesian filters (Jonsen et al., 2005; Breed et al., 2006; Lopez et al., 2014). The persistence in a CRW can be formulated in two ways: a constant angle and speed (Codling et al., 2004; Faugeras and Maury, 2007) or a constant speed along two orthogonal axes (Lopez et al., 2014). The second approach makes the assumption that movements along these axes are independent. Although this assumption may be an abstraction of reality, it allows formulation of a linear model. Therefore, the second approach will be used in this thesis. The correlation of the CRW may also be a disadvantage in some cases. If the previous speed is based on an erroneous point, the influence of this error may persist longer, sidetracking correct positions in the process. Abrupt changes in swimming speed or direction may also go unnoticed for a while, especially if time-steps are large. Therefore, a model with less persistence may work better.

Johnson et al. (2008) formulated a new model, the continuous-time correlated random walk model (CTCRW) that forms a compromise between the RW and CRW. It assumes a certain persistence in travelling direction and speed, but this correlation fades with time. So with a long enough time between measurements, the model will fall back from CRW to RW behaviour. Most other CRWs solve this by considering multiple behaviour modes (Morales et al., 2004). The fundamental difference between

that approach and the CTCRW is that the former allows switches between the RW and CRW during every time-step, while the latter describes the global affinity for both movement modes. As such, the CTCRW makes no assumptions about time specific behaviour. Furthermore, Johnson et al. (2008) formulated the model as a linear state space model. Thus, processing with the regular KF and RTSS is possible. The main disadvantage of the CTCRW is that two model parameters have to be estimated, while the CRW and RW only require one estimation. Since its development, the model's validity was proven in a wide range of studies and led to a revival of the basic KF (Wells et al., 2013; Rode et al., 2015; Laidre et al., 2016; Baylis et al., 2017; Joyce et al., 2017).

In conclusion, the CTCRW seems to be the best option for this specific case study. However, the basic RW model is still interesting for the premise of this study as it makes no assumption about the travel direction. Due to its simplicity and relevance, the regular CRW was also tested. Together, the CRW and RW allow a decomposition of the CTCRW to see which of the two components is the most relevant. Furthermore, these simpler models may still be the best choice if they show a similar performance since they are computationally lighter.

2.2.5 Additional outlier filtering

Although the KF may be an effective measure to reduce the influence of noise, it is not well suited to handle false position readings. It can reduce the influence of these errors, but as the error on these false positions will never be infinitely large, the filter will still incorporate them to an extent. As the scale of these errors can be large relative to actual fish movements, they can sidetrack the path of the fish, even if the measurement has a low reliability. Ignoring them leads to a biased interpretation of the fish's behaviour (Bradshaw et al., 2007). Furthermore, the KF requires a Gaussian distribution of the measurement error. False positives with large errors can create a heavy tail in the distribution, causing deviations from this assumption. Therefore, it is advisable to remove these multipath errors as much as possible before applying the KF.

An HPE threshold is a popular way to remove these false positions with VEMCO systems (Espinoza et al., 2011a; Coates et al., 2013; McMahan et al., 2013; Meckley et al., 2014). However, the HPE does not account for many of the processes that cause false positions, as Section 2.1.3 explains. Therefore, this method is unlikely to remove all false positions and may remove correct points in the process. This study mainly uses the HPE threshold to benchmark other filtering methods against this widely used technique.

Because of these shortcomings, Vergeynst (2017) created an intuitive method to remove unreliable data. The receiver clusters picking up the signals are grouped into three groups: good, bad and neutral. This classification is based on how well these clusters position the synchronization and reference tags with a known location. This classification may capture some error causing mechanisms such as bad geometries of the receiver clusters, highly reflective receiver locations or poorly performing receivers. By ignoring positions calculated by the worst performing clusters, the false positions can be removed.

A filter based on fish swimming speeds may be a more natural way of removing false positions. As erroneous positions are not directly related to the fish track, they can lay far away from the fish's path. If such an error occurs in the middle of a correct track, an exceptionally high speed is needed to jump to this false point and back. McConnell et al. (1992) used this principle to identify and remove errors. This filter averages out the recorded swimming speed over two points before and after every position and rejects the points of which the speed is biologically infeasible. Since its development, this speed filter successfully removed outliers in multiple studies (Vincent et al., 2002; Austin et al., 2003; Johnson et al., 2008). However, some caution is necessary, as biological filters can bias the results. If the maximum swimming speed is chosen too low, actual fish positions can be classified as errors. This way, the fastest parts of the fish trajectory are removed (Patterson et al., 2008; Meckley et al., 2014). This can bias the results because it systematically excludes a specific behaviour type (e.g. quickly fleeing from danger).

To account for this weakness of the speed filter, we opt to use only the highest swimming speeds reported in literature. This is a conservative approach, since the speed gate was designed to use a maximum speed that can be held for a few time-steps (McConnell et al., 1992). For European eels, Videler and Wardle (1991) reported the maximum burst speed is 7.5 body lengths per second. Swimming speeds of 3.5 and 5.3 body lengths per second can be sustained for 3 and 0.7 seconds respectively. For Atlantic Salmon, Bainbridge (1957) mentions speeds between 5.8 and 12.2 body lengths per second. The highest speeds recorded are for salmon leaping out of the water. These are excluded in this thesis as it is considered an unlikely occurrence in a canal. The highest remaining speed is then 8 body lengths per second. Wardle (1975) also reports that small salmon can reach speeds of 8 body lengths per second. Based on this information the speed threshold is set at 7.5 and 8 body lengths per second for eels and salmon respectively.

In addition to the standard speed filter, two possible extensions were tested. Austin et al. (2003) improved the speed filter by adding an extra filtering stage. Before running the standard filter, points are excluded if the swimming speed to all four

neighbours are higher than the threshold. This extra step decreased the number of false negatives and simultaneously removed more outliers. Freitas et al. (2008) added a third stage to this filter. This step removes more outliers, with a reasonable loss of correct positions. After the same first two stages, points that require a turning angle that is higher than a predefined maximum are removed. These three methods were implemented to evaluate if the added stages increase performance as reported.

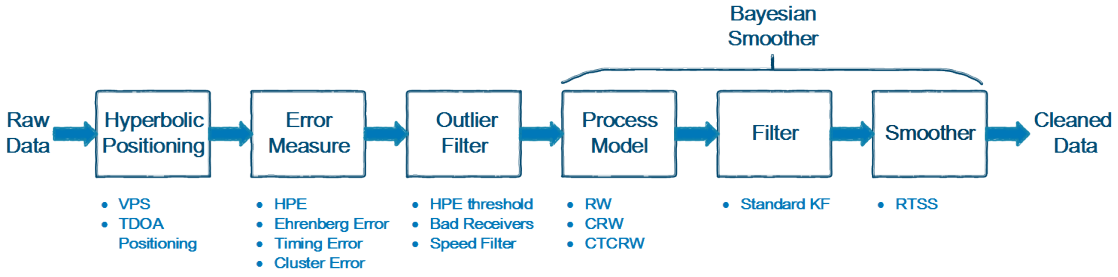

Figure 2.4: Block diagram that shows the required steps in the traditional approach. Below the blocks, all tested alternatives are summed up.

Figure 2.4 summarizes the different steps followed by the classic approach towards data clean-up of noisy fish telemetry data. It also shows all possibilities that will be considered in the search for the optimal algorithm following this approach. This best technique will then be compared to a new, radically different approach: the YAPS-algorithm, created by Baktoft et al. (2017). This algorithm is discussed in the next section.

2.3 A new approach: YAPS

Baktoft et al. (2017) designed a new algorithm to handle noisy telemetry data: Yet Another Positioning Solver (YAPS). This method approaches the acoustic telemetry problem from a fundamentally different angle. It uses raw TOA data to perform a Maximum Likelihood analysis of a state-space model that describes acoustic signal transmissions and fish behaviour. So far, results seem promising: YAPS outperformed the tested alternatives by calculating more positions and deviating less from the true track.

By using TOA instead of TDOA, YAPS can calculate more positions. Since the actual time of transmission is not usually known, most classic methods use the first detecting hydrophone as a reference to calculate the TDOA. This way, the transmission time is considered an extra unknown. Therefore, a minimum of three hydrophones is needed to determine a position in a two dimensional tracking problem: one for every unknown (transmission time and longitudinal and latitudinal position). If less hydrophones pick

up the signal, their information cannot be used (Li et al., 2014). In contrast, YAPS regards all transmissions as random values with a well defined probability distribution. The algorithm then maximises the likelihood of all TOAs occurring simultaneously by varying the transmission locations. That way, all TOA information can be used to determine positions, even if picked up by less than three receivers (Baktoft et al., 2017).

The TOA approach also minimises the impact of errors. In the classic TDOA system, every position is calculated based on three hydrophones. If one of these detections is erroneous, the calculated position can be far from the real one. If more than three hydrophones recorded the signal, the position is determined multiple times. This way, the impact of a wrong detection can be reduced, but it remains substantial. YAPS omits this problem by basing the positioning on all available detections (Baktoft et al., 2017). The wrong detection is compared not only to the other two TOAs, but to all previous and following transmissions. Therefore, it is less likely that this error will affect the positioning considerably.

The current version of YAPS makes several assumptions that have to be kept in mind. So far, the model ignores the influence of depth. Also, it assumes the variation of the sound speed (i.e. due to changes in temperature and depth) can be modelled as a random walk process. Fish movement is also described by a basic random walk process. Furthermore, the error distribution is assumed to be the sum of a zero mean Gaussian distribution and a scaled t-distribution with three degrees of freedom. Finally, the time interval between transmissions is assumed to be constant. This last assumption poses a problem for our case as VEMCO uses transmitters with random burst intervals (Pincock, 2012). This deviation from ideal conditions has to be kept in mind when evaluating the performance. Many of these assumptions can be removed from the model by expanding or altering its components. This is facilitated by the transparent and flexible structure of the model.

YAPS differs from the traditional approach in several ways. Firstly, it performs positioning and data clean-up simultaneously, while the classic approach requires the sequential application of different algorithms and filters. Secondly, it minimises the effect of noise for all points simultaneously, contrary to Bayesian filters, that take a recursive, point by point approach. It is also a completely transparent process, while the classic approach involves positioning and error determination steps that are often black-box. Because of this, it can be used for all telemetry systems and opens the door to one, universal method. Like many traditional methods, it uses a movement model to estimate the likelihood of positions based on expected fish behaviour. The main difference is that, in this first version, a regular random walk model is used, whereas most classic approaches implement more complex extensions of this model.

Finally, the residuals (related to the positioning error) are modelled as a combination of a Gaussian and a Student's t-distribution. Therefore, YAPS can better cope with multipath errors, which create long tails in the residuals. Further technical details about the workings of this algorithm are provided in Section 3.9.

Due to its different approach and advantages, we tested YAPS on our case study. Since it is a new method, it has not been rigorously compared to other well established methods. So far, YAPS was mainly tested on simulated data. Beyond that its performance was evaluated for one test track and compared to unfiltered TDOA positioning data and unfiltered positioning data from Lotek. Comparing the algorithm against a system that implements a noise and error filtering step was considered beyond the scope of the original paper (Baktoft et al., 2017). This thesis evaluates its potential more strictly by giving it a fair competitor: the best performing system from the classical approach. This way, we can truly establish if this new system is better than the old ones. Furthermore, the algorithm is pushed to its limits by testing it on our noisy dataset with random and large burst intervals. Lastly, its performance is tested on real fish data, while so far it has only been used for tracks performed by boat.

CHAPTER 3

METHODOLOGY

3.1 Description of the case study

The site of this study is located upstream of a navigation lock complex on the Albert canal in Ham. Twelve receivers (VR2W-69kHz from VEMCO) were placed throughout this site to track fish (see Figure 3.1 for the set-up). Ten of these were collocated with synchronization tags, needed for time synchronization of the independent receivers. In addition, three reference tags emit signals every ten minutes, just like the synchronization tags. Because the actual positions of these tags are known, the calculated positions can be used to evaluate system performance.

The fish were surgically implanted with acoustic transmitters and released upstream of the test site in different deployments. VEMCO's V13 and V13-P transmitters, with burst intervals between 17 and 33 seconds, were used for the European eels. These have random burst intervals of 17 to 33 seconds. Salmon smolts from a hatchery were implanted with V7 transmitters, with burst intervals of 15 to 30 or 40 to 80 seconds. In addition, a boat carrying a GPS-device and V7 and V13-P transmitters was used to drive test tracks through the study site. Data from these test tracks will be used to evaluate the performance of the positioning and clean-up techniques.

The sound speed was calculated as a function of environmental conditions. The site was fitted with a temperature sensor, which makes hourly measurements, and a conductivity sensor to determine the salinity every ten minutes. These temperature and salinity data were then used to calculate the sound speed via the Mackenzie (1981) equation:

$$\begin{aligned} c(z,S,T_w) = {} & 1448.96 + 4.591T_w - 5.304e^{-2}T_w^2 + 2.374e{-}4T_w^3 + 1.34(S-35) \\ & + 1.63e^{-2}z + 1.675e^{-7}z^2 - 1.025e^{-2}T_w(S-35) - 7.139e^{-13}z^3T_w\,; \end{aligned} \tag{3.1}$$

with z the depth, S, the salinity in p.p.t. and T_w the water temperature in °C. Because depth information is not available for most transmitters and its influence on the speed of sound is minimal (Smith, 2013), we used a depth of zero meters.

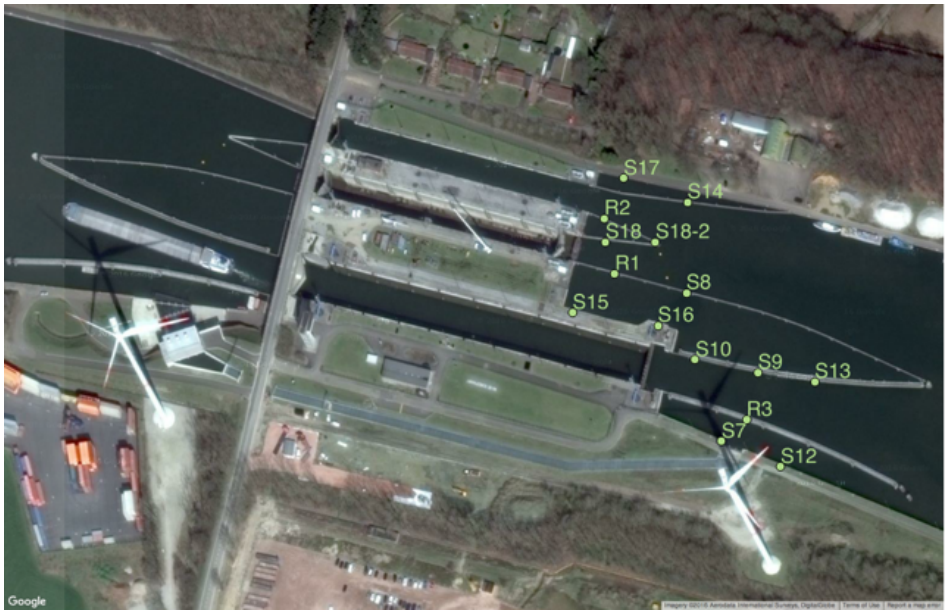

Figure 3.1: Top view of the study site. The green dots represent the locations of the receivers (collocated with synchronization tags, 'S') and reference tags ('R').

3.2 Hyperbolic positioning

Before the TOA data was fed to the hyperbolic positioning and YAPS algorithms, it was cleaned up by removing impossible arrival times. From the TOA matrix, the time delay between signals can be calculated. If this delay is smaller than the minimum burst interval, one of the two detections is erroneous (i.e. a reflected signal arriving later). In this case, the signal detected by the least amount of receivers was removed. This is based on the assumption that a reflected signal will be picked up by less receivers than the original transmission. VEMCO uses a similar method to filter out false detections (Pincock, 2012).

The hyperbolic positioning algorithm then estimates the track using this TOA matrix. Because the transmission time is unknown, the first detection is used as a reference. Subsequently, the TDOA between this reference and the other detecting receivers is calculated. Assuming a uniform speed of sound, this time difference is linked to a range difference:

$$(t_i - t_1)c = \|\boldsymbol{p} - \boldsymbol{h}_i\| - \|\boldsymbol{p} - \boldsymbol{h}_1\|,$$

with $\boldsymbol{h}_1$ the position of the first detecting receiver, $\boldsymbol{h}_i$ the position of receiver i, $\boldsymbol{p}$ the position of the transmitter, t_i the TOA of receiver i and c the sound speed. For a two dimensional tracking problem, $\boldsymbol{h}_i = (h_{i,1}, h_{i,2})^T$, with $h_{i,1}$ the position of receiver i in the first dimension, and $\boldsymbol{p} = (p_1, p_2)^T$. $\|\boldsymbol{p} - \boldsymbol{h}_i\|$ is the euclidean distance between

positions $\boldsymbol{p}$ and $\boldsymbol{h}_1$. This relationship is then used to find the optimal value of the true position.

Our data proved to be too noisy for the analytical methods of Wahlberg et al. (2001) and Spiesberger and Fristrup (1990), so we implemented a more robust Least squares (LS) approach. The cost function of Li et al. (2016) was minimized iteratively for every detection:

$$J_{TDOA} = \sum_{i=2}^{N}((t_i - t_1)c - \|\boldsymbol{p}^* - \boldsymbol{h}_i\| + \|\boldsymbol{p}^* - \boldsymbol{h}_1\|)^2\,,$$

with $\boldsymbol{p}^*$ the calculated transmitter position and N is the number of detecting hydrophones.

A genetic algorithm reduces the influence of initial estimates and increases the chance of finding the global minimum, in contrast with the local optimizers used by all current methods (Li et al., 2016). Therefore, we used the genetic algorithm of Storn and Price (1997), which is available as `scipy.optimize.differential_evolution` in the SciPy package (Jones et al., 2018) of Python.

To remove positions that were caused by erroneous TOAs or local minima, we filtered this data by removing impossible coordinates (i.e. too far from the array, far outside the canal)

3.3 Error sensitivity measures

The error measures described in Section 2.1.4 do not accurately predict the positioning error, so using them directly to clean up data is not advisable. However, they can still provide a rough indication of the reliability of the calculated positions. The KF needs such a measure to determine the relative importance of the measured and predicted state. This indicator does not need to capture all sources of noise and errors, as these are dealt with by the KF and outlier filter respectively. Therefore, we still use the error measures to describe the relative error sensitivity. Besides the HPE, we tested the performance of several more transparent alternatives. The basics of their determination are outlined below.

The timing error uses the accuracy data available from the fixed tags to estimate the reliability of a position. For every calculated position, a time interval of five minutes before and after the detection is defined. The error measure is then the median of the known errors (HPEm) of the positioned stationary tags within this time interval. This error measure may capture some of the environmental disturbances present at the

time of detection. We chose a time interval of five minutes as a compromise between sample size and temporal accuracy. The median is used to reduce the influence of outliers.

The cluster error incorporates the reliability of the receiver cluster that calculated the position. This method groups all positions of the fixed tags according to the receivers used for their calculation. For each of these receiver clusters, the average HPEm is calculated. The error sensitivity of a fish position is then the mean HPEm of the cluster that was used to calculate this position. This method is inspired by the receiver classification of Vergeynst (2017).

The error measure defined by Ehrenberg and Steig (2002) calculates the positional accuracy as a function of hydrophone geometry, distance from the hydrophones, uncertainty of the TOA, and inaccuracies of the sound speed. Information on the latter two processes was not available, so we removed them from the error calculation. Therefore, the error measure loses its physical relevance and can no longer be expressed in meters. However, it still captures some important error mechanisms and like HPE, it may still serve as a relative measure of error sensitivity. We rewrote the error definition for a two dimensional positioning problem and using all detecting hydrophones (instead of only three).

The total location error, Δp, is defined as:

$$\Delta p = \sqrt{\Delta p_1^2 + \Delta p_2^2},$$

with Δp_1 and Δp_2 the errors of the longitudinal and latitudinal position respectively. These values are calculated as follows:

$$\begin{bmatrix} \Delta p_1 \\ \Delta p_2 \\ \Delta Rm \end{bmatrix} = \boldsymbol{M}^{-1} \begin{bmatrix} t_1 \\ t_2 \\ \vdots \\ t_N \end{bmatrix} \Delta c\,.$$

t_i is again the TOA of receiver i, and ΔR_m is the error in the range calculation, caused by the conversion of the analog arrival time to a digital number (quantization error). Δc is the uncertainty of the calculated sound speed, which is unknown and set to 1.

The matrix $\boldsymbol{M}$ is calculated as:

$$\boldsymbol{M} = \begin{bmatrix} m_{11} & m_{12} & 1 \\ m_{21} & m_{22} & 1 \\ \vdots & \vdots & \vdots \\ m_{N1} & m_{N2} & 1 \end{bmatrix}, \text{with } m_{ij} = \frac{h_{ij} - p_j}{R_i} \text{ and } R_i = \sqrt{(h_{i1} - p_1)^2 + (h_{i2} - p_2)^2},$$

where h_{ij} is the position of receiver i in dimension j. If N is greater than three, the inverse of $\boldsymbol{M}$ does not exist and a least squared approximation has to be used. This total location error (Δp) will be tested as a transparent alternative to the HPE.

3.4 The Kalman filter

This section outlines the basic concepts of the KF implementation, based on Chapter 4 of 'Bayesian Filtering and Smoothing', by Sarkka (2013). For a more in-depth explanation and proof of the presented formulae, this book can serve as a concise reference. Section 3.4.1 outlines the general principle of the KF and Section 3.4.2 provides the iterative approach that is actually implemented.

3.4.1 General equations

The Kalman filter is based on two main assumptions. Firstly, the state $\boldsymbol{x}_k$, the measurement noise $\boldsymbol{r}_k$ and the process noise $\boldsymbol{q}_k$ have to be normally distributed:

$$\begin{aligned} \boldsymbol{x}_k &\sim \mathrm{N}(\boldsymbol{m}_k, \boldsymbol{P}_k), \\ \boldsymbol{r}_k &\sim \mathrm{N}(0, \boldsymbol{R}_k) \\ \boldsymbol{q}_k &\sim \mathrm{N}(0, \boldsymbol{Q}_k), \end{aligned}$$

where $\boldsymbol{P}_k$ is the total covariance of state $\boldsymbol{x}_k$ at time step k and $\boldsymbol{R}_k$ and $\boldsymbol{Q}_k$ are the covariance matrices of the measurement and process model respectively. Secondly, the measurement and process models have to be linear, so they can be written in their linear state-space form.

If these assumptions are met, the closed form solutions of the the Bayesian filtering equations (see Eq. 2.1) are given by:

$$\begin{aligned} \boldsymbol{x}_k &= \boldsymbol{A}_{k-1}\boldsymbol{x}_{k-1} + \boldsymbol{q}_{k-1}, \\ \boldsymbol{y}_k &= \boldsymbol{H}_k\boldsymbol{x}_k + \boldsymbol{r}_k. \end{aligned}$$

Here, $\boldsymbol{A}_{k-1}$ and $\boldsymbol{H}_k$ are the transition matrices of the process and measurement model respectively. Their construction for the different movement models is discussed in Section 3.6.

3.4.2 Iterative filtering algorithm

$\boldsymbol{x}_k$ is the true state of the system, which is unknown in reality. The KF estimates this state as the mean of its Gaussian distribution ($\boldsymbol{m}_k$), which is computed in two steps:

The prediction step:

$$\begin{aligned} \boldsymbol{m}_k^* &= \boldsymbol{A}_{k-1}\boldsymbol{m}_{k-1}\,, \\ \boldsymbol{P}_k^* &= \boldsymbol{A}_{k-1}\boldsymbol{P}_{k-1}\boldsymbol{A}_{k-1}^T + \boldsymbol{Q}_{k-1}\,, \end{aligned} \tag{3.2}$$

and the update step:

$$\begin{aligned} \boldsymbol{v}_k &= \boldsymbol{y}_k^m - \boldsymbol{H}_k\boldsymbol{m}_k^*\,, \\ \boldsymbol{S}_k &= \boldsymbol{H}_k\boldsymbol{P}_k^*\boldsymbol{H}_k^T\,, \\ \boldsymbol{K}_k &= \boldsymbol{P}_k^*\boldsymbol{H}_k^T\boldsymbol{S}_k^{-1}\,, \\ \boldsymbol{m}_k &= \boldsymbol{m}_k^* + \boldsymbol{K}_k\boldsymbol{v}_k\,, \\ \boldsymbol{P}_k &= \boldsymbol{P}_k^* - \boldsymbol{K}_k\boldsymbol{S}_k\boldsymbol{K}_k^T\,. \end{aligned} \tag{3.3}$$

$\boldsymbol{m}_k^*$ and $\boldsymbol{P}_k^*$ are the predicted state and covariance respectively and $\boldsymbol{y}_k^m$ is the actual measurement. By iterating this set of equations over all the observation times, the optimal estimations of the true states ($\boldsymbol{x}$) and their uncertainties ($\boldsymbol{P}$) can be computed. For the first time step, $\boldsymbol{m}$ is initialized as the first measured position ($\boldsymbol{m}_0 = \boldsymbol{y}_0^m$) and $\boldsymbol{P}$ as the measurement noise matrix of this first position ($\boldsymbol{P}_0 = \boldsymbol{R}_0$). Figure 3.2 shows one filtering step for a one dimensional positioning problem to illustrate the meaning of the parameters used.

3.5 RTSS implementation

The method outlined in the last section only uses the information of the previous and current times steps. Applying a Bayesian smoother after the filter incorporates measurements of later time steps as well to increase the overall reliability. We opted for the Rauch-Tung-Striebel smoother due to its similarities with the forward KF. This section describes its implementation, based on Chapter 8 of 'Bayesian Filtering and Smoothing' by Sarkka (2013).

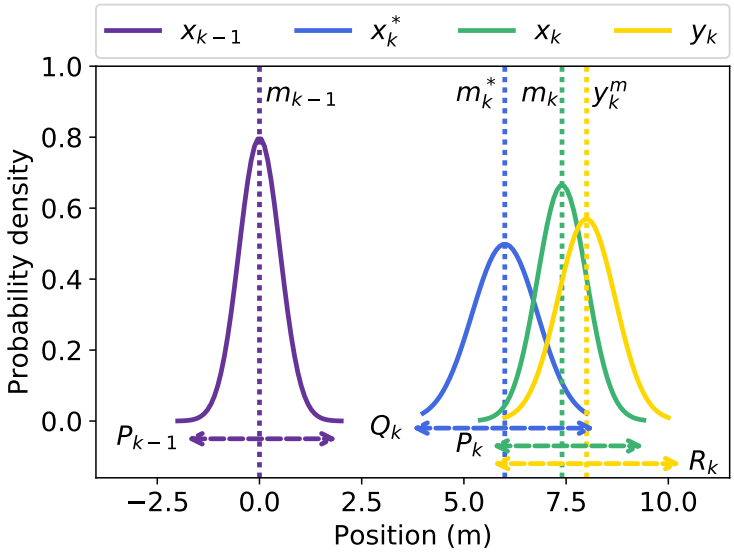

Figure 3.2: Illustration of one Kalman filter iteration for a one dimensional positioning problem. The probability distribution of the current state (x_{k-1}), with mean m_k and variance P_k, is used to predict the next position. This predicted position (x_k^*) is then combined with the measured position (y_k) to obtain the optimal estimate of the next state (x_k).

After running the KF algorithm outlined above, we can compute the smoothed positions as follows:

$$
\begin{aligned}
\boldsymbol{m}_{k+1}^* &= \boldsymbol{A}_k \boldsymbol{m}_k\,, \\
\boldsymbol{P}_{k+1}^* &= \boldsymbol{A}_k \boldsymbol{P}_k \boldsymbol{A}_k^T + \boldsymbol{Q}_k\,, \\
\boldsymbol{G}_k &= \boldsymbol{P}_k \boldsymbol{A}_k^T [\boldsymbol{P}_{k+1}^*]^{-1}\,, \\
\boldsymbol{m}_k^S &= \boldsymbol{m}_k + \boldsymbol{G}_k [\boldsymbol{m}_{k+1}^S - \boldsymbol{m}_{k+1}^*]\,, \\
\boldsymbol{P}_k^S &= \boldsymbol{P}_k + \boldsymbol{G}_k [\boldsymbol{P}_{k+1}^S - \boldsymbol{P}_{k+1}^*] \boldsymbol{G}_k^T\,,
\end{aligned}
$$

with $\boldsymbol{m}_k^S$ the smoothed optimal estimate and $\boldsymbol{P}_k^S$ its covariance matrix.

This algorithm runs backwards, starting from the second-to-last position and ending with the first one ($\boldsymbol{m}_0$). Since these equations require the next smoothed position $\boldsymbol{m}_{k+1}^S$ and its covariance $\boldsymbol{P}_{k+1}^S$, the last position (at time step T) cannot be smoothed. Therefore the smoothing recursion is initialised by copying the KF results: $\boldsymbol{m}_T^S = \boldsymbol{m}_T$ and $\boldsymbol{P}_T^S = \boldsymbol{P}_T$.

3.6 Definition of the transition matrices

The state-space formulation of the RW and CRW model in this section are based on those of Lopez et al. (2014). We excluded the signal frequency from the model as it is not a relevant parameter for the VEMCO system.

The RW model assumes that fish movement follows a normal distribution with the last position ($\boldsymbol{m}_{k-1}$) as a mean. The transition and covariance matrices then become:

$$\boldsymbol{A}_k = \begin{bmatrix} 1 & 0 \\ 0 & 1 \end{bmatrix}, \boldsymbol{H}_k = \begin{bmatrix} 1 & 0 \\ 0 & 1 \end{bmatrix}, \boldsymbol{Q}_k = \begin{bmatrix} 2D_{RW}\Delta t_k & 0 \\ 0 & 2D_{RW}\Delta t_k \end{bmatrix},$$

with Δt_k the time between the previous and current observation and D_{RW} the diffusivity, which has to be estimated based on the data (see Section 3.7). Here, $\boldsymbol{m}_k^*$ is defined as $(p_{k,1}^*, p_{k,2}^*)^T$, with $p_{k,1}^*$ the predicted position in the first dimension.

In the CRW, the random walk component is the speed instead of the position. Thus, the state must include the position and speed in both dimensions: $\boldsymbol{m}_k^* = (p_{k,1}^*, p_{k,2}^*, s_{k,1}^*, s_{k,2}^*)^T$, with $p_{k,1}^*$ the predicted positions in the first dimension and $s_{k,1}^*$ the estimated speed along this axis. Since no speed measurements are available, $\boldsymbol{m}_k$ remains equal to $(m_{k,1}, m_{k,2})^T$. The predicted speeds are removed through multiplication with $\boldsymbol{H}_k$. The CRW model thus defines the following matrices:

$$\boldsymbol{A}_k = \begin{bmatrix} 1 & 0 & \Delta t_k & 0 \\ 0 & 1 & 0 & \Delta t_k \\ 0 & 0 & 1 & 0 \\ 0 & 0 & 0 & 1 \end{bmatrix}, \boldsymbol{H}_k = \begin{bmatrix} 1 & 0 & 0 & 0 \\ 0 & 1 & 0 & 0 \end{bmatrix}, \boldsymbol{Q}_k = \begin{bmatrix} 0 & 0 & 0 & 0 \\ 0 & 0 & 0 & 0 \\ 0 & 0 & 2D_{CRW}\Delta t_k & 0 \\ 0 & 0 & 0 & 2D_{CRW}\Delta t_k \end{bmatrix},$$

with D_{CRW} the diffusivity of the swimming speed, which has to be estimated.

The construction of the CTCRW model given below is based on its first publication by Johnson et al. (2008). The full derivations of the equations are provided in this paper. $\boldsymbol{H}_k$ is the same as with the CRW model, the other matrices are defined as follows:

$$\boldsymbol{A}_k = \begin{bmatrix} 1 & 0 & (1-e^{-\beta\Delta t_k})/\beta & 0 \\ 0 & 1 & 0 & (1-e^{-\beta\Delta t_k})/\beta \\ 0 & 0 & e^{-\beta\Delta t_k} & 0 \\ 0 & 0 & 0 & e^{-\beta\Delta t_k} \end{bmatrix}, \boldsymbol{Q}_k = \begin{bmatrix} V_{pos,k} & 0 & C_k & 0 \\ 0 & V_{pos,k} & 0 & C_k \\ C_k & 0 & V_{speed,k} & 0 \\ 0 & C & 0 & V_{speed,k} \end{bmatrix},$$

with V_{pos} and V_{speed} the variance of the position and speed respectively and C the covariance between the position and speed. These are defined as:

$$V_{pos,k} = \frac{\sigma^2}{\beta^2}\left[\Delta t_k - \frac{2}{\beta}(1-e^{-\beta\Delta t_k}) + \frac{1}{2\beta}(1-e^{-2\beta\Delta t_k})\right],$$
$$V_{speed,k} = \frac{\sigma^2}{2\beta}\left[1-e^{-2\beta\Delta t_k}\right],$$
$$C_k = \frac{\sigma^2}{2\beta^2}\left[1-2e^{-\beta\Delta t_k}+e^{-2\beta\Delta t_k}\right].$$

β and σ are unknown model parameters that have to be estimated. β describes how strongly the movement is correlated to previous time steps. Small β values result in a strong correlation, and predictions will be similar to those of the CRW model (see Figure 3.3). σ expresses the overall variability of the velocity. The negative Δt in the exponents causes a reduction of the dependence on the previous observation over time. If there is a long pause between observations, the speed of the previous time step is not relevant any more and the model falls back on standard RW behaviour.

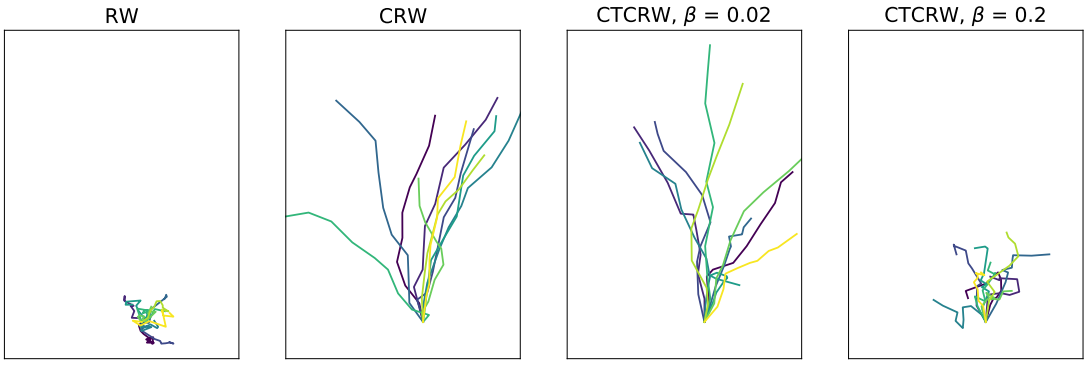

Figure 3.3: Illustration of the differences between the random walk models. Each plot depicts 10 simulated tracks of 10 time steps each. The CRW and CTCRW simulations were all given the same initial speed of 1 m/s in the upwards direction to illustrate their persistence. The diffusivity of the position and speed are the same in all simulations.

3.7 Parameter estimation

As described in Section 3.4, $\boldsymbol{Q}_k$ captures how well the behaviour models predict actual fish movement. Since no true, accurately known fish tracks are available for this study, these behaviour models cannot be validated. Thus, the model parameters (D_{RW}, D_{CRW}, β and σ) have to be estimated. Choosing these parameters arbitrarily is not advisable, as their value can heavily influence filter performance. Large values of $\boldsymbol{Q}_k$ will assign a low confidence to the model predictions, thereby reducing the filter's effect. On the other hand, low values will incorporate too little information of the measurements. Thus, it is crucial that these parameters are representative of real fish

movement. The Bayesian filtering algorithms can use the unfiltered fish tracks to estimate these parameters by maximizing their marginal posterior probability: $p(\boldsymbol{\theta}|\boldsymbol{y}_{1:T})$, with $\boldsymbol{\theta}$ a vector containing all unknown parameters.

Chapter 12 of the book by Sarkka (2013) discusses the three most widely used parameter estimation methods: direct optimization of the posterior distribution, expectation-maximization and Markov chain Monte Carlo methods. The latter two are used when direct optimization is not possible. Due to the simplicity of our filtering problem, the first method is preferable since it is more stable and is easier to compute. The energy function is an example of this method. It calculates the negative logarithm of the posterior distribution to expedite the optimization.

The energy function is calculated recursively for every time step, using the filter parameters of that step. All filtering equations (Eqs. 3.2 and 3.3) are now a function of the unknown parameters $\boldsymbol{\theta}$. The energy function incorporates some of these filter parameters to calculate the overall reliability of the process model:

$$\varphi_k(\boldsymbol{\theta}) = \varphi_{k-1}(\boldsymbol{\theta}) + \frac{1}{2} log \|2\pi \boldsymbol{S}_k(\boldsymbol{\theta})\| + \frac{1}{2} \boldsymbol{v}_k(\boldsymbol{\theta})^T \boldsymbol{S}_k^{-1}(\boldsymbol{\theta}) \boldsymbol{v}_k(\boldsymbol{\theta}).$$

The energy function of the final step ($\varphi_T(\boldsymbol{\theta})$) is then minimized to obtain the best estimate of the parameters $\boldsymbol{\theta}$.

3.8 Additional outlier filters

As mentioned in Section 2.2.5, an additional filter is required to remove the worst outliers. This section explains how the different tested methods were implemented.

The simplest and most used method is simply choosing an HPE threshold. Positions with a HPE higher than this value are removed. We used the relationship between the HPEm and HPE to set the threshold at an HPE where the expected error is 2.5 meters.

The data can also be filtered by removing positions calculated by bad performing clusters (Vergeynst, 2017). This method uses the calculated and known positions of the fixed tags to classify the receiver clusters. First an accuracy goal and confidence level have to be defined (in our case 2.5 meters and 95% respectively). If a receiver cluster positions less than 95% of the stationary transmitters within 2.5 meters of their true position, the cluster is classified as a bad performing one and all positions of this cluster are removed. This classification is only performed for clusters that detected more than 10 positions to limit the effects of small sample sizes.

The speed filter of McConnell et al. (1992) takes a more heuristic approach. The filter averages out the speeds from the two previous and next points. If this average speed ($\overline{s_k}$) exceeds a predefined maximum mean velocity, the current point is removed. This filter is then iteratively applied to all points. By averaging the speed over four time steps, the threshold defines the maximum speed that can be sustained for more than two minutes (with 30 second burst intervals). The maxima reported in literature are burst speeds that are held for only a few seconds. We only use the first point before and after the current one, to filter points based on burst speeds instead of maximum mean velocities. The average speed at time step k then becomes:

$$\overline{s_k} = \sqrt{\frac{1}{2}(s_{k-1,k}^2 + s_{k,k+1}^2)}.$$

$\overline{s_k}$ is then compared to the threshold values from Section 2.2.5.

The two stage filter of Austin et al. (2003) precedes this speed filter by a step that deletes positions where all four speeds to and from the current position are higher than $\overline{s_k}$. Freitas et al. (2008) added a third stage after the previous two: the angle filter. This stage rejects turning angles larger than 165°, as these are considered unrealistic for fish. The turning angle of position k is calculated using the cosine rule:

$$\phi_k = 180° - \left| \arccos\left(\frac{\|\boldsymbol{p}_{k+1} - \boldsymbol{p}_k\|^2 + \|\boldsymbol{p}_{k-1} - \boldsymbol{p}_{k-1}\|^2 - \|\boldsymbol{p}_{k+1} - \boldsymbol{p}_{k+1}\|^2}{2\,\|\boldsymbol{p}_{k+1} - \boldsymbol{p}_k\|\,\|\boldsymbol{p}_k - \boldsymbol{p}_{k-1}\|} \right) \right|,$$

with $\|\boldsymbol{p}_{k+1} - \boldsymbol{p}_k\|$ the euclidean distance between position k and $k+1$.

3.9 YAPS implementation

Section 2.3 explained why the YAPS algorithm shows potential as a new filtering and positioning system. This section first discusses the basics of the algorithm as created by Baktoft et al. (2017). Afterwards it sums up the adaptations we made to this method to better fit our case-specific needs.

3.9.1 Standard YAPS formulation

Like Bayesian filters, YAPS models the probability of a location in two ways. Firstly the process components predict the likelihood of the current state, using the last observation. These process components are:

- The time interval between transmissions:

$$p(\Delta t_{P,k}|\Delta t_{P,k-1}) \sim \mathrm{N}(\Delta t_{P,k-1}, \sigma_{bi}^2), \tag{3.4}$$

with σ_{bi} the standard deviation of the burst interval and $t_{P,k}$ the time-of-ping at time step k. Note that this transmission time is unknown and has to be estimated using the TOAs. This model component assumes the burst interval (Δt_P) is relatively constant and normally distributed.

- The position of the fish is modelled as a Gaussian RW in both dimensions:

$$p(p_{j,k}^*|p_{j,k-1}^*) \sim \mathrm{N}(p_{j,k-1}^*, 2D_{xy}\Delta t_{P,k}), \tag{3.5}$$

with D_{xy} the diffusivity. $p_{j,k}^*$ is the current estimate of the position at time k in dimension j. This RW model will constrain calculated fish positions to biologically plausible ones, like the KF.

- The speed of sound is also modelled as a Gaussian RW process to incorporate variations in temperature, salinity and depth:

$$p(c_{1,k}|c_{1,k-1}) \sim \mathrm{N}(c_{k-1}, 2D_c\Delta t_{P,k}), \tag{3.6}$$

with D_c the diffusivity of the sound speed.

Secondly, the observation components estimate the likelihood of the state estimates based on the measurements. This is done separately for every detecting hydrophone:

- The predicted TOA ($t_{i,k}^*$) at hydrophone i (with known position $\boldsymbol{h}_i$) at time k is given by:

$$t_{i,k}^* = t_{P,k} + \frac{\|\boldsymbol{h}_i - \boldsymbol{p}_k^*\|}{c_k}.$$

- The residual $\epsilon_{i,k}$ between this predicted TOA and the measured TOA can now be calculated as: $\epsilon_{i,k} = t_{i,k} - t_{i,k}^*$.

- The probability distribution of this residual is modelled as a combination of a Gaussian and a Student's t-distribution:

$$p(\epsilon_{i,k}) \sim (1-\theta_{mix})\,\mathrm{N}(0, \sigma_\epsilon^2) + \frac{\theta_{mix}\, t(0,3)}{\theta_{scale}}, \tag{3.7}$$

with $t(0,3)$ a zero-mean t-distribution with three degrees of freedom and σ_ϵ the residual standard deviation. θ_{mix} and θ_{scale} are a mixture and scaling parameter respectively, which have to be estimated. The t-distribution permits a longer

tail towards large residuals. This way, YAPS can deal with multipath errors that typically fall far from the mean.

The distributions given by Eqs.3.4-3.7 can be used to calculate the track by maximizing the likelihood of the simultaneous occurrence of all estimated positions. The values that have to be optimized consist of two groups: unknown random variables ($\boldsymbol{p}$, t_P, and c for every transmission) and unknown parameters ($\sigma_{bi}, D_{RW}, D_c, \sigma_\epsilon, \theta_{mix}$, and θ_{scale}). For a given set values, the probabilities of all components are calculated and their negative logarithms are summed up. This results in one global cost function that is minimized by varying the values of the random variables and unknown parameters. The error sensitivity measure for every position is then the uncertainty of its estimation, given as an output by the minimization algorithm.

The actual model used for positioning is built in Template Model Builder (Kristensen et al., 2016), inputs and outputs are processed in an interface in R (R Core Team, 2014). Baktoft made the current YAPS version available on Github (`https://github.com/baktoft/yaps_sciRep`).

3.9.2 Creating a more robust version

The transparent structure of YAPS allowed us to make some tweaks to the algorithm. YAPS uses one big optimization step with many degrees of freedom. Suboptimal data and conditions where the assumptions are not met can sidetrack the optimization algorithm. In our case, high levels of multipath errors and missing detections in our data, combined with random burst intervals, resulted in runtime errors or unrealistic results. In addition, we have water temperature data available. This extra source of information can be used to stabilize the performance. Therefore we adapted the algorithm in two ways.

Firstly, we removed the speed of sound as a random variable. We calculated the speed of sound for every arrival time using Eq. 3.1. This was fed to the model as a known parameter and Eq. 3.6 was removed to lower the degrees of freedom. This version is referred to as 'YAPS-SS'.

Secondly, we redefined the distribution of the time interval. The actual burst interval is pseudo-random in our case: the time between transmissions is distributed between known limits according to a fixed (but unknown) pattern, generated by VEMCO upon initialization of the transmitter. Thus, the assumption made by Eq. 3.4 is not valid. To make YAPS more robust in dealing with this suboptimal situation, we redefined this equation as:

$$p(\Delta t_{P,k} | \Delta t_{P,k-1}) \sim \mathrm{N}(\mu_{bi}, \sigma_{bi}^2),$$

with μ_{bi} the global average of the burst interval, which is the mean of the known limits. If for example the burst interval is distributed between 17 and 33 seconds, the largest possible difference between $\Delta t_{P,k-1}$ and $\Delta t_{P,k}$ is 16 s. For our reformulation, the difference between $\Delta t_{P,k}$ and μ_{bi} is limited to 8 s. This smaller deviation from the mean creates shorter tails in the distribution and makes the normality assumption more plausible. Therefore, the algorithm will be sidetracked less. Although this method is more robust, it still assumes a normal distribution of the burst interval, while this is not true in our case. This deviation from reality has to be kept in mind during the performance evaluation. The combination of both adaptations is called YAPS-BI from now on.

3.10 Performance evaluation measures

A quantitative evaluation requires the definition of objective performance measures. The VEMCO positioning system is designed to calculate positions close to the hydrophone array. Positions far from this array will be more erroneous, resulting in a strong influence on the total positioning error. This way, poor performance inside the array could be compensated by good performance further away. Since we are mainly interested in the behaviour near the sluice complex, we defined four extra performance measures that focus more on the area of interest.

The local error is defined as the average distance between known and calculated position, but only for positions close to the array. This proximity is defined as any location within 150 meters of the central receiver (S8, see Figure 3.1).

The track length simply calculates the total length of the calculated track in meters. Comparison to the known actual track length gives some insight into the performance. Noisy tracks are typically longer because calculated positions jump around the true ones. A reduction in track length is an indication of noise reduction. However, a shorter track can also be caused by over-filtering, which leaves out important characteristics of the path.

Additionally, we report the third quartile of the positioning error distribution, and the correctly positioned percentage. The former describes the effect of the algorithms on the worst outliers, while the latter focusses on the fine scale precision. A correct position is defined as one that falls within 2.5 meters of the true value.

Finally, we calculated the range and bearing error, defined by Ren et al. (2012). These weigh the deviations from the true track by the distance to the receiving hydrophones. Both measures require the definition of an origin with a known location. We used

receiver S8 as this reference point. The range error is then the absolute difference of the distances from the known position to the origin, and from the calculated position to the origin. The bearing error is the angle formed by the lines that connect the calculated and known position to the origin. This angle can again be calculated using the law of cosines.

CHAPTER 4

RESULTS AND DISCUSSION

This chapter first evaluates the algorithms via the real data of the test tracks. The selection of the most promising methods is primarily based on test track ’255’. Results of the other two test tracks are included in Appendix A. They will mainly be used to validate the conclusions drawn from track ’255’.

Although these tracks reflect the potential of the different methods for our case-specific conditions, they don not give a quantitative or definitive answer for several reasons. Firstly, the test tracks do not resemble actual fish movement: they mainly consist of straight lines and unrealistically high speeds. Additionally, they spend a disproportional amount of time outside the array, which biasses results towards these regions. Thirdly, the tracks contain relatively little positions and were all generated in two days time. Thus, they do not describe all influencing factors correctly. Finally, results from the three test tracks often contradict each other, which illustrates the risk of basing results on a few tracks alone. Therefore, the definitive conclusions are drawn from the simulation study, which provides a more controlled environment and larger sample size.

Sections 4.1 and 4.2 select the optimal configuration for the traditional (KF) and new approach (YAPS) respectively. Section 4.3 then compares the best configurations of both approaches. Afterwards, the simulation study in Section 4.4 quantitatively and definitely confirms the optimal technique under varying environmental conditions. Finally, Section 4.5 shows the effect of the best methods on actual fish positioning data.

4.1 The traditional approach: The Kalman Filter

4.1.1 Hyperbolic positioning

Before positioning, the TOA data has to be preprocessed as outlined in Section 3.2. For test track ’255’, this clean-up removed 47 of the 255 detections (18.43%). Before this step, a lot of detections arrived right after the previous transmission (see Figure

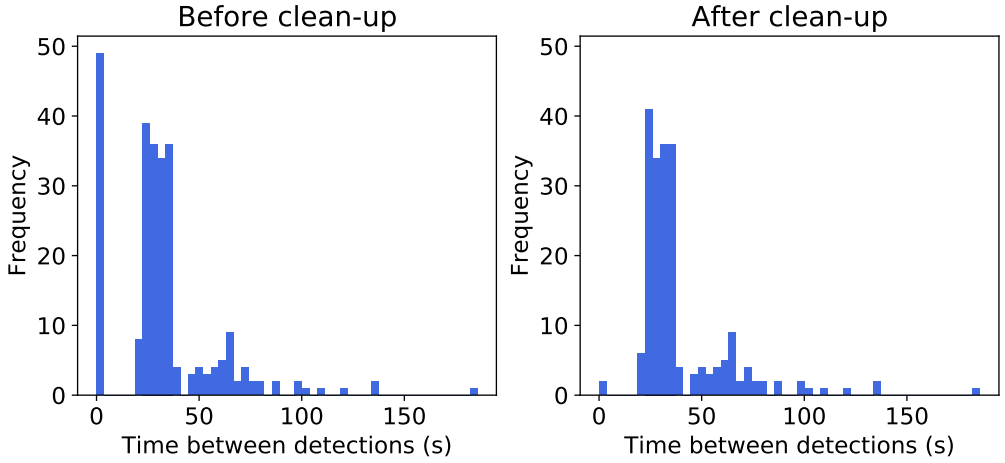

Figure 4.1: Two histograms that show the effect of the clean-up step on the TOA matrix for test track '255'. The transmitter (VEMCO model V13-P) has a burst interval that varies between 20.6 and 36.6 seconds.

4.1), being either reflected signals that are detected again or errors caused by a unsynchronized receiver clocks. These erroneous detections are effectively removed by the clean-up algorithm. The TOA matrix was subsequently fed to the LS-positioning system, both with a local and genetic optimizing algorithm.

Using a genetic algorithm significantly lowers the positioning error compared to a local optimization, but VPS remains superior. The standard LS positioning system resulted in an average error of 20.90 meters, while the genetic algorithm generated an error of 13.94 meters. However, VPS still outperforms both systems, with an average deviation of 5.80 meters. Total track lengths and a qualitative analysis (Figure 4.2) confirm that the LS positioned track is still heavily distorted. With respective track lengths of 3090, 2710 and 2194 meters, the local optimization, genetic algorithm and VPS tracks are all significantly longer than the true length of 1784 meters. The amount of calculated positions is comparable for all techniques, with 146 for VPS and 145 for both LS systems. This means that 30% of the transmissions were unusable for all TDOA systems. This was as expected, since TDOA positioning systems require at least three hydrophones to calculate a two-dimensional position. Additionally, eighth positions were removed with both LS systems because they fell outside of the predefined bounds ([-10,300] horizontally, [-50,200] vertically).

The results reveal VPS is not a transparent positioning system. Although both algorithms use the same TDOA principle, the VPS track looks less noisy and shows some distinctly different features. This indicates the system uses a fundamentally different approach to ours. Additionally, the raw TOA data contains 153 transmissions that were detected by more than three hydrophones, while VPS recorded only 146 posi-

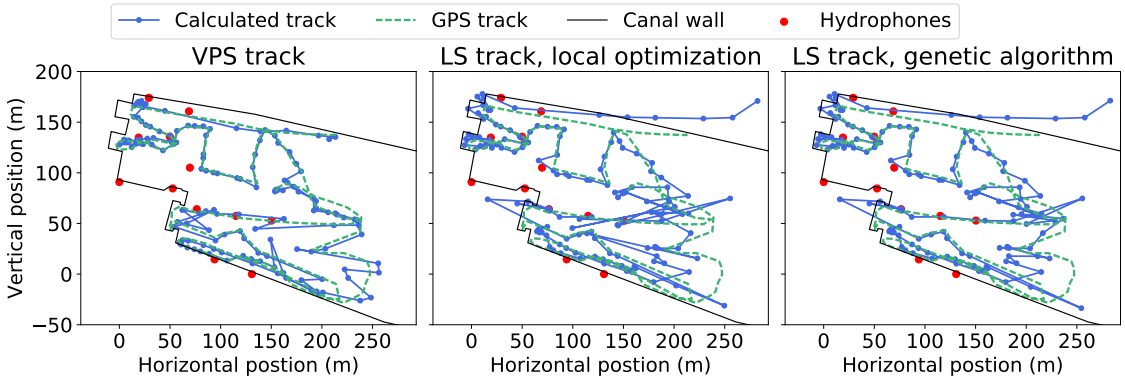

Figure 4.2: Calculated and true tracks for the three considered positioning systems.

tions. This shows the VPS removed seven positionable transmissions. Such a filtering step is not described in VEMCO's documentation (Smith, 2013).

VPS will be used to position all test and fish tracks. A further optimization of the LS positioning is beyond the scope of this thesis, as we focus on clean-up techniques. The LS positioning will only be used to position the simulated data, since no VPS tracks are available. However, the results highlight the need for a clean-up step, even when using VPS data. An average error of 5.8 meters and a track length increase of 410 meters are still large for a close confined space, like a canal, and hampers fine-scale movement analysis.

4.1.2 Error sensitivity measures

The KF requires an indication of the reliability of each calculated position to construct the covariance matrix of the measurement model ($\boldsymbol{R}_k$). For this purpose, the performance of the error measures, outlined in Section 3.3, is first evaluated through the coefficient of determination of the linear regression between the true and calculated error. Figure 4.3 shows these regressions for the four tested error measures. However, the sample size for the test tracks is small and all R squared values are low, so this figure should not be over-analysed. Therefore, we tested the performance of the best two measures in the Kalman filter/ smoother.

The timing error shows a poor correlation to the true error. The low correlation suggests variations in environmental conditions have a minor impact on the system's performance. Since the test track was generated in two hours, the water temperature changed only by 0.1 °C. Such a small temperature change will not affect the positioning error substantially. Thus, the timing error is not relevant in a close-confined space where fish will not reside for long.

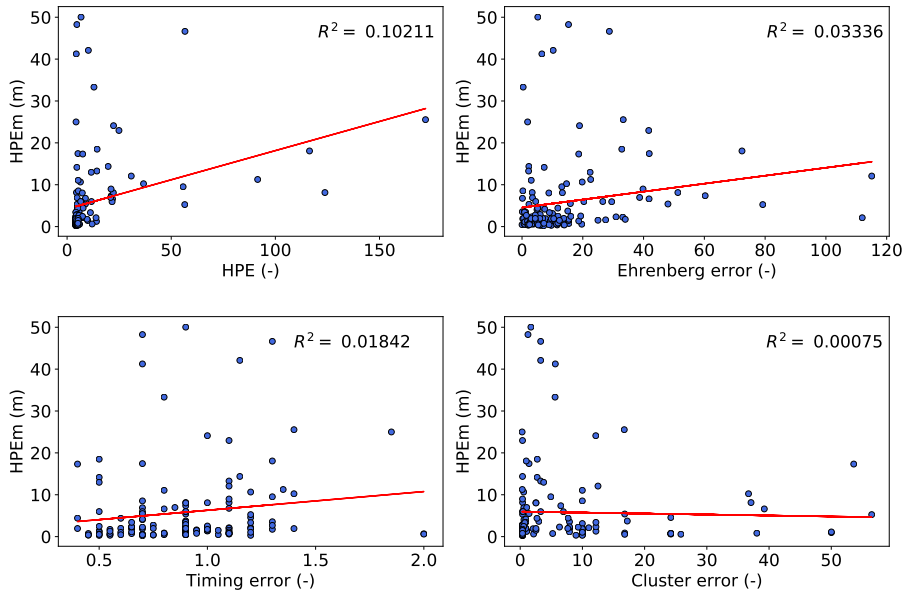

Figure 4.3: Regression analysis of all tested error measures. These are the HPE, supplied by VEMCO, the error measure defined by Ehrenberg and Steig (2002), and the timing and cluster error as defined in Section 3.3. The red line shows the calculated regression between the calculated and true error (HPEm).

The cluster error does not capture the error-inducing processes properly. The coefficient of determination is nearly zero, and the correlation between true and calculated error is negative. This is possibly the result of the cluster error's simplified approach, as it does not account for the relative position of transmitters and receivers. For example, some clusters may perform poorly when the transmission comes from one side, but well from another. Because of its low performance, the cluster error will not be used further.

The HPE and Ehrenberg error are the best options, but the correlation with the true error is still poor. Of these two, the HPE shows the highest coefficient of determination ($R^2 = 0.10$). By incorporating hydrophone geometry, temporal variations, and the uncertainty of the calculated sound speed, it describes the true error better than the other measures. The Ehrenberg error still captures some of the error-inducing processes, despite its simplifications. By only using the hydrophone geometry and distance between transmission and detection, it can explain one third of the variance captured by th HPE ($R^2 = 0.03$). Additionally, the Ehrenberg error is more transparent and applicable to all systems, which may compensate for its lower correlation with the true error.

For the other two test tracks, the HPE also shows the least poor correlation to the true error (Figures A.1 and A.5 in Appendix A). In general all R-squared values are low for these tracks as well. For track '53429', the Ehrenberg error performs poorly, while the cluster error works significantly better, and almost equals the HPE. For test track

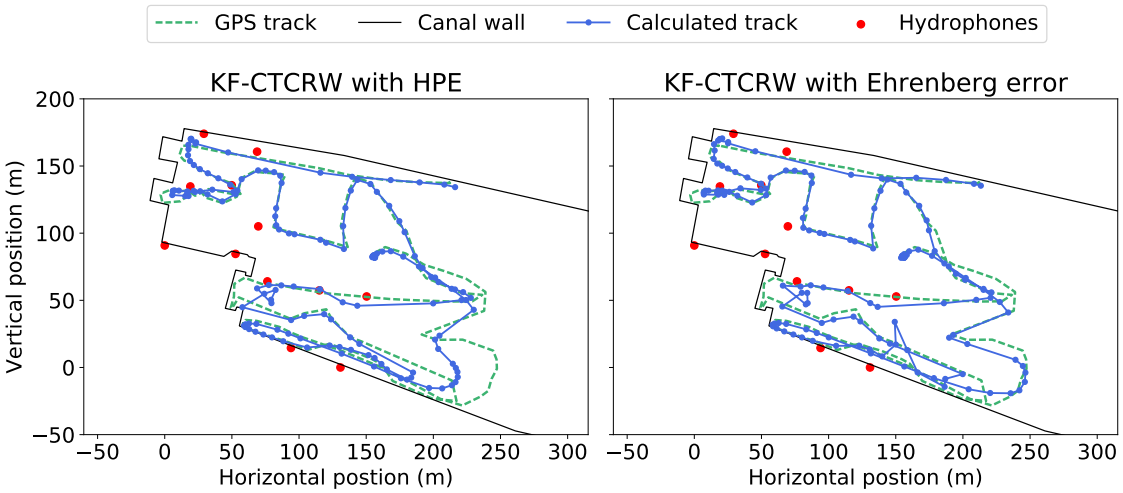

Figure 4.4: Comparison of the KF results using HPE or the Ehrenberg error as an error sensitivity measure. Tracks were generated with the CTCRW as the behaviour model and unfiltered VPS data as an input.

'16200', the Ehrenberg error approaches the performance of HPE. Here, the cluster error shows a poor correlation to the true error, with again a negative correlation.

Next, we tested the performance of the HPE and Ehrenberg error as the measurement noise parameter in the KF. Differences between the methods are small (Table B.1 in Appendix B.1). The HPE outperforms the Ehrenberg error for the KF, but after the smoothing step, results of both methods are similar. The HPE works best close to the hydrophone array: it always achieves the lowest local error. The Ehrenberg error performs slightly better for the total error measures after smoothing. For the other two test tracks, performance of the two measures is also similar, but the Ehrenberg error performs worse in virtually all cases, both locally and globally, and both with the KF and RTSS (Tables A.2 and A.7 Appendix A).

The Ehrenberg error fails to capture some clearly erroneous positions (e.g. the peak at coordinate (150,0) in Figure 4.4), which the HPE does manage to reduce. This illustrates the HPE incorporates some additional uncertainty factors during the VPS-positioning, which the other error measures cannot access because of the black box approach.

Based on these results, we select HPE as the optimal error measure. The HPE shows the highest correlation with the true error and outperforms the Ehrenberg error in most cases, especially close to the receiver array. Its lower performance far from the array is of secondary concern as we are mainly interested in fish behaviour near the navigation lock complex. The black-box approach is not a downside in this case, as the cleaning approach already lost its transparency by using VPS. Because the HPE is calculated during VPS-positioning, it incorporates the same undescribed processes

Table 4.1: Performance of the different filter combinations for test track '255', using HPE as an error sensitivity measure. For every performance indicator, the best behaviour model is underlined, both for the KF and RTSS.

	Total			**Local**				
	Error (m)	Correct (%)	Q3 (m)	Error (m)	Correct (%)	Range (°)	Bearing (m)	Length (m)
VPS	5.80	59.59	5.98	4.54	56.85	4.30	2.31	2194
RW-KF	8.89	38.36	8.78	5.35	38.36	5.83	3.56	1666
RW-RTSS	7.85	47.26	8.55	4.48	47.26	6.10	2.69	1481
CRW-KF	5.83	53.42	6.32	4.60	52.05	3.91	2.59	1929
CRW-RTSS	6.29	45.89	6.32	4.47	45.21	4.40	2.69	1573
CTCRW-KF	6.36	49.32	6.60	4.66	48.63	4.03	2.83	1828
CTCRW-RTSS	6.37	47.26	6.81	4.44	45.89	4.54	2.65	1541

and predicts the true error more accurately. However, its correlation with the true error is still weak. Because many processes influence the true error and these show complex interactions (Binder et al., 2016), defining a perfect error measure is currently infeasible. All error measures merely give an idea of how sensitive a position is to errors, and other filtering steps are needed to remove noise and errors.

We will still use the Ehrenberg error with LS positioned data in the simulation study, as HPE values cannot be calculated there. Ehrenberg error still showed great potential, often approaching the performance of HPE. Since it can be determined for all raw data, it can contribute to one, generalized, clean-up method for all positioning systems. Additionally, it creates a completely transparent alternative when combined with LS positioning.

4.1.3 Selection of the optimal behaviour model

This part evaluates the three random walk models described in Section 3.6. All models were tested for the unfiltered VPS data and the cleaned track from the next section. It is important to keep in mind that the properties of test tracks may be different from actual fish behaviour. Therefore, we will not focus on small differences in performance, but rather look for a model that is robust in all situations. This way, we are most confident the model is capable of mimicking actual fish behaviour. In this section, we focus on the behaviour models, the performance of the KF and RTSS is evaluated in Section 4.1.5.

The CRW and CTCRW models show a similar performance for most tests, while the RW model fails to describe the true track (Table 4.1). The RW model has the lowest performance for all considered indicators, both for the filtered and smoothed track (Table 4.1). The track length and visualisation in Figure 4.5 reveal that this smooths

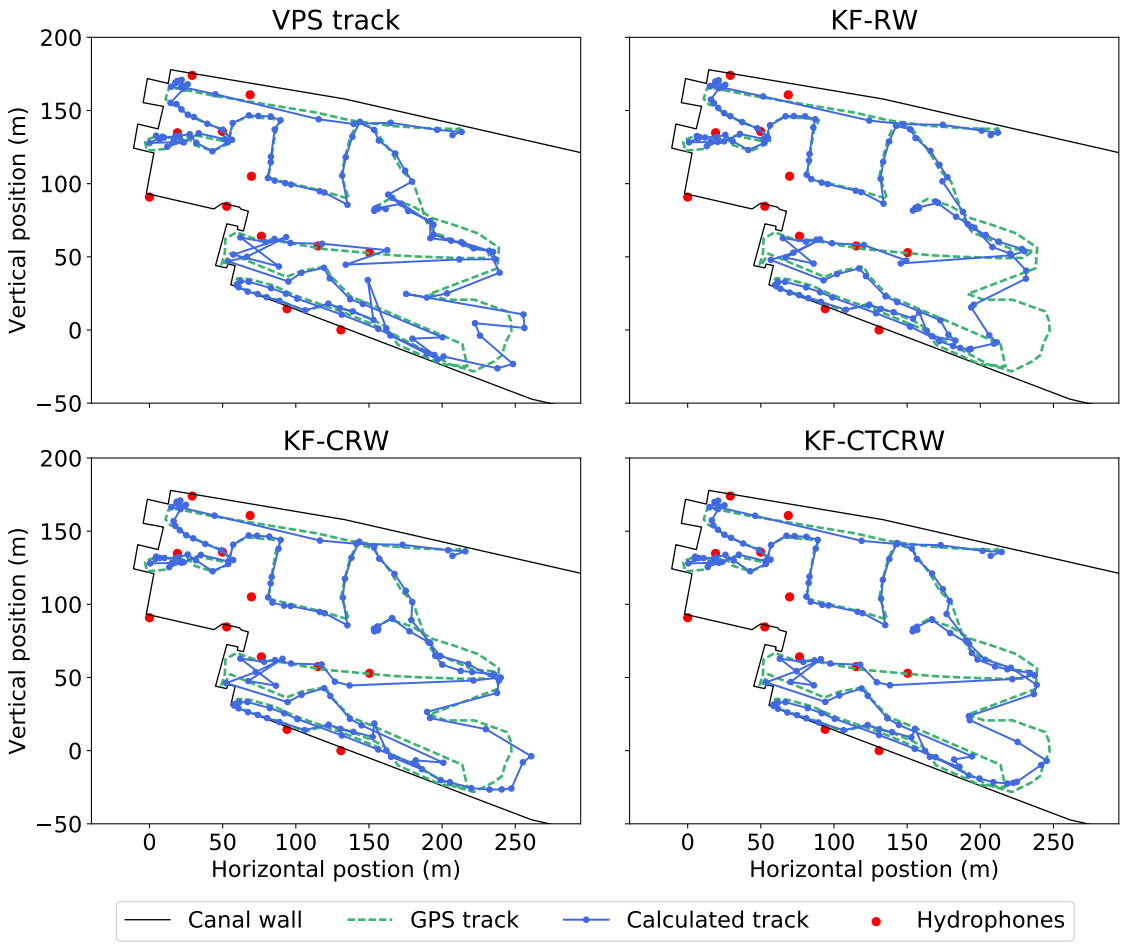

Figure 4.5: The raw VPS track and results of the KF for all three behaviour models. The KF used the HPE as the measurement error and unfiltered VPS data as an input.

out track features too strongly far from the array, causing the large error. For the KF track, the CRW model gives the lowest total error, but the local error is nearly equal for the CTCRW and CRW. The range and bearing errors affirm the CRW model produces the best overall tracks, although differences are small. A qualitative analysis of Figure 4.5 shows this difference is mainly caused by the turn at the bottom right of the track, which the CRW describes more accurately. Inside the array, the CRW and CTCRW models produce nearly identical tracks, resulting in a similar local error. For the smoothed track, all indicators are nearly identical for both models. The CRW track is now smoothed out further from the array, thereby losing its advantage over the CTCRW (Figure B.1 in Appendix B.1). Finally, the CTCRW model is marginally better at removing the worst outliers (see Figure 4.6).

These conclusions hold when the KF is preceded by an outlier filter (see Tables and Figures in Appendix B.2.2). The other two test tracks also affirm the results, but the CTCRW model generally outperforms the CRW for these tracks (see Tables A.1 and A.6 in Appendix A).

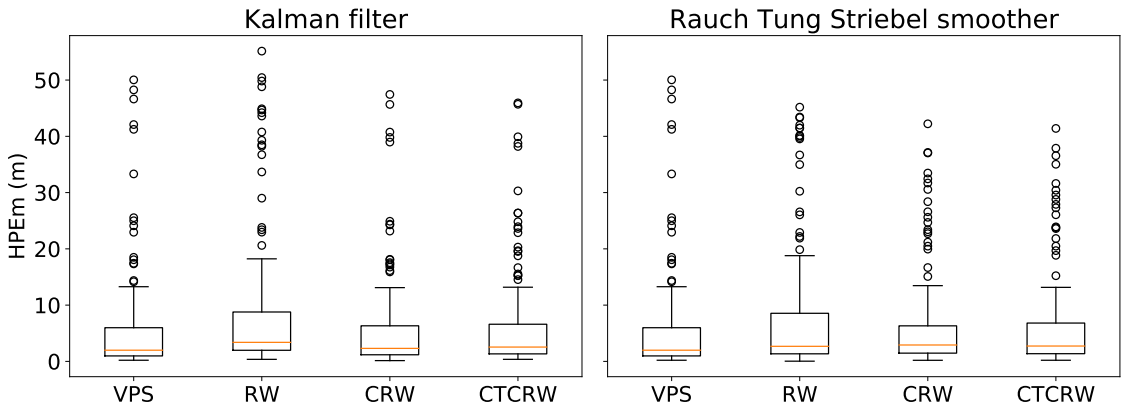

Figure 4.6: Boxplot of the error distribution after applying the KF (left) and RTSS (right) to the raw VPS data of test track ’255’, with HPE as the measurement error.

Although differences are small, the CTCRW shows the most robust performance and will be used as the optimal model in the traditional approach. Even though the CRW model gives a low overall error, it works best far from the receiver array, while we are mainly interested in fish behaviour near the locks. In this region, the CTCRW usually performs best. In addition, the CTCRW has a consistently good performance over all tracks, while the outcome for track ’16200’ shows the CRW performs poorly in certain conditions. Theoretically, this is a logical conclusion: as the CTCRW captures both CRW and RW behaviour, it can describe a wider variety of tracks. The CTCRW’s flexibility, in combination with its overall good performance, makes it the most relevant movement model.

4.1.4 Outlier filtering

The performance of Bayesian filters and smoothers is suboptimal for tracks containing a high level of multipath errors. The track accuracy deteriorates after Kalman filtering/smoothing, because the algorithms get sidetracked by erroneous positions (see Table 4.1). Therefore, the KF will be preceded by an additional outlier filter. The tested filters and their performance are summarized in Table 4.2. Again, we define a correct position as one that falls within a radius of 2.5 meters of the true position. By this definition, a false positive is an estimated position that is not removed by the outlier filter, while it is further than 2.5 meters from the true position. The results in this table are analysed below.

The HPE filter is a suboptimal outlier filter, although the performance measures in Table 4.2 suggest that it is the best outlier filter. It strongly reduces the positioning error and removes the most false positives, with an acceptable amount of correct positions removed. However, the HPE method lowers the overall error by simply

Table 4.2: Overview of the tested outlier filters and their performance. The number '2' and '4' behind the names of the speed filters denote the number of points used by the filter.

	Excluded (%)	False neg. (%).	False pos. (%)	Avg. error (m)	95th perc. (m)
Unfiltered	0	0	40.41	5.80	24.77
HPE	20.55	3.42	23.29	3.95	14.95
Cluster	19.86	13.01	33.56	5.96	23.36
Speed 2	2.05	0	38.36	5.64	23.99
Speed 4	2.05	0	38.36	5.64	23.99
Two-stage 2	3.42	0	36.99	5.36	22.95
Two-stage 4	2.05	0	38.36	5.64	23.99
Three-stage 2	9.59	2.74	33.56	4.90	18.26
Three-stage 4	8.90	2.74	34.25	4.90	18.24

removing all points far from the array (see Figure 4.7). Quantitatively, this causes a drop in error, as these positions are hardest to determine and thus furthest from the real position. Meanwhile, virtually nothing changes near the hydrophone array and most erroneous positions in this area remain. For the other test tracks, the threshold shows a much lower performance: about half of the removed positions were correct. By removing one-fifth of the data on average, a lot of valuable information is lost. Especially since erroneous detections could be corrected by the KF. In conclusion, the HPE threshold is too indiscriminate as an outlier filter.

For all types of speed filter, using two neighbouring points is better than four. The inclusion of two extra points mainly lowers the amount of bad positions removed, but does not improve the retention of correct positions (see Table 4.2). Thus the two-point version is considered an improvement and only this version will be discussed further.

Of all speed filters, the three-stage filter has the best overall performance. The simplest speed filter defined by McConnell et al. (1992) works well, as it removes incorrect positions without creating false negatives. The two-stage filter of Austin et al. (2003) only improves this by removing additional bad positions without touching the good ones. With the additional angle filter, three stage filter of Freitas et al. (2008) removes a lot more false positives and the error is lowered significantly, but the amount of false negatives increases as well. Quantitative analysis of the track (Figure 4.7) indicates that the removal of these correct positions has no effect on the shape or properties of the track, while the additional filter does remove some clearly visible errors. Therefore, we argue that the three stage filter is the best compromise between outlier removal and information retention.

Excluding bad receiver clusters shows potential, but is not as robust as the other methods. For test track '255', this method heavily trims the data: it removes one fifth of the positions. The majority of these removed points were correct (see Table 4.2).

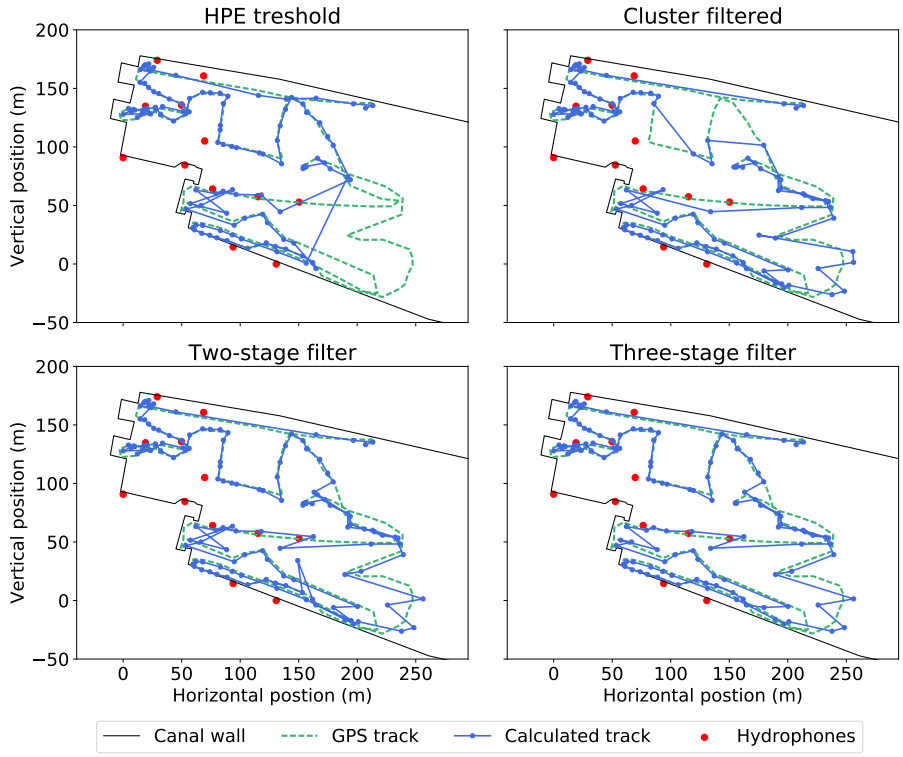

Figure 4.7: Visualization of the tracks obtained by applying the outlier filters to unfiltered VPS data

These false negatives significantly change the properties of the track (see Figure 4.7). On the other hand, this method intercepts some erroneous detections at the bottom of the track, which the two stage filter cannot remove. Additionally, its performance varies widely between tracks. For test track '53429', it is the best performing method, removing most outliers.

For the other two test tracks, the quantitative data suggest that all outlier filters performed poorly. In all cases, more than half of the removed positions were false negatives. This impedes a proper quantitative comparison of the different methods, as most perform worse than the unfiltered data. Nonetheless, qualitative analysis of Figures A.2 and A.6 confirms the conclusions outlined above.

In conclusion, the three-stage filter is the optimal outlier filter for the test tracks, although its performance for fish tracks may differ. It consistently removes the worst outliers without altering the track's properties. Furthermore, it works well both inside and outside the receiver array. This filter will be used in the optimal traditional method together with the KF and RTSS. However, all tests so far removed the 5% highest speeds, as maximum swimming speeds are not relevant for the boat tracks. For fish tracks, removing the highest speeds can bias the tracks as it removes biologically relevant processes (Patterson et al., 2008; Meckley et al., 2014). Therefore, we

Table 4.3: Performance of the subsequent filtering steps for test track '255'. Outliers, were filtered with the three-stage filter, and HPE was used as measurement error.

	Total			**Local**				
	Error (m)	Correct (%)	Q3 (m)	Error (m)	Correct (%)	Range (°)	Bearing (m)	Length (m)
VPS	5.80	59.59	5.98	4.54	56.85	4.30	2.31	2194
Outl. filter	4.90	62.88	5.35	3.98	59.85	3.65	1.94	1958
CTCRW-KF	5.68	52.27	5.03	4.23	52.27	3.76	2.45	1733
CTCRW-RTSS	5.74	50.00	5.55	4.16	48.48	4.20	2.34	1502

will solely use it with the maximum reported swimming speeds, which can alter its performance.

We will also test the receiver cluster method as an outlier filter on the fish tracks. This method showed some potential but was inconsistent. However, fish tracks have different properties, it may perform better there and could be an alternative to the three-stage filter. Its simplicity would make it a useful tool to efficiently clean up the large datasets.

4.1.5 Evaluation of the optimal filter combination

As reasoned in Section 4.1.1, the optimal traditional approach uses VPS for positioning. The VPS track is first filtered with the three-stage filter, after which the KF and RTSS are applied, with HPE as the error measure and the CTCRW as the process model. Figure 4.8 and the top and bottom two rows of Table 4.3 provide a qualitative and quantitative overview of this method. This section analyses the impact and necessity of the different filtering steps.

The KF is an essential clean-up step for this study. As mentioned above, our main interest is the accuracy within the hydrophone array, near the locks. Therefore, we focus on the local error measures, range and bearing error, and qualitative figures. If a minimal total error is desired, the three-stage filter on its own would suffice. However, this filter neglects some erratic and unnatural jumps in the track (see Figure 4.8). The KF is able to reduce the impact of these sudden deviations. Purely qualitatively, the KF track looks less erratic or noisy. The track length confirms the KF track is closer to the true shape of the track: it is 51 meters shorter than the true length, while the outlier filtered track is still 194 meters too long. Even though the average error increases, the third quartile error is lowered. The boxplots in Figure 4.9 confirm that the KF further reduces the impact of the worst outliers. Thus, the KF moves some correct points further away from their optimal position to smooth out the worst outliers. We

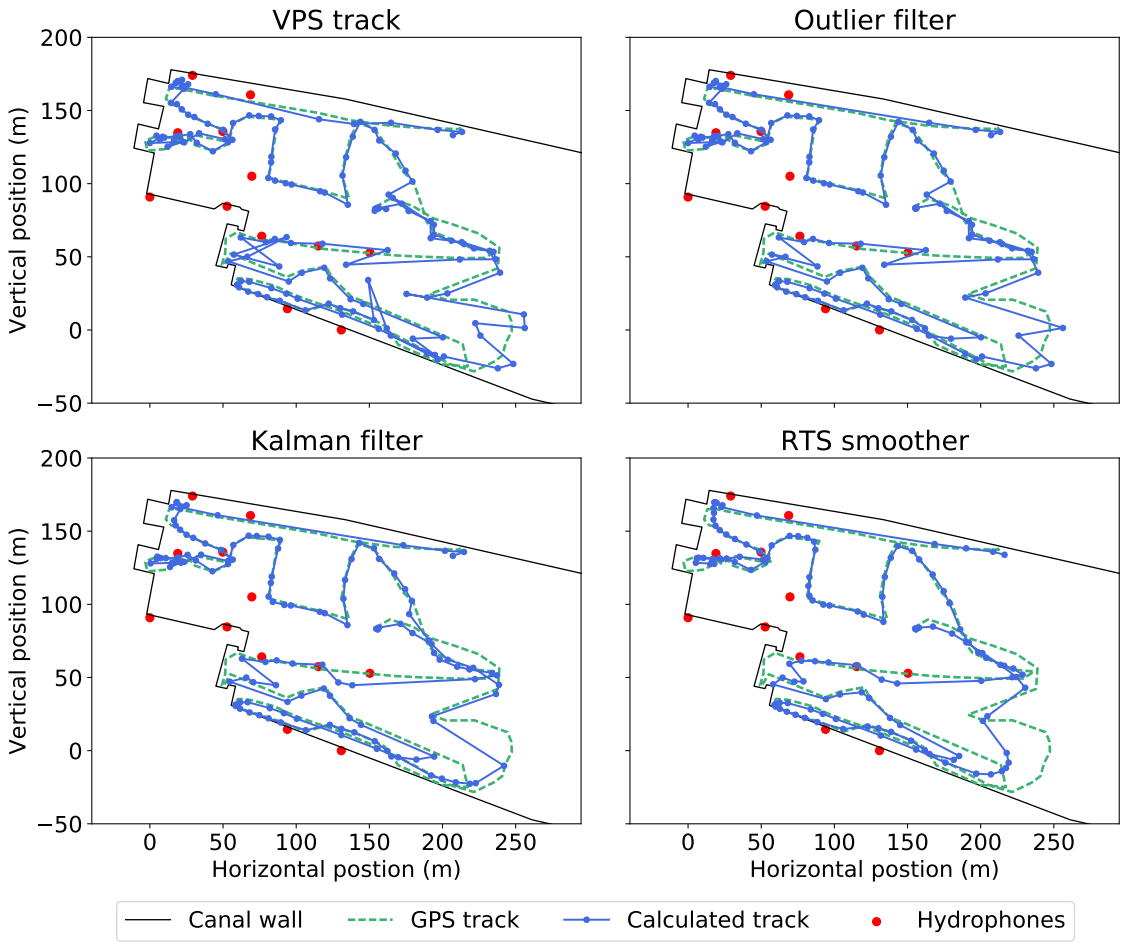

Figure 4.8: Visualization of the tracks obtained after every filtering step of the optimal traditional configuration.

consider this an acceptable compromise, since the presence of outliers will influence the described behaviour more than minor error increases of correct positions.

The RTSS can further reduce the worst outliers, but with a greater cost for the correct positions. It decreases the size of the largest errors (see Figure 4.9), but the third quartile increases as good positions are pushed further from their true value to smooth the track. While the total error increases, the local error decreases. The track is now cutting off sharp corners (see Figure 4.8), which makes its length 282 meters shorter than the true length. On the other hand, the effects of errors are qualitatively almost completely removed. If noise and error levels are extremely high, the RTSS causes an overall improvement for all performance measures (see Appendix B.3 for the result on the LS positioned track). However, since our data are not that heavily distorted, the smoothing is considered too extensive.

For the other two test tracks, all performance indicators are improved by the outlier filter and worsened by the KF and RTSS. Visual inspection, however, shows that the KF removes some additional erratic behaviour, while most deviations from the true track

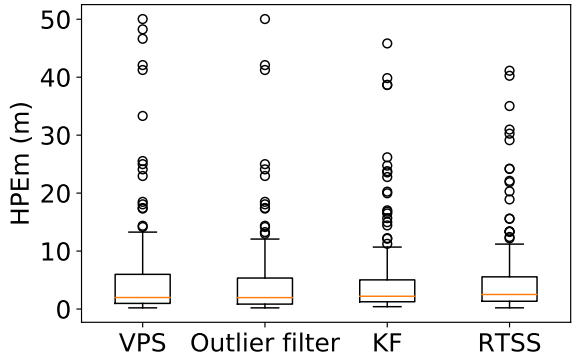

Figure 4.9: Boxplots of the error distributions after every filtering step of the optimal traditional configuration.

occur far from the array (see Figures A.3 and A.7). Therefore the KF is considered a valuable addition here too. The RTSS again mainly smooths out the track too much, without significantly reducing outliers. Thus the RTSS is again not a valuable addition to data with these noise characteristics.

In addition to removing outliers, the KF and RTSS increase the relevance of the error measure. As mentioned before, the current error measures do not express all error inducing processes, resulting in poor correlations with the true error. By incorporating the plausibility of a point given the previous and next position, the KF and RTSS improve the relevance of the error measure. This additional information triples and quadruples the R^2-value for the KF and RTSS respectively (see Figure 4.10). The correlation increase can be explained in two ways. Firstly, the filter will move wrong positions if the process model suggests that they are unlikely, even when the HPE is low (i.e. pull points down on the scatter plot). Secondly, the large difference between the measured and predicted position increases the overall uncertainty of the position (i.e. push points to the right). The overall improvement of the correlation is possible even though the outlier filter first halves the coefficient of determination.

In the context of this case study, the combination of the outlier filter and KF will provide the most consistent results. The outlier filter on its own can properly lower the average error, but too many artefacts remain, especially near the hydrophone array. The KF can further reduce the impact of large errors at a relatively low cost for correct positions. Additionally, the resulting error measure is more relevant and can improve the reliability of the data in subsequent studies. For VPS data, the RTSS is too strong in its smoothing. The reduced impact of outliers and increased error relevance do not outweigh the decreased average performance. However, it remains a valuable step in more noisy conditions. Therefore, we will use it on the LS positioned tracks in the simulation studies as these are heavily distorted.

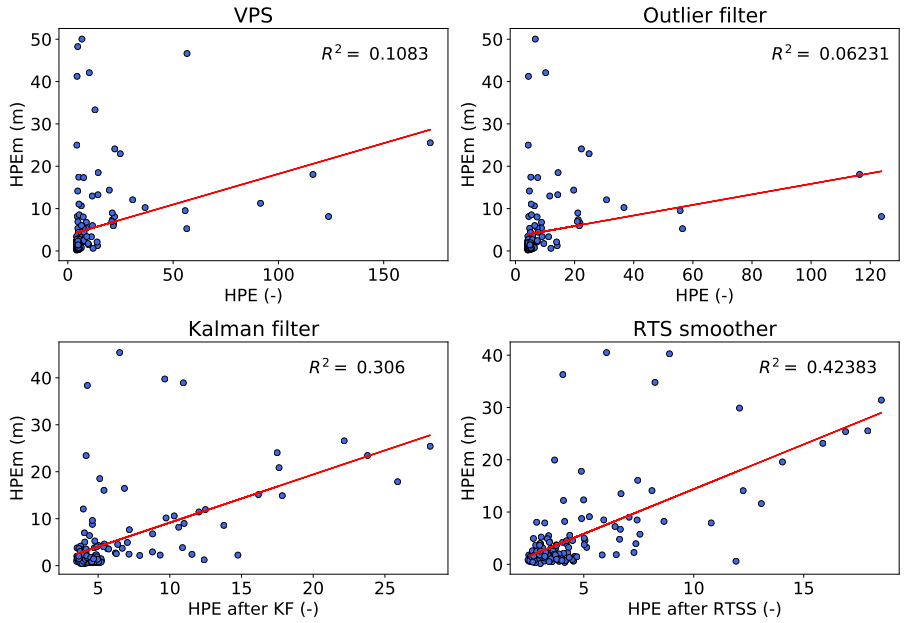

Figure 4.10: Results of the regression analysis between the true and calculated error after each filtering step of the optimal configuration of the traditional approach.

4.2 YAPS

In this section, we compare the original YAPS version of Baktoft et al. (2017) to our two adapted versions. Quantitative results are provided in Table 4.4, the calculated tracks are visualized in Figure 4.11.

Table 4.4: Performance measures for all implemented YAPS versions.

	Total Error	Corr. %	Q3	Local Error	Corr. %	Range	Bearing	Length
YAPS	6.73	45.0	7.22	4.69	44.0	4.91	2.68	1746
YAPS-SS	9.77	27.5	7.98	4.64	27.5	8.13	2.89	1538
YAPS-BI	6.84	48.5	7.82	4.75	47.5	4.98	2.88	1725

YAPS-BI almost matches the accuracy of the standard YAPS algorithm, while YAPS-SS is inferior to both. The original YAPS scores better for almost all performance measures, but differences with YAPS-BI are small. Visualization of the tracks in Figure 4.11 confirms YAPS and YAPS-BI produce virtually the same result. YAPS-SS scores worse for all performance indicators and the plotted tracks show that it deviates most from the true track. Imperfect sound speed data is the most likely cause for this poor performance. Since these data are directly used with YAPS-SS, small deviations can sidetrack the algorithm. YAPS-BI also uses the same calculated sound speeds, but can compensate this shortcoming with an improved burst interval definition.

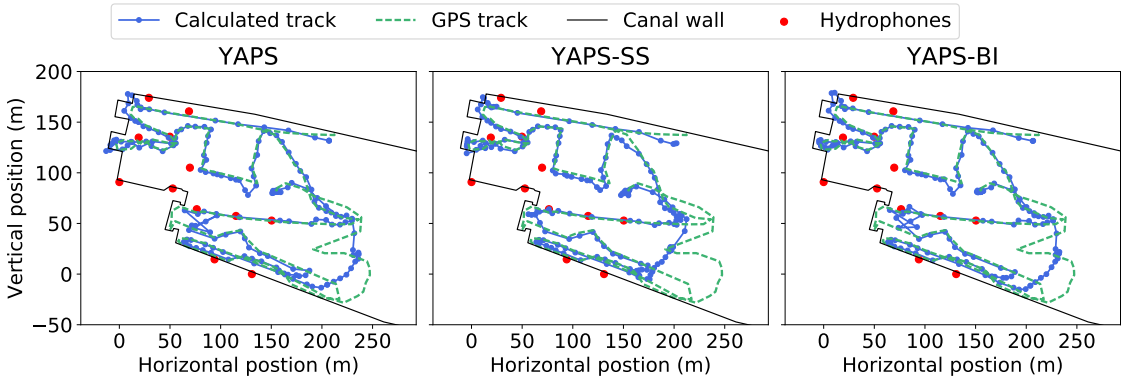

Figure 4.11: Visualization of the tracks obtained from the three tested YAPS versions.

For test track ’53429’, the standard YAPS version fails to predict the track properly (Table A.4). Even inside the hydrophone array, YAPS results are far off (see Figure A.4). Here, YAPS-BI is superior, with an average error reduction of five to six meters. YAPS-SS also works better for this track, but not as well as YAPS-BI. None of the versions can properly predict the track outside the array.

Despite its similar quantitative performance, YAPS-BI significantly improves the YAPS algorithm. The main goal of our adaptations was to improve the robustness of the algorithm to the harsh conditions of our case study. The poor performance of YAPS for track ’53429’ shows the standard version is not consistent in all circumstances. Additionally, these results only show the optimal outcomes, obtained after several runs. In previous attempts, the standard YAPS failed to optimize all parameters and crashed, or got lost in a local optimum, generating erratic tracks (example given in Figure B.5). Additionally, the decreased complexity of the optimization with our adaptations led to a strong improvement in running time. The standard YAPS algorithm took 41 seconds to calculate the track, while YAPS-SS and YAPS-BI needed only 25 and 21 seconds respectively (averages of 10 runs for test track ’255’). Due to its higher robustness, comparable performance and lower running time, YAPS-BI is considered the best version and will be used for the simulation study and fish tracking.

4.3 Selection of the optimal clean-up method

This section first compares the performance of the best traditional approach from Section 4.1.5 to YAPS-BI. Afterwards, we test the performance of a combined approach, where the KF and RTSS are applied to the YAPS results.

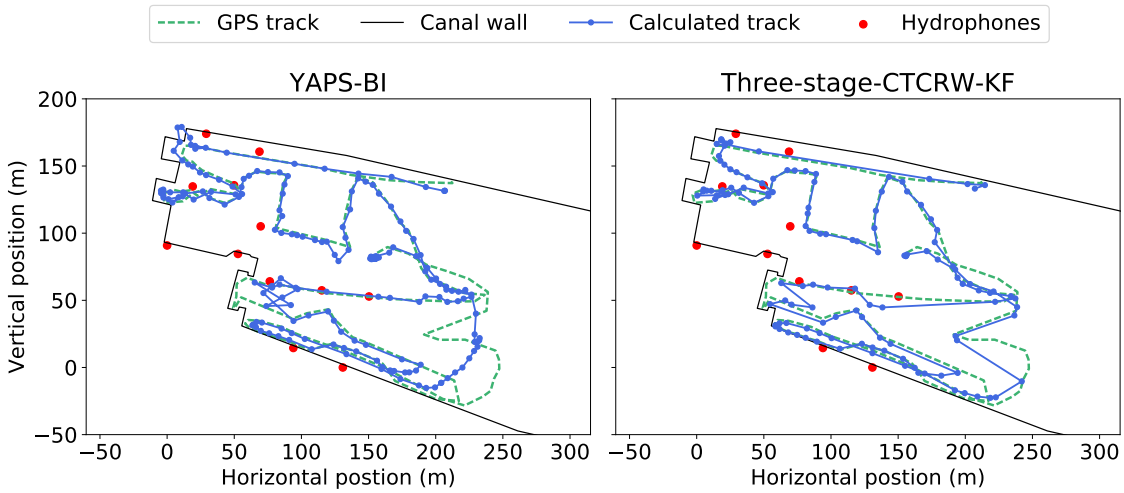

Figure 4.12: Comparison of the final results of the new (YAPS-BI) and the traditional approach (VPS, the three-stage filter and the KF with the CTCRW as the process model and the HPE as the measurement error).

4.3.1 A comparison: old versus new

The best obtained tracks from the traditional (KF) and new (YAPS) approach are visualized in Figure 4.12. For quantitative data, we refer to Tables 4.3 and 4.4. Before interpreting the results, it is important to keep in mind that YAPS is operating under suboptimal conditions. The original algorithm was build solely for stable burst intervals. Our adapted version, YAPS-BI, can better cope with random burst intervals, but it still assumes they are normally distributed. In the future, new YAPS versions that can cope with random burst intervals may improve its performance (Source: 'yapsr' package in R, unpublished).

The KF approach is more accurate than the newly developed method for this test track. Quantitatively, the traditional configuration outperforms YAPS for all considered indicators. On average, the former's average prediction error is one meter lower and the correctly positioned percentage is 3-5% higher. Its range and bearing error are significantly lower. The track length is similar for both systems, and about 50 meters shorter than the true length. This suggest both methods smooth out some features of the true track. Visualization shows that both tracks follow the true path quite well, but still contain some artefacts. The YAPS track is still more noisy overall, and fails to capture the true track far from the array. YAPS does calculate 200 positions, while the traditional filter only retains 132 positions. However, more positions do not necessarily add valuable information if they are far from the true values. For test track '53429', the traditional approach outperforms YAPS even clearer: deviations for YAPS double or triple those of the KF (see Tables A.1 and A.4). Taking all these factors into consideration, the traditional approach works better for these tests. However,

both test tracks follow the exact same trajectory, so these conclusions may not hold for other tracks.

The error measure calculated by YAPS is more relevant than any of the error measures of the traditional approach. With an R^2 of 0.23 (Figure 4.14), it more than doubles the performance of HPE, which only captured 10% of the true error's variance. However, Kalman filtering still leads to a better correlation ($R^2 = 0.29$).

The usage of a RW behaviour model may be partly responsible for YAPS's poor performance. Our analysis of the behaviour models showed that the RW model strongly smooths out tracks outside the array, which is detrimental for its overall performance (see Section 4.1.3). Comparison of the plotted results confirms that the YAPS track strongly resembles that of the smoothed RW track (see Figure B.3 in Appendix B.1). YAPS performance could thus be improved by using a CTCRW model instead of an RW model. The development of such an algorithm was out of the scope of this thesis.

4.3.2 A combination of old and new

Visualization of the YAPS track shows it still contains some noise, but describes the general track behaviour well within the array. Additionally, the error measure accompanying the data is quite relevant in comparison to the HPE. Such circumstances are ideal for noise removal with the Kalman filter/ smoother. Therefore, this section tests the combined effect of the traditional and new methods. In this context, YAPS is regarded as an advanced positioning system instead of a clean-up technique. The performance indicators of these extra steps are given in Table 4.5, the effect on the track and error measure are visualized in Figures 4.13 and 4.14 respectively.

Overall, the combination of YAPS and traditional Kalman filtering outperforms either of the methods alone. Applying the filtering algorithms to the YAPS track significantly improves most accuracy measures. The local and bearing error reach lower values than any of the tests so far. The percentage of correct positions and total error improves compared to YAPS alone, but the traditional approach remains superior. Additionally,

Table 4.5: Performance indicators for YAPS data after each filtering step of the traditional approach.

	Total			**Local**				
	Error	Corr. %	Q3	Error	Corr. %	Range	Bearing	Length
YAPS track	6.73	45.00	7.22	4.69	44	4.91	2.68	1746
Outlier	6.57	45.51	7.03	4.19	44.38	5.10	2.27	1646
KF	6.75	46.63	7.45	4.30	44.94	5.22	2.33	1614
RTSS	6.54	50.56	7.15	4.08	48.88	5.13	2.23	1550

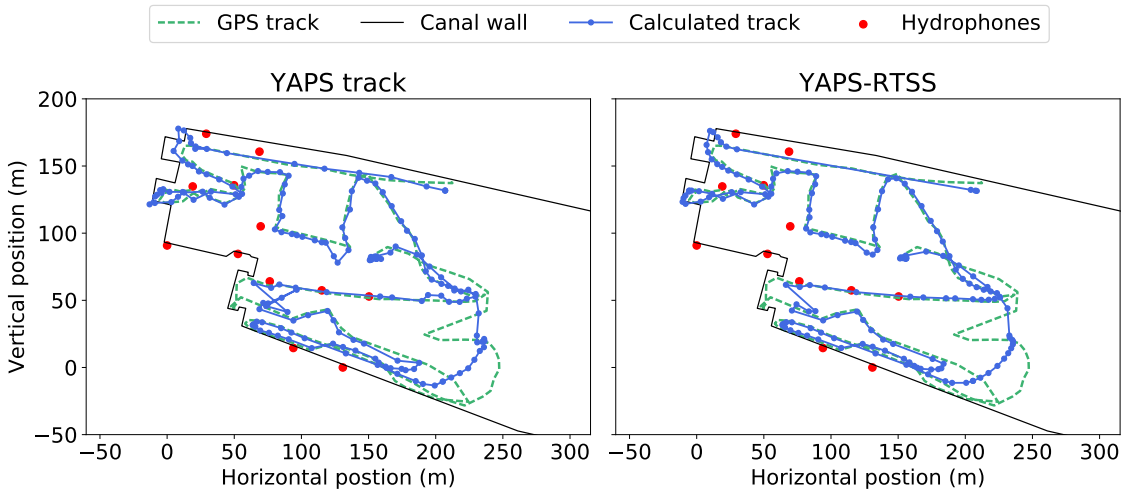

Figure 4.13: Visualization of the YAPS track before and after applying the traditional filtering algorithms.

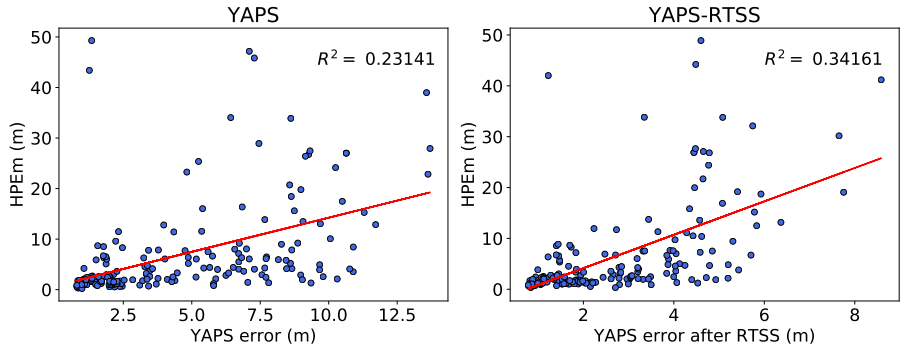

Figure 4.14: Regression analysis for the true and calculated error measure before and after filtering YAPS data with the traditional filtering algorithms.

the correlation between the calculated and true error increases again because of the filtering/smoothing. With a a coefficient of determination of 0.34, this is a more viable error measure than that of both methods separately. The smoothed track in Figure 4.13 shows little changes on the right side of the track, which was already heavily smoothed by YAPS. The main visual changes occur at the erroneous zones near the lock doors on the left. Thus, the reduced track length (194 m shorter), is mainly the result of noise removal instead of excessive smoothing. As mentioned before, we are mainly interested in the accuracy near the navigation lock and inside the array. Since the combination of YAPS and the KF gives the lowest recorded error in this region, it may be the most relevant clean-up technique. However, we cannot base the conclusion on this test track alone, as it contains relatively few points, and improvements are small. Whether this combined approach is worth the extra computational burden, will be evaluated during the simulation study in the next section.

4.4 Simulation study

Because only a limited amount of test data is available, and results of the different test tracks often contradicted each-other, we performed a simulation study to confirm our conclusions. Additionally, the test tracks do not represent actual fish movements: they consist of straight lines and unnatural turns. By simulating tracks, we can test the filtering systems on more natural behaviour (Figure C.1 in Appendix C shows an example of a simulated track). Finally, these simulations allow us to vary the amount of noise and multipath errors, and quantify how these factors affect the performance of the different methods. We tested the best traditional and new approach, as well as the combination of both.

Tracks were simulated using the R-package of YAPS (`yapsr`, from personal communication). This tool first generates fish tracks via a CRW model. Then, it uses a random walk model for the sound speed and user-defined burst interval limits to create TOA data for this track. Subsequently, the track can be distorted with missing detections and multipath errors to mimic real data. We simulated 200 tracks of 250 points each. The transmissions were generated for a random burst interval between 20.6 and 36.6 seconds to recreate the exact conditions of VEMCO's V13-P receiver (used in test track '255'). The probability of missing detections (p(NA)) was varied between 0 and 0.5 with increments of 0.1 and the probability of multipath errors (p(MP)) from 0 to 0.15 with increments of 0.03. All possible combinations of these two parameters were tested for all tracks, so in total 7200 TOA matrices were simulated. The simulated tracks remained close to the hydrophone array, so the total average error is an appropriate performance measure. Additional figures can be found in Appendix C, average error data is given in Table C.1.

4.4.1 Comparison of YAPS and Kalman filtering

YAPS performs well, even in the harsh and suboptimal conditions of our case study. As mentioned before, YAPS-BI is not fully adapted to random burst intervals. Despite this shortcoming, the average error of YAPS results remained below our accuracy goal of 2.5 meters, even for the harshest conditions (see Figure 4.16 and Table C.1 for a more detailed overview). With an average computation time of 3 seconds, it is much faster than the traditional approach, which on average requires 28 seconds for positioning, 52 seconds for estimation of the model parameters and 1 second for Kalman filtering/smoothing. One of YAPS's disadvantages is that it sometimes fails to find an optimal path, which results in a fatal error. This occurred in 2.7% of the simulations. Usually, a simple retry resolved the issue. Additionally, YAPS by definition

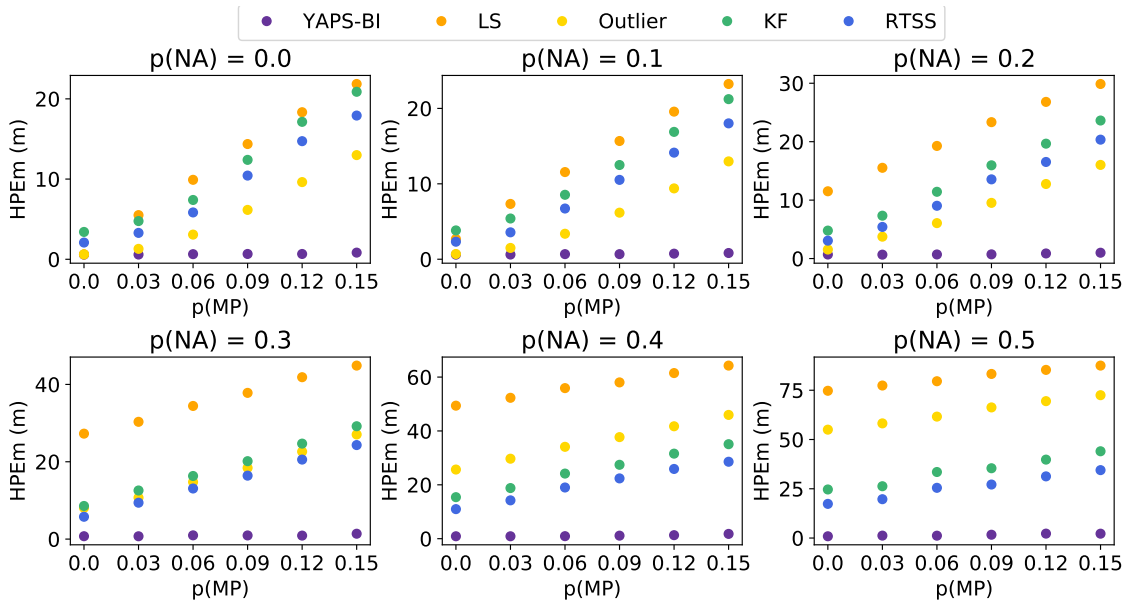

Figure 4.15: Average error for all tested filtering algorithms for all simulated scenarios.

calculates one position per detected transmission, while the outlier in the traditional filter removes 10 to 40% of the transmissions, depending on the noise conditions (see Figure C.2 in Appendix C).

Simulations confirm that the optimal configuration of the traditional approach depends on the site-specific conditions. For ideal circumstances, with little missing detections or multipath errors, an outlier filter alone reduces the average error the most (see Figure 4.15). In these conditions, applying a KF and RTSS increases the average error again, because good positions are sidetracked to reduce the influence of outliers. As the conditions worsen, the outlier filter cannot remove all errors properly, and the KF and RTSS become crucial for an overall error reduction. Track lengths, shown in Figure C.3, confirm the outlier filter effectively decreases the worst outliers at low noise levels. For harsher conditions, tracks are up to 20 times too long after outlier filtering. Even with these large amounts of noise, the RTSS smoother can lower the track lengths down to their original size. These results show the KF and RTSS smoother are great tools for noise removal and error reduction, but for fine-scale applications, other methods provide more satisfactory results.

YAPS's robustness and accuracy make it the optimal clean-up technique. Even though the traditional approach is suboptimal, the simulations with a low p(NA) (few missing detections) and p(MP) (few multipaths) prove YAPS is the superior method. With p(NA) and p(MP) set to zero, LS accuracy approaches that of YAPS with an average error of 0.62 and 0.58 meters respectively (see Table C.1). Applying the outlier filter does not lower this error, and the KF and RTSS even raise this error to 3.41 and 2.09 meters respectfully. For simulations with a p(NA) between 0 and 0.1 and a p(MP) between 0

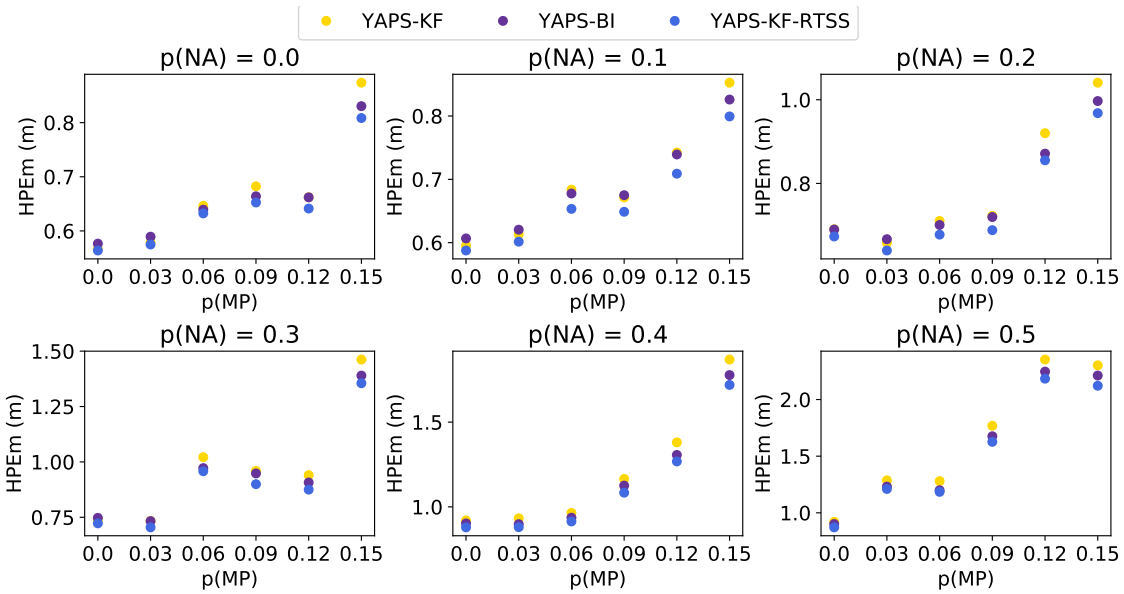

Figure 4.16: Average error of the simulated YAPS track before and after applying the KF and RTSS.

and 0.09, the average LS error varies between two and ten meters, which is similar to the accuracy range of VPS. Thus, these tracks are representative of the conditions in which the traditional approach has to perform well. For these simulations, the outlier filter significantly reduces the error, but it rarely achieves the accuracy of YAPS, which remains below 2.3 meters for even the harshest conditions. Subsequently applying the KF and RTSS only raises this error further (see Table C.1). While the traditional approach can greatly improve tracks under harsh circumstances, its performance and optimal configuration are case specific. Consequently, it is not a reliable option for fish tracks, where no validation is possible. YAPS, on the other hand, can achieve sub meter accuracies, both for ideal situations and harsh environments. Finally, YAPS is completely transparent and adjustable for users. The optimal traditional approach still requires black box positioning and error definition, since the transparent alternatives are less accurate. Therefore, YAPS is the optimal positioning and data clean-up technique, providing positioning data that is accurate, reliable and verifiable.

4.4.2 Combination of YAPS and Kalman filtering/smoothing

The previous section showed YAPS is preferable over the traditional method. In Section 4.3.2 we saw that YAPS's performance can potentially be improved by applying the Kalman filter/smoother to the resulting track. This section tests if this is generally the case, and if the improvements are worth the additional computational burden.

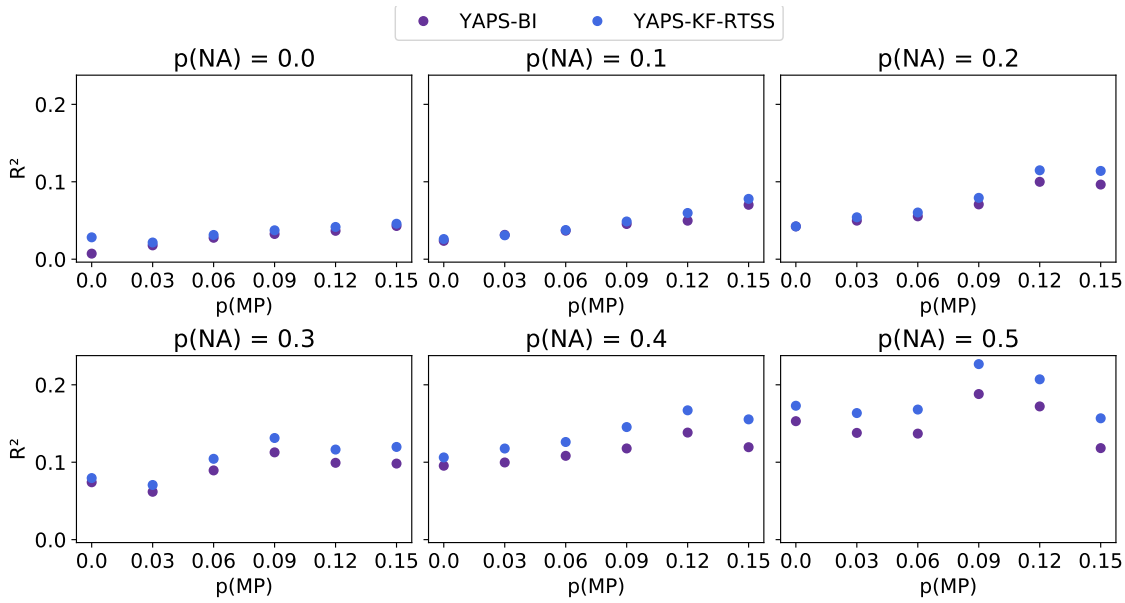

Figure 4.17: Average coefficients of determination for the linear regression between the true and calculated error for all simulated scenarios.

Applying the traditional filtering algorithms to the YAPS tracks results in small, yet consistent improvements in accuracy. Even though the KF initially increases the average error in most cases, subsequent RTS smoothing always achieves the lowest error (see Figure 4.16). While this accuracy increase is minimal (average error decreases 0.0262 m, or 2.7%), it is consistent over all simulations, thus still significant (95% confidence interval: [0.0254,0.0271], p-value below the machine limits). The size of the improvement increases as conditions become harsher (higher p(NA) and p(MP)). Thus, this additional step can increase the system's robustness in suboptimal conditions without hindering its performance in more favourable settings. This is especially valuable for fish positioning, where a consistent performance is crucial.

The additional filtering step increases the relevance of the error measure significantly. Like with the test track, the Bayesian filter and smoother add information about a position's plausibility, based on biologically possible behaviour. This increases the relevance of the error measure with 17% (R^2 increase from 0.081 to 0.095, averaged over all simulated tracks). This improvement is again consistent over all simulations, and therefore significant (p value: 8.05E -214, 95% confidence interval: [0.013,0.015]). Like with the accuracy, the size of the improvement increases with p(NA) and p(MP) (see Figure 4.17).

Overall, the combined approach is an improvement over the YAPS filter alone. Although the size of the improvement is minimal, and in good conditions even negligible, the change is always positive. Thus, this extra step has no disadvantages besides the additional computation time. The time required for the traditional ap-

proach is mainly determined by the parameter estimation. These parameters showed little variance between simulations (95% confidence intervals of [0.0144,0.0151] for β and [0.0118, 0.0121] for σ). Thus, they only have to be estimated once, given a large enough sample size. With known parameters, the filtering steps only require an additional 0.21 seconds for YAPS data. As the size of the positive impact increases in harsher conditions, the added step improves the overall reliability at little to no cost. Therefore, we opt to use the combined approach for the fish tracks. Nevertheless, YAPS on its own suffices to achieve desirable accuracy levels, so this additional step is not crucial in all applications.

4.5 Fish tracks

While the KF was slightly more accurate than YAPS for the test tracks, the latter was clearly superior in the simulation study. A combination of YAPS and Kalman filtering led to the lowest error in both studies, although differences were small. As mentioned before, both the test track and simulation study are not completely representative for fish tracks. Therefore, this final evaluation compares the performance of the separate and combined approaches for actual fish tracks. For these data, no true tracks are known, so only a qualitative analysis of the plotted tracks can be performed. We focus on how the methods handle some clearly erroneous points (i.e. positions on land, sudden changes in location or direction, extremely high speeds and chaotic, unnatural behaviour). Additionally, we shortly evaluate the cluster classification method, because so far results were mixed, but the technique showed some potential. The conclusions in this section hold for all available results. The most relevant tracks, where fish interact with the navigation lock, are shown at the end of this section, some additional tracks are provided in Appendix D. All plots also show the unfiltered VPS tracks, which serve as a reference of the current situation, that has to be improved. The code used to clean the tracks, and example data are available in an open GitHub repository (`https://github.com/vanwyck/Thesis_fish_data_cleanup`). This repository also contains a link to all cleaned fish tracks (only accessible with a UGent-account).

The receiver cluster classification method removed some errors, but overall the results of this technique were too noisy to consider it a reliable clean-up method (see Figure D.1 in Appendix D). Its successful removal of errors illustrates the importance of hydrophone geometry in the occurrence of erroneous positions. However, the three-stage filter combined with the KF performs better in virtually all cases, so the cluster method will not be discussed further.

The traditional approach improves the tracks considerably, but most remain too erroneous for further use. The KF removes some clearly erroneous track jumps and reduces the impact of noise (see Figure4.18). However, this method still relies on VPS data, which are heavily distorted. Even though the KF improves these data, it can rarely remove all artefacts (e.g. Figure 4.20). Consequently, most tracks remain unusable or unreliable.

YAPS shows a much more consistent performance, and is clearly superior to the traditional approach. Firstly, YAPS tracks always look biologically plausible and contain few obvious errors. They often look similar to the successfully cleaned KF tracks, which indicates the obtained track is correct (e.g. Figure 4.20). Secondly, YAPS even returns realistic tracks in situations where VPS data is highly erroneous, and the traditional method fails (e.g. Figure 4.21 and 4.22). Thirdly, YAPS can track the fish further from the array. This produces longer tracks that containing features that are not present in the VPS data (e.g. in Figures 4.19 and4.20, where fish can be tracked inside the lock, or D.2, where it is tracked far outside the array). This is a result of the fundamentally different approach, which allows YAPS to use transmissions detected by less than three hydrophones. Finally, YAPS calculates more points than the VPS, providing a higher resolution for subsequent interpretation of the track.

Despite the improved stability of YAPS-BI, not all tracks can be positioned. When the raw TOA data are too noisy, YAPS fails to find a solution (Figure D.3 in Appendix D). While VPS does calculate a track for these transmissions, the track is often so erroneous that even after Kalman filtering it remains unusable. In this sense, the fatal errors make YAPS more reliable: if data are too noisy, there is no result, but also no wrong result, which could be misinterpreted (like with VPS).

Applying the KF and RTSS to the YAPS results further improves the tracks and is a valuable extra step. Although YAPS outperforms the traditional approach, it still contains noisy sections (e.g. Figure 4.20). Additionally, errors in the TOA data can cause sudden unnatural track jumps (e.g. Figure D.4 in Appendix D) and even positions on land (Figure 4.23). Using a combined approach clearly reduces the impact of all these artefacts. Purely qualitatively, the tracks look smoother and more biologically plausible. The KF parameters showed little variation (95% confidence intervals of [0.009, 0.012] for β and [0.04, 0.05] for σ), and were fixed ($\beta = 0.0105$, $\sigma = 0.045$). Using global parameters had little influence on the performance of the KF (all images referred to above used these values). The extra filtering step took 0.5 seconds on average, while the YAPS positioning required 4.5 seconds on its own. Because the combined approach clearly reduces noise and error levels, at a negligible computational cost, we consider it an overall improvement compared to YAPS on its own.

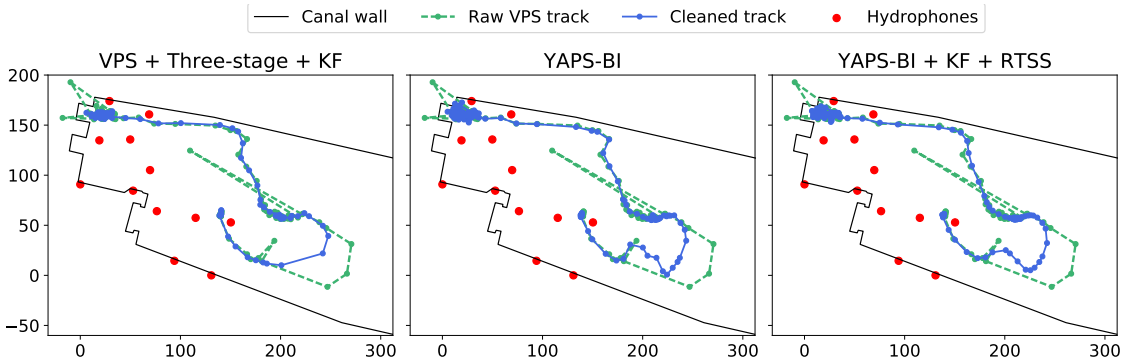

Figure 4.18: Filtered tracks for a European eel with tag number '103'. The track was generated on 27/05/16 between 19:04 and 20:36. Both the KF and YAPS remove all visible errors and return a usable track.

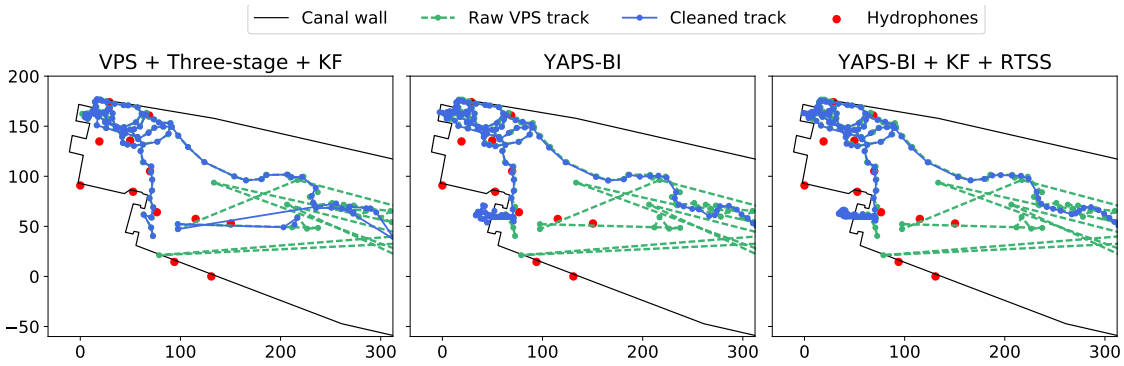

Figure 4.19: Filtered tracks for a European eel with tag number '108'. The track was generated between on 19/12/15 between 16:45 and 18:28. In the YAPS results, the fish is clearly entering the navigation lock after several attempts.

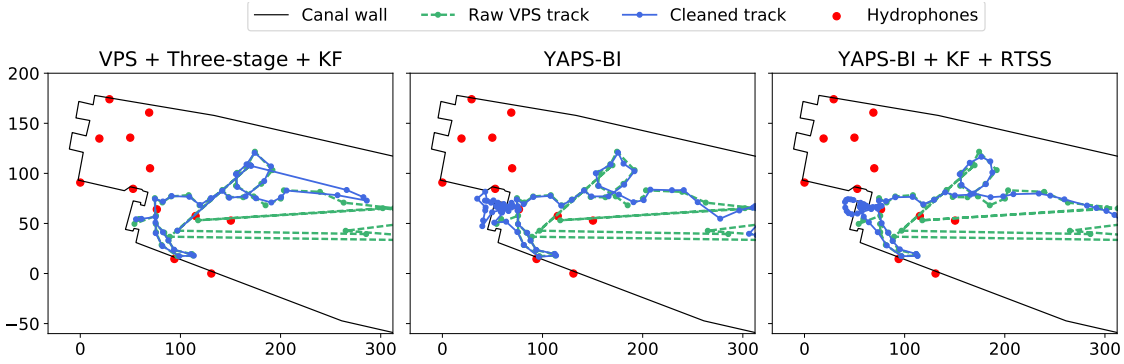

Figure 4.20: Filtered tracks for a European eel with tag number '103'. The track was generated between on 02/06/16 between 19:46 and 20:40. In the YAPS results, the fish is clearly entering the navigation lock. This was the final observation of this fish at the study site.

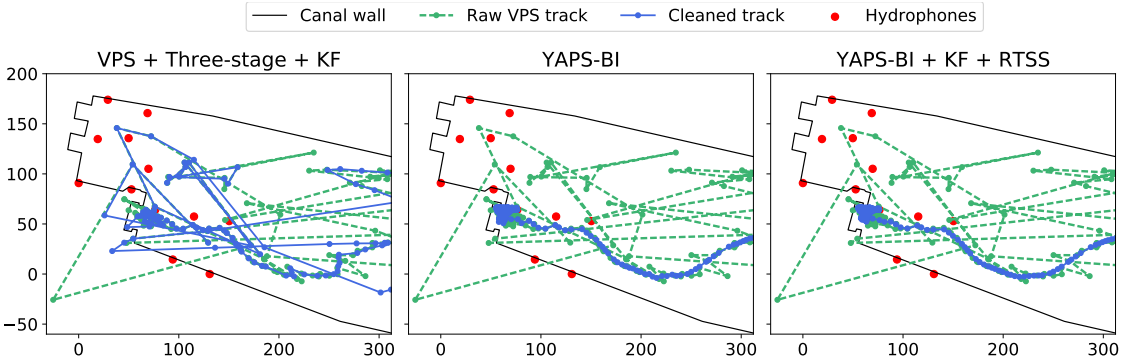

Figure 4.21: Filtered tracks for a European eel with tag number '38740'. The track was generated between 21:00 on 28/12/15 and 00:39 on 29/12/15. This was again the last observation of this fish at the study site. The KF results are too distorted to distinguish the true track.

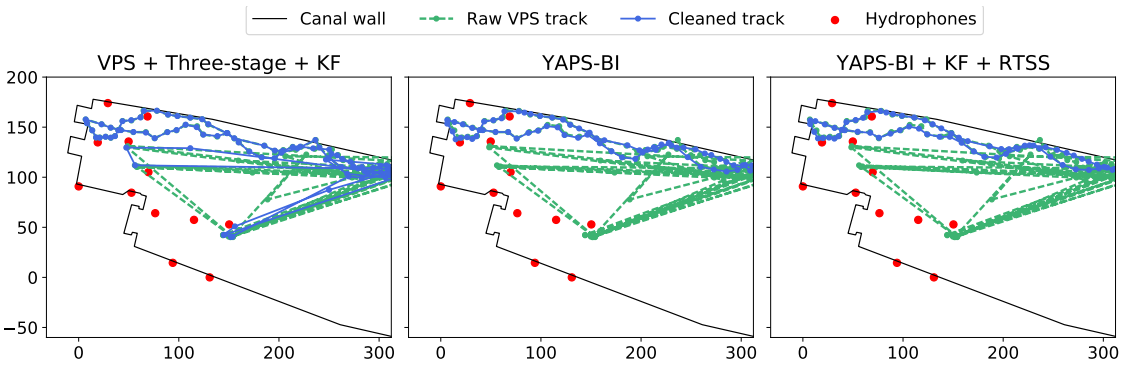

Figure 4.22: Filtered tracks for a European eel with tag number '108'. The track was generated between 07:11 and 08:28 on 20/12/15. This example shows how heavily distorted VPS data can be, while YAPS contains no errors.

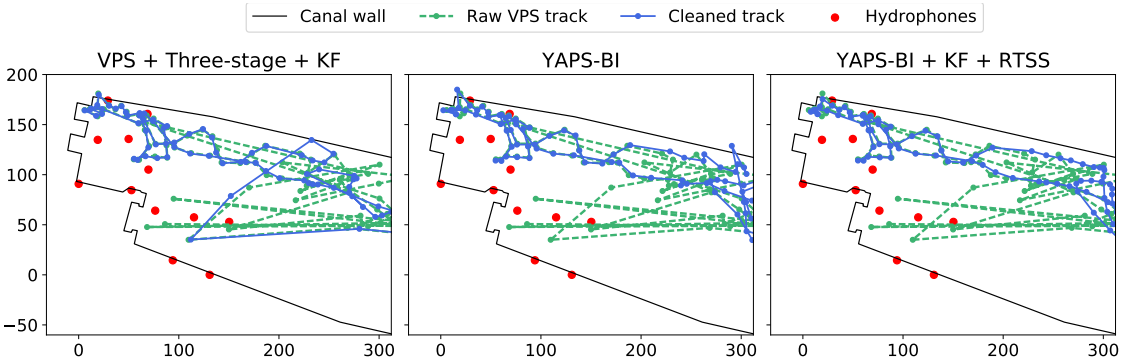

Figure 4.23: Filtered tracks for a European eel with tag number '103'. This track was generated on 09/05/2016 between 21:29 and 22:37. YAPS results contain an erroneous position on land at the right side of the track, which is effectively removed by the KF.

CHAPTER 5

CONCLUSION

In this thesis, we tested and optimized a wide variety of data clean-up techniques. We evaluated their performance under real-life conditions, with random burst intervals, high levels of missing detections and multipath errors. We based this evaluation on a combination of test tracks, realistic simulated data, and actual fish tracks. By taking all these factors into account, we can confidently say that the results of this thesis are representative of the real performance of the methods. Most previous studies focus on the optimization of the newly developed method and compare its performance to unoptimized alternatives. This way, these studies merely prove that the new technique is better than the tested alternative, but absolute conclusions are not possible. Since we optimized all relevant methods one-by-one, we can assure that the best method to come out of this thesis is the most reliable clean-up technique for noisy fish data currently available.

A combination of VPS positioned data, filtered via the three stage speed filter and CTCRW-KF, is the best method to clean up data through the traditional approach. Clearly, the VPS data is highly optimized by the company and therefore outperforms all other tested positioning systems and error measures. An outlier filter is crucial for realistic datasets, as the quantity and size of the errors is too large for the KF alone. The three-stage filter is the best compromise between removing errors and retaining correct positions. These filtered data are then processed via the KF, but not the RTSS. While the former can strongly reduce the impact of the worst outliers and thereby increase the overall accuracy, the latter smooths out the data too strongly and moves correct positions too far from their true values. We showed that the RTSS is a viable option when noise levels are extremely high, but such conditions will not produce usable, accurate results. Of the tested behaviour models, the CTCRW is the most reliable and versatile. However, the fact that most optimized traditional method is based on a black-box system, stresses the need for a transparent alternative that performs as good (or even better).

YAPS outperformed even this optimized traditional system in multiple ways. Although its overall accuracy remained slightly lower for the test track, the simulation study and fish track analysis showed its performance is much more consistent and robust

under varying levels of disturbances. Overall, it created more realistic tracks and none of them contained extreme inconsistencies, like the traditional approach. Furthermore, the TOA approach allows YAPS to calculate more positions, but also points further away from the array. This revealed some track features that were not present in the traditional approach. Finally, this method shows potential to become a universal positioning and clean-up system, facilitating a fair comparison between studies. The system is completely transparent and users can easily redefine some of its components to fit their case specific needs. Additionally, it is usable for any positioning system, as long as raw TOA data are available. For these reasons, this new approach is clearly superior to the traditional one.

YAPS-BI is an overall improvement of the standard algorithm. By using known burst interval limits and calculated sound speeds, we increased the robustness of the method and halved the computation time. The adapted version resulted in less errors and never generated completely erroneous tracks, unlike the standard version. These improvements were possible without influencing the accuracy significantly.

Applying the KF to the YAPS tracks consistently improved the results in several ways. The test tracks, simulations, and real fish tracks all showed that the additional filtering step further removed noise and artefacts from the calculated tracks. Additionally, the test track and simulations showed that the relevance of the error sensitivity measure increases after Kalman filtering. Despite the sometimes small size of the impact, we proved it is consistently positive: none of the results suggest that the additional filtering step would reduce the accuracy of the track. Finally, the computation time of this extra step is small compared to the YAPS algorithm on its own. Therefore, we consider the combination of YAPS-BI and a CTCRW-KF the best technique currently available to clean up noisy fish data with high levels of multipath errors.

CHAPTER 6

PERSPECTIVES

YAPS is the best system currently available, but it is still a new algorithm, and further improvements are still possible. Firstly, YAPS-BI remains suboptimal for random burst intervals. Although our adaptation made the algorithm more robust, the assumption of a normally distributed burst interval is not met. A complete redefinition of the TOA component of the model, using the known burst interval limits, can further improve the performance of the algorithm. Secondly, stability issues need to be addressed further. Despite our improvements, some good quality VPS tracks could not be positioned by YAPS. These advancements are not due to the YAPS algorithm, but mainly to the Template Model Builder. Such a stability update occurred during the writing of this thesis, which significantly increased the stability of the optimization and reduced computation time. Finally, a redefinition of the movement model may improve YAPS performance. Our evaluation of the behaviour models indicated that the regular RW model is inferior to the CTCRW in all cases. YAPS uses the RW model, and analysis of the test track showed that this resulted in the same shortcomings as the RW-KF combination. Therefore, a more realistic behaviour model can make the YAPS-algorithm more representative of actual fish movement.

Including known acceleration data from accelerometers implanted in the fish can further improve the performance of both the new and traditional approach. Currently, the speed filters, CRW, CTCRW, and YAPS estimate swimming speeds based on the calculated positions, and no validation of this speed is possible. The acceleration data can be compared to the calculated change of swimming speeds to evaluate their reliability. This additional source of information will affect all methods differently, so a brief re-evaluation of the models may be in order to confirm YAPS is still the most desirable option. Unfortunately, data of the latest deployment, including the accelerometer data arrived too late to be implemented and reviewed in this thesis.

TDOA positioning can be further improved by testing different optimization techniques. All positioning systems found in literature used local optimizers. A wrong selection of initial values is detrimental to the performance these systems. Therefore, most new TDOA algorithms focus on the determination of these initial values. Our use of the genetic algorithms exemplifies that global optimization algorithms can cre-

ate better performing and more robust positioning systems. We chose this algorithm merely to test the effect of a global optimizer, and considered further improvements to the positioning system beyond the scope of this thesis. The genetic algorithm is probably not the most time efficient method, and the results still contain many artefacts. A study focussing on the performance of these different optimization algorithms can thus greatly improve the efficiency and accuracy of TDOA-positioning.

The results of this thesis can now be used in further research to investigate fish behaviour and relate this to hydraulic conditions near sluices.

BIBLIOGRAPHY

Allen, K. R. (1944). Studies on the Biology of the Early Stages of the Salmon (Salmo salar). 4. The smolt migration in the Thurso River in 1939. *The Journal of Animal Ecology*, 13(1):63–85.

Alós, J., Palmer, M., Balle, S., and Arlinghaus, R. (2016). Bayesian state-space modelling of conventional acoustic tracking provides accurate descriptors of home range behavior in a small-bodied coastal fish species. *PLoS ONE*, 11(4).

Anderson-Sprecher, R. (1994). Robust estimates of wildlife location using telemetry data. *Biometrics*, 50(2):406–16.

Anderson-Sprecher, R. and Ledolter, J. (1991). State-Space Analysis of Wildlife Telemetry Data. *Journal of the American Statistical Association*, 86(415):596–602.

Andrews, K. S., Tolimieri, N., Williams, G. D., Samhouri, J. F., Harvey, C. J., and Levin, P. S. (2011). Comparison of fine-scale acoustic monitoring systems using home range size of a demersal fish. *Marine Biology*, 158(10):2377–2387.

Austin, D., McMillan, J. I., and Bowen, W. D. (2003). A three-stage algorithm for filtering erroneous Argos satellite locations. *Marine Mammal Science*, 19(2):371–383.

Bainbridge, B. Y. R. (1957). The speed of swimming of fish as related to size and the frequency and amplitude of the tail beat. *The Journal of Experimental Biology*, 35(1937):109–133.

Baktoft, H., Gjelland, K. Ø., Økland, F., and Thygesen, U. H. (2017). Positioning of aquatic animals based on time-of-arrival and random walk models using YAPS (Yet Another Positioning Solver). *Scientific Reports*, 7:14294.

Baylis, A. M. M., Orben, R. A., Costa, D. P., Tierney, M., Brickle, P., and Staniland, I. J. (2017). Habitat use and spatial fidelity of male South American sea lions during the nonbreeding period. *Ecology and Evolution*, 7(11):3992–4002.

Belpaire, C., Buysse, D., Breine, J., Verreycken, H., Ovidio, M., Nzau Matondo, B., De Meyer, J., Adriaens, D., Roland, K., Kestemont, P., and Vlietinck, K. (2013). Report on the eel stock and fishery in Belgium 2012/2013. Technical report, EIFAAC/ICES WGEEL.

Benelux Committee of Ministers (2009). Beschikking inzake de vrije migratie van vissoorten in de hydrografische stroomgebieden van de Beneluxlanden (M(2009)1). *Gemeenschappelijke memorie van toelichting*, pages 1–6.

Biesinger, Z., Bolker, B. M., Marcinek, D., Grothues, T. M., Dobarro, J. A., and Lindberg, W. J. (2013). Testing an autonomous acoustic telemetry positioning system for fine-scale space use in marine animals. *Journal of Experimental Marine Biology and Ecology*, 448:46–56.

Binder, T. R., Holbrook, C. M., Hayden, T. A., and Krueger, C. C. (2016). Spatial and temporal variation in positioning probability of acoustic telemetry arrays: Fine-scale variability and complex interactions. *Animal Biotelemetry*, 4(1):1–15.

Boyd, J. D. and Brightsmith, D. J. (2013). Error Properties of Argos Satellite Telemetry Locations Using Least Squares and Kalman Filtering. *PLoS ONE*, 8(5).

Bradshaw, C. J. A., Sims, D. W., and Hays, G. C. (2007). Measurement error causes scale-dependent threshold erosion of biological signals in animal movement data. *Ecological applications : a publication of the Ecological Society of America*, 17(2):628–38.

Breed, G. A., Bowen, W., McMillan, J., and Leonard, M. (2006). Sexual segregation of seasonal foraging habitats in a non-migratory marine mammal. *Proceedings of the Royal Society B: Biological Sciences*, 273(1599):2319–2326.

Clark, J. S. and Bjørnstad, O. N. (2004). Population time series: process variability, observation errors, missing values, lags, and hidden states. *Ecology*, 85(11):3140–3150.

Coates, J. H., Hovel, K. A., Butler, J. L., Peter Klimley, A., and Morgan, S. G. (2013). Movement and home range of pink abalone Haliotis corrugata: Implications for restoration and population recovery. *Marine Ecology Progress Series*, 486:189–201.

Codling, E., Hill, N., Pitchford, J., and Simpson, S. (2004). Random walk models for the movement and recruitment of reef fish larvae. *Marine Ecology Progress Series*, 279:215–224.

Ehrenberg, J. E. and Steig, T. W. (2002). A method for estimating the "position accuracy" of acoustic fish tags. *ICES Journal of Marine Science*, 59:140–149.

Ellis, T., McNames, J., Zurk, L., Lotz, J., and Ecochard, J.-L. (2007). Echosounder Depth Tracking with the Extended Kalman Filter. In *OCEANS 2007*, pages 1–7. IEEE.

Ennola, K., Sarvala, J., and Dévai, G. (1998). Modelling zooplankton population dynamics with the extended Kalman filtering technique. *Ecological Modelling*, 110(2):135–149.

Espinoza, M., Farrugia, T. J., and Lowe, C. G. (2011a). Habitat use, movements and site fidelity of the gray smooth-hound shark (Mustelus californicus Gill 1863) in a newly restored southern California estuary. *Journal of Experimental Marine Biology and Ecology*, 401(1-2):63–74.

Espinoza, M., Farrugia, T. J., Webber, D. M., Smith, F., and Lowe, C. G. (2011b). Testing a new acoustic telemetry technique to quantify long-term, fine-scale movements of aquatic animals. *Fisheries Research*, 108(2-3):364–371.

European Council (2007). Council Regulation (EC) No 1100/2007: Establishing measures for the recovery of the stock of European eel.

Faugeras, B. and Maury, O. (2007). Modelling fish population movements: from an individual-based representation to an advection-diffusion equation Modelling fish population movements: from an individual- based representation to an advection-diffusion equation. *Journal of Theoretical Biology*, 247:837–848.

Forester, J. D., Ives, A. R., Turner, M. G., Anderson, D. P., Fortin, D., Beyer, H. L., Smith, D. W., and Boyce, M. S. (2007). State-space models link elk movement patterns to landscape characteristics in Yellowstone National Park. *Ecological Monographs*, 77(2):285–299.

Freitas, C., Lydersen, C., Fedak, M. A., and Kovacs, K. M. (2008). A simple new algorithm to filter marine mammal Argos locations. *Marine Mammal Science*, 24(2):315–325.

Freyhof, J. (2014). Salmo salar. The IUCN Red List of Threatened Species 2014: e.T19855A2532398.

Furey, N. B., Dance, M. A., and Rooker, J. R. (2013). Fine-scale movements and habitat use of juvenile southern flounder Paralichthys lethostigma in an estuarine seascape. *Journal of Fish Biology*, 82(5):1469–1483.

Goodwin, R. A., Politano, M., Garvin, J. W., Nestler, J. M., Hay, D., Anderson, J. J., Weber, L. J., Dimperio, E., Smith, D. L., and Timko, M. (2014). Fish navigation of large dams emerges from their modulation of flow field experience. *Proceedings of the National Academy of Sciences of the United States of America*, 111(14):5277–82.

Hanson, K. C., Cooke, S. J., Suski, C. D., Niezgoda, G., Phelan, F. J. S., Tinline, R., and Philipp, D. P. (2007). Assessment of largemouth bass (Micropterus salmoides) behaviour and activity at multiple spatial and temporal scales utilizing a whole-lake telemetry array. *Hydrobiologia*, 582(1):243–256.

Hassan, R. M., Scholes, R., and Ash, N. (2005). *Ecosystems and Human Well-being - Current State and Trends: Findings of the Condition and Trends Working Group of the Millennium Ecosystem Assessment*. Island Press.

Hesthagen, T. and Garnås, E. (1986). Migration of Atlantic salmon smolts in River Orkla and Central Norway in relation to management of a hydroelectric station. *North American Journal of Fisheries Management*, 6(3):376–382.

Hilborn, R. (2013). Ocean and dam influences on salmon survival. *Proceedings of the National Academy of Sciences of the United States of America*, 110(17):6618–9.

Jacoby, D. and Gollock, M. (2014). Anguilla anguilla. The IUCN Red List of Threatened Species 2014: e.T60344A45833138.

Jensen, A. and Chen, Y. (2013). Tracking tagged fish with swarming Unmanned Aerial Vehicles using fractional order potential fields and Kalman filtering. *2013 International Conference on Unmanned Aircraft Systems, ICUAS 2013 - Conference Proceedings*, pages 1144–1149.

Johnson, D. S., London, J. M., Lea, M.-A., and Durban, J. W. (2008). Continuous-time correlated random walk model for animal telemetry data. *Ecology*, 89(5):1208–15.

Jones, E., Oliphant, T., Peterson, P., et al. (2001-2018). SciPy: Open source scientific tools for Python. http://www.scipy.org/ [Online; Accessed 2018-04-15].

Jonsen, I. D., Flemming, J. M., and Myers, R. A. (2005). Robust state-space modeling of animal movement data. *Ecology*, 86(11):2874–2880.

Jonsen, I. D., Myers, R. A., and Flemming, J. M. (2003). Meta-analysis of animal movement using state-space models. *Ecology*, 84(11):3055–3063.

Jonsen, I. D., Myers, R. A., and James, M. C. (2006). Robust hierarchical state-space models reveal diel variation in travel rates of migrating leatherback turtles. *Journal of Animal Ecology*, 75(5):1046–1057.

Joyce, T. W., Durban, J. W., Claridge, D. E., Dunn, C. A., Fearnbach, H., Parsons, K. M., Andrews, R. D., and Ballance, L. T. (2017). Physiological, morphological, and ecological tradeoffs influence vertical habitat use of deep-diving toothed-whales in the Bahamas. *PLOS ONE*, 12(10):e0185113.

Kristensen, K., Nielsen, A., Berg, C. W., Skaug, H., and Bell, B. M. (2016). TMB : Automatic Differentiation and Laplace Approximation. *Journal of Statistical Software*, 70(5):1–21.

Laidre, K. L., Moon, T., Hauser, D. D. W., McGovern, R., Heide-Jørgensen, M. P., Dietz, R., and Hudson, B. (2016). Use of glacial fronts by narwhals (Monodon monoceros) in West Greenland. *Biology letters*, 12(10):20160457.

Lam, C. H., Nielsen, A., and Sibert, J. R. (2008). Improving light and temperature based geolocation by unscented Kalman filtering. *Fisheries Research*, 91(1):15–25.

Li, X., Deng, Z., and Rauchenstein, L. (2016). Contributed Review: Source-localization algorithms and applications using time of arrival and time difference of arrival measurements. *Review of Scientific*, 041502(2016).

Li, X., Deng, Z. D., Sun, Y., Martinez, J. J., Fu, T., McMichael, G. A., and Carlson, T. J. (2014). A 3D approximate maximum likelihood solver for localization of fish implanted with acoustic transmitters. *Scientific Reports*, 4:1–9.

Limburg, K. E. and Waldman, J. R. (2009). Dramatic Declines in North Atlantic Diadromous Fishes. *BioScience*, 59(11):955–965.

Lopez, R., Malarde, J.-P., Royer, F., and Gaspar, P. (2014). Improving Argos Doppler Location Using Multiple-Model Kalman Filtering. *IEEE Transactions on Geoscience and Remote Sensing*, 52(8):4744–4755.

Lowther, A. D., Lydersen, C., Fedak, M. A., Lovell, P., and Kovacs, K. M. (2015). The Argos-CLS Kalman Filter: Error Structures and State-Space Modelling Relative to Fastloc GPS Data. *PLOS ONE*, 10(4):e0124754.

Mackenzie, K. V. (1981). Discussion of sea water soundâĂŘspeed determinations. *The Journal of the Acoustical Society of America*, 70(3):801–806.

Mao, J., Lee, J. H., and Choi, K. (2009). The extended Kalman filter for forecast of algal bloom dynamics. *Water Research*, 43(17):4214–4224.

McConnell, B. J., Chambers, C., and Fedak, M. A. (1992). Foraging ecology of southern elephant seals in relation to the bathymetry and productivity of the Southern Ocean. *Antarctic Science*, 4(04):393–398.

McCormick, S. D., Hansen, L. P., Quinn, T. P., and Saunders, R. L. (1998). Movement, migration, and smolting of Atlantic salmon (Salmo salar). *Canadian Journal of Fisheries and Aquatic Sciences*, 55(S1):77–92.

McMahan, M. D., Brady, D. C., Cowan, D. F., Grabowski, J. H., and Sherwood, G. D. (2013). Using acoustic telemetry to observe the effects of a groundfish predator (Atlantic cod, Gadus morhua) on movement of the American lobster (Homarus americanus). *Canadian Journal of Fisheries and Aquatic Sciences*, 70(11):1625–1634.

Meckley, T. D., Holbrook, C. M., Wagner, C., and Binder, T. R. (2014). An approach for filtering hyperbolically positioned underwater acoustic telemetry data with position precision estimates. *Animal Biotelemetry*, 2(1):7.

Morales, J. M., Haydon, D. T., Frair, J., Holsinger, K. E., and Fryxell, J. M. (2004). Extracting more out of relocation data: Building movement models as mixtures of random walks. *Ecology*, 85(9):2436–2445.

Nations, C. S. and Anderson-Sprecher, R. C. (2006). Estimation of animal location from radio telemetry data with temporal dependencies. *Journal of Agricultural, Biological, and Environmental Statistics*, 11(1):87–105.

Nielsen, A., Bigelow, K. A., Musyl, M. K., and Sibert, J. R. (2006). Improving light-based geolocation by including sea surface temperature. *Fisheries Oceanography*, 15(4):314–325.

Niezgoda, G., Benfield, M., Sisak, M., and Anson, P. (2002). Tracking acoustic transmitters by code division multiple access (CDMA) -based telemetry. *Hydrobiologia*, 483:275–286.

nv De Scheepvaart (2017). *Technische gegevens kanalen - Albertkanaal - Sluizen*. http://descheepvaart.empuls.be/Rubriek/Beroepsvaart/Kanalen/Albertkanaal.aspx [Online; Accessed: 2017-10-24].

O'Dor, R. K., Andrade, Y., Webber, D. M., Sauer, W. H. H., Roberts, M. J., Smale, M. J., and Voegeli, F. M. (1998). Applications and performance of Radio-Acoustic Positioning and Telemetry (RAPT) systems. *Hydrobiologia*, 372(165536):1–8.

Patterson, T. A., Thomas, L., Wilcox, C., Ovaskainen, O., and Matthiopoulos, J. (2008). State-space models of individual animal movement. *Trends in Ecology and Evolution*, 23(2):87–94.

Pedersen, M. W., Righton, D., Thygesen, U. H., Andersen, K. H., and Madsen, H. (2008). Geolocation of North Sea cod (Gadus morhua) using hidden Markov models and behavioural switching. *Canadian Journal of Fisheries and Aquatic Sciences*, 65(11):2367–2377.

Pincock, D. G. (2012). False detections: What they are and how to remove them from detection data. Technical Report DOC-004691 Version 03, VEMCO.

Piraino, M. N. and Szedlmayer, S. T. (2014). Fine-Scale Movements and Home Ranges of Red Snapper around Artificial Reefs in the Northern Gulf of Mexico. *Transactions of the American Fisheries Society*, 143(4):988–998.

R Core Team (2014). *R: A Language and Environment for Statistical Computing*. R Foundation for Statistical Computing, Vienna, Austria. URL http://www.R-project.org/.

Ren, H., Daniel Deng, Z., Carlson, T. J., Sun, Y., Fu, T., Martinez, J. J., Matzner, S., and Myers, J. R. (2012). Localization of Southern Resident killer whales using two star arrays to support marine renewable energy. *OCEANS 2012 MTS/IEEE: Harnessing the Power of the Ocean*.

Rode, K. D., Wilson, R. R., Regehr, E. V., St. Martin, M., Douglas, D. C., and Olson, J. (2015). Increased Land Use by Chukchi Sea Polar Bears in Relation to Changing Sea Ice Conditions. *PLOS ONE*, 10(11):e0142213.

Røed, H., Porter, G., Gourlay, J., and DeVitre, R. (2001). The Status of Wild Atlantic Salmon: A River by River Assessment. Technical report, WWF.

Roy, R., Beguin, J., Argillier, C., Tissot, L., Smith, F., Smedbol, S., and De-Oliveira, E. (2014). Testing the VEMCO Positioning System : spatial distribution of the probability of location and the positioning error in a reservoir. *Animal Biotelemetry*, 2:1.

Royer, F., Fromentin, J.-M., and Gaspar, P. (2005). A state-space model to derive bluefin tuna movement and habitat from archival tags. *Oikos*, 109(3):473–484.

Sarkka, S. (2013). *Bayesian Filtering and Smoothing*. Cambridge University Press.

Scheel, D. and Bisson, L. (2012). Movement patterns of giant Pacific octopuses, Enteroctopus dofleini (Wülker, 1910). *Journal of Experimental Marine Biology and Ecology*, 416-417:21–31.

Sengupta, A., Foster, S. D., Patterson, T. A., and Bravington, M. (2012). Accounting for location error in Kalman filters: Integrating animal borne sensor data into assimilation schemes. *PLoS ONE*, 7(8).

Sibert, J. R., Lutcavage, M. E., Nielsen, A., Brill, R. W., and Wilson, S. G. (2006). Interannual variation in large-scale movement of Atlantic bluefin tuna (Thunnus thynnus) determined from pop-up satellite archival tags. *Canadian Journal of Fisheries and Aquatic Sciences*, 63(10):2154–2166.

Sibert, J. R., Musyl, M. K., and Brill, R. W. (2003). Horizontal movements of bigeye tuna (Thunnus obesus) near Hawaii determined by Kalman filter analysis of archival tagging data. *Fisheries Oceanography*, 12(3):141–151.

Simpfendorfer, C. A., Heupel, M. R., and Collins, A. B. (2008). Variation in the performance of acoustic receivers and its implication for positioning algorithms in a riverine setting. *Canadian Journal of Fisheries and Aquatic Sciences*, 65(3):482–492.

Simpfendorfer, C. A., Huveneers, C., Steckenreuter, A., Tattersall, K., Hoenner, X., Harcourt, R., and Heupel, M. R. (2015). Ghosts in the data: false detections in VEMCO pulse position modulation acoustic telemetry monitoring equipment. *Animal Biotelemetry*, 3(1):55.

Smith, F. (2013). Understanding HPE in the VEMCO Positioning System (VPS). Technical Report DOC-005457-01 Version 1.0, Vemco.

Spiesberger, J. L. and Fristrup, K. M. (1990). Passive Localization of Calling Animals and Sensing of their Acoustic Environment Using Acoustic Tomography. *The American Naturalist*, 135(1):107–153.

Stevens, M., Buysse, D., Neucker, T. V. D., Gelaude, E., Jacobs, Y., Mouton, A., Coeck, J., and Vessem, J. V. (2011). Wetenschappelijke ondersteuning van de uitvoering van het palingbeheerplan . Technical Report 0, Instituut voor Natuur- en Bosonderzoek.

Storn, R. and Price, K. (1997). Differential Evolution âĂŞ A Simple and Efficient Heuristic for global Optimization over Continuous Spaces. *Journal of Global Optimization*, 11(4):341–359.

Sullivan, P. J. (1992). A Kalman Filter Approach to Catch-at-Length Analysis. *Biometrics*, 48(1):237.

Trevorrow, M. V. (1998). Boundary scattering limitations to fish detection in shallow waters. *Fisheries Research*, 35(1-2):127–135.

van Ginneken, V. J. T. and Maes, G. E. (2005). The European eel (Anguilla anguilla, Linnaeus), its Lifecycle, Evolution and Reproduction: A Literature Review. *Reviews in Fish Biology and Fisheries*, 15(4):367–398.

Vergeynst, J. (2017). *JennaVergeynst/code_cluster_classification: First release of cluster classification code*. https://github.com/JennaVergeynst/code_cluster_classification [Online; Accesed:2018-03-26].

Verreycken, H., Belpaire, C., Van Thuyne, G., Breine, J., Buysse, D., Coeck, J., Mouton, A., Stevens, M., Van Den Neucker, T., De Bruyn, L., and Maes, D. (2014). IUCN Red List of freshwater fishes and lampreys in Flanders (north Belgium). *Fisheries Management and Ecology*, 21(2):122–132.

Videler, J. J. and Wardle, C. S. (1991). Fish swimming stride by stride: speed limits and endurance. *Reviews in Fish Biology and Fisheries*, 1(1):23–40.

Vincent, C., Mcconnell, B. J., Ridoux, V., and Fedak, M. A. (2002). Assessment of Argos location accuracy from satellite tags deployed on captive gray seals. *Marine Mammal Science*, 18(1):156–166.

Wahlberg, M., Møhl, B., and Teglberg Madsen, P. (2001). Estimating source position accuracy of a large-aperture hydrophone array for bioacoustics. *The Journal of the Acoustical Society of America*, 109(1):397–406.

Wardle, C. S. (1975). Limit of fish swimming speed. *Nature*, 255(5511):725–727.

Wells, R. S., McHugh, K. A., Douglas, D. C., Shippee, S., McCabe, E. B., Barros, N. B., and Phillips, G. T. (2013). Evaluation of Potential Protective Factors Against

Metabolic Syndrome in Bottlenose Dolphins: Feeding and Activity Patterns of Dolphins in Sarasota Bay, Florida. *Frontiers in Endocrinology*, 4:139.

Welsh, J. Q., Fox, R. J., Webber, D. M., and Bellwood, D. R. (2012). Performance of remote acoustic receivers within a coral reef habitat: Implications for array design. *Coral Reefs*, 31(3):693–702.

APPENDIX A

RESULTS FOR OTHER TEST TRACKS

A.1 Test track ’53429’

This test track was generated at the same time as test track ’255’, but with a V7 transmitter instead of a V13P, so noise characteristics may be different.

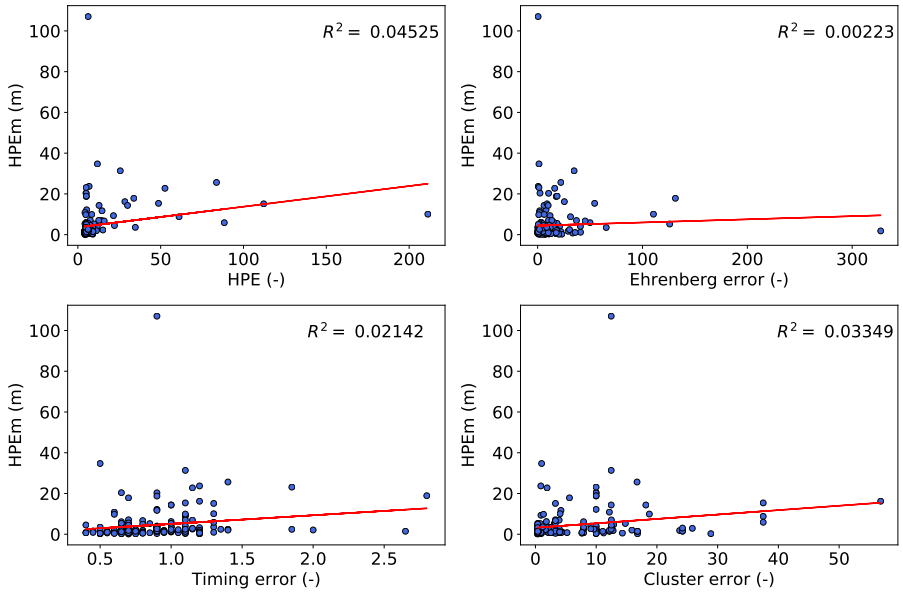

Figure A.1: Regression analysis of all tested error measures. The red line shows the calculated regression between the calculated and true error (HPEm).

Table A.1: Quantitative data for all behaviour models for test track ’53429’, using HPE as an error measure. For every performance indicator. The best behaviour model is underlined, both for the KF and RTSS.

	Total			**Local**				
	Error (m)	Correct (%)	Q3 (m)	Error (m)	Correct (%)	Range (°)	Bearing (m)	Length (m)
VPS	4.63	66.67	3.65	3.95	66.11	3.27	1.93	2203
Outlier	3.61	71.79	2.86	2.71	71.15	2.68	1.48	1734
RW-KF	5.58	51.28	4.44	3.39	51.28	3.94	2.26	1476
RW-RTSS	6.25	62.82	3.50	4.24	62.18	5.19	1.93	1284
CRW-KF	3.57	62.82	3.23	2.80	62.18	2.51	1.52	1699
CRW-RTSS	5.03	54.49	4.07	3.74	53.85	3.93	1.82	1374
CTCRW-KF	4.15	62.82	3.26	2.82	62.18	2.88	1.71	1572
CTCRW-RTSS	4.81	60.90	3.81	3.39	60.26	3.83	1.65	1378

Table A.2: Quantitative data for all filter combinations for test track ’53429’, using the Ehrenberg error. Should be compared to Table A.1. Underlined values are better than those obtained with the HPE.

	Total		**Local**				
	Error (m)	Correct (%)	Error (m)	Correct (%)	Range (°)	Bearing (m)	Length (m)
VPS	4.63	66.67	3.95	66.11	3.27	1.93	2203
Outlier	3.61	71.79	2.71	71.15	2.68	1.48	1734
RW-KF	6.78	39.10	4.71	38.46	4.87	3.02	1447
RW-RTSS	6.03	53.21	4.26	52.56	4.83	2.09	1334
CRW-KF	4.95	52.56	3.78	50.64	3.60	2.18	1693
CRW-RTSS	5.12	51.92	3.85	50.64	3.97	2.07	1418
CTCRW-KF	5.49	48.72	3.90	48.08	3.99	2.38	1536
CTCRW-RTSS	5.23	51.28	3.79	50.00	4.14	1.96	1410

Table A.3: Overview of the tested outlier filters and their performance for test track ’53429’.

	Excluded (%)	False neg. (%).	False pos. (%)	Avg. error (m)	95th perc. (m)
Unfiltered	0	0	40.41	5.80	24.77
HPE	17.12	8.22	31.51	5.89	25.54
Cluster	16.44	8.90	32.88	5.57	24.90
Speed	5.48	3.42	38.36	5.90	25.08
Two-stage	4.79	4.11	39.73	5.98	25.05
Three-stage	8.90	6.85	38.36	6.09	25.21

Table A.4: Performance measures for all implemented YAPS versions for test track ’53429’.

	Total		**Local**				
	Error (m)	Correct (%)	Error (m)	Correct (%)	Range (°)	Bearing (m)	Length (m)
YAPS	18.23	21.29	11.45	21.29	15.63	5.09	1031
YAPS-SS	15.24	25.74	8.96	25.74	12.58	4.49	1204
YAPS-BI	12.52	32.67	6.99	32.67	10.12	3.83	1293

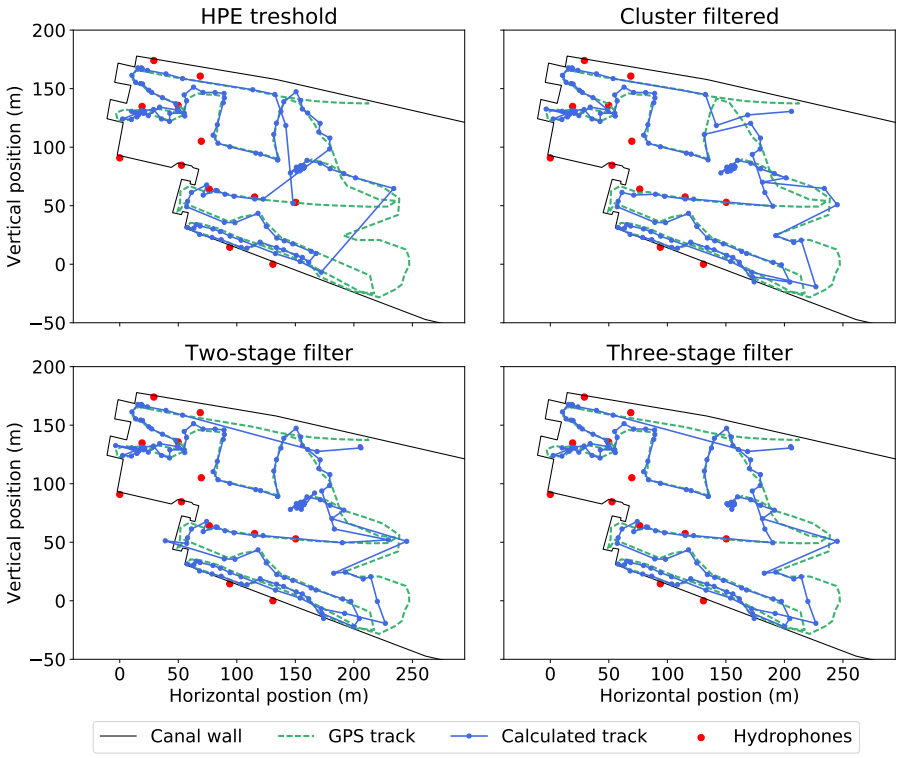

Figure A.2: Visualization of the tracks obtained by applying the outlier filters to unfiltered VPS data

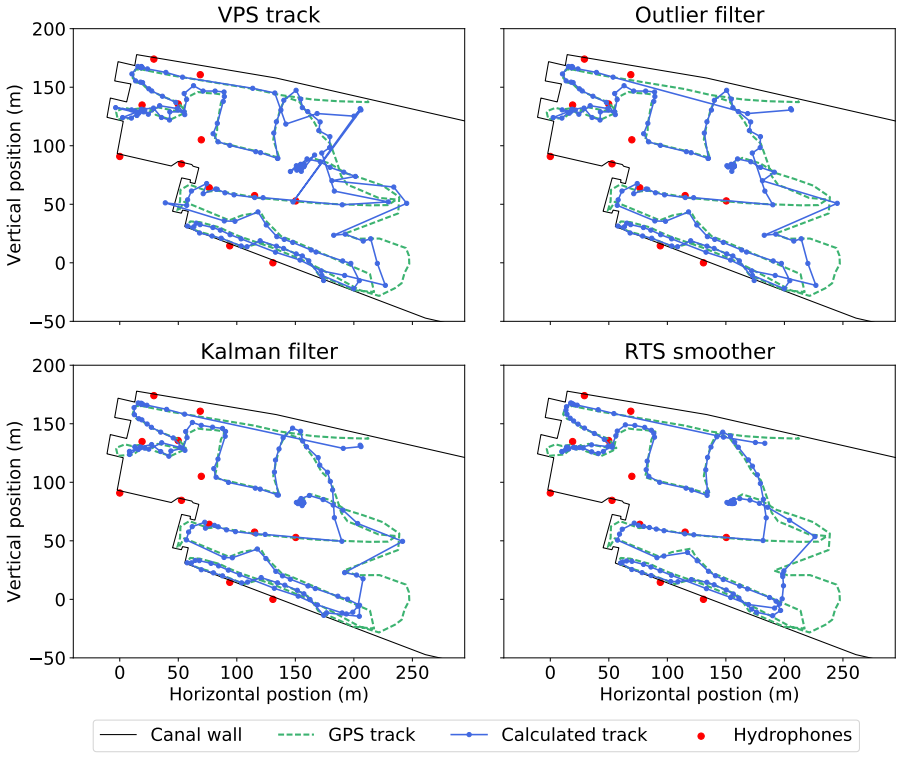

Figure A.3: Plot of the contribution of the different steps for the traditional approach using the CTCRW model and the HPE as an error measure.

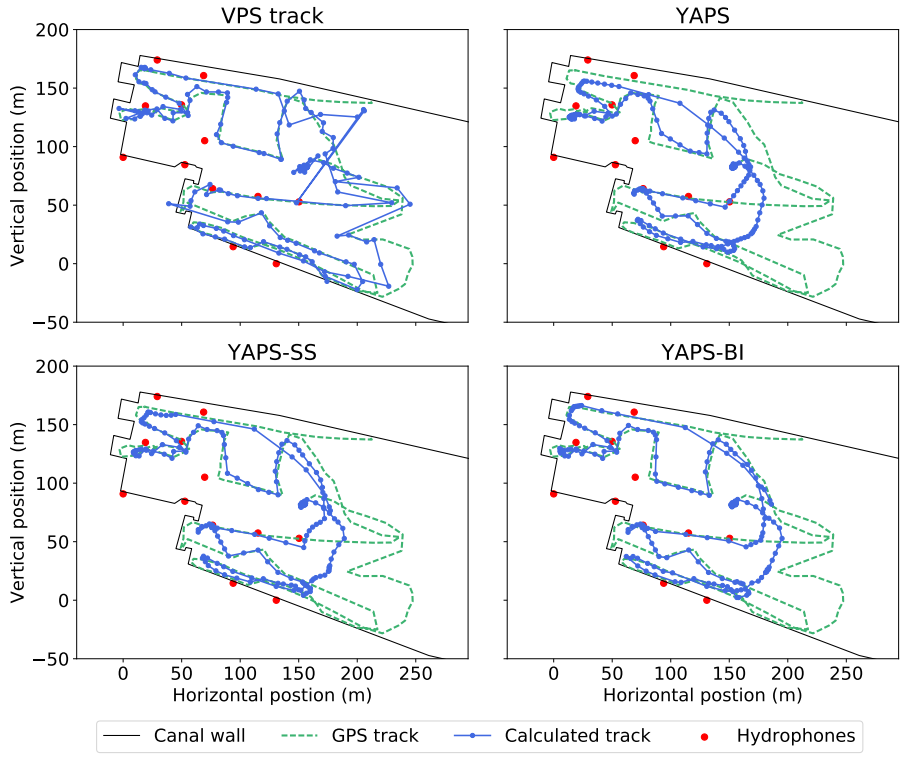

Figure A.4: Visualization of the tracks obtained from the three tested YAPS versions.

Table A.5: Performance indicators for YAPS data after each filtering step of the traditional approach.

	Total		**Local**				
	Error (m)	Correct (%)	Error (m)	Correct (%)	Range (°)	Bearing (m)	Length (m)
YAPS track	12.52	32.76	6.99	32.67	10.12	3.83	1293
KF	13.24	23.76	7.72	23.76	10.56	4.18	1242
RTSS	12.95	28.71	7.35	28.71	10.73	3.88	1178

A.2 Test track ’16200’

This test track was generate the day after the previous two. Here a V13 receiver was dragged behind the boat.

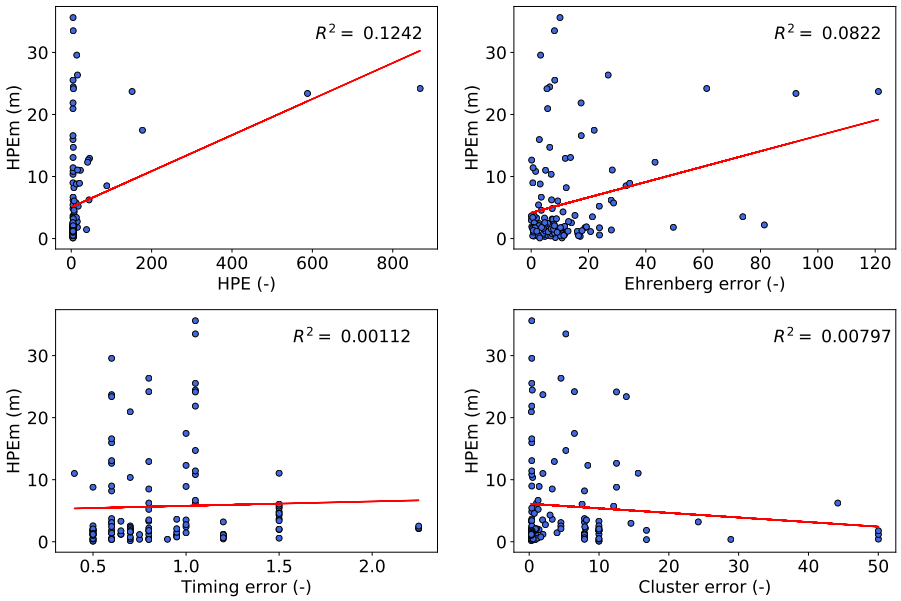

Figure A.5: Regression analysis of all tested error measures. The red line shows the calculated regression between the calculated and true error (HPEm).

Table A.6: Quantitative data for all behaviour models, using HPE as an error measure. The best behaviour model is underlined, both for the KF and RTSS.

	Total			**Local**				
	Error (m)	Correct (%)	Q3 (m)	Error (m)	Correct (%)	Range (°)	Bearing (m)	Length (m)
VPS	5.69	55.91	6.21	4.65	53.54	4.40	2.04	1674
Outlier	5.32	58.20	5.98	4.58	55.74	4.05	2.00	1585
RW-KF	10.31	15.57	9.94	6.57	14.75	7.40	4.08	1238
RW-RTSS	8.14	45.90	7.34	4.68	45.08	6.63	2.51	1129
CRW-KF	7.10	46.72	6.31	4.89	45.90	5.16	2.75	1591
CRW-RTSS	5.63	43.44	6.65	4.78	42.62	4.08	2.29	1267
CTCRW-KF	6.69	48.36	5.92	4.84	46.72	4.82	2.57	1464
CTCRW-RTSS	5.62	45.90	6.52	4.58	45.08	4.18	2.20	1259

Table A.7: Quantitative data for all behaviour models, using the Ehrenberg error. Should be compared to Table A.6. Underlined values are better than those obtained with the HPE.

	Total Error (m)	Correct (%)	**Local** Error (m)	Correct (%)	Range (°)	Bearing (m)	Length (m)
VPS	5.69	55.91	4.65	53.54	4.40	2.04	1674
Outlier	5.32	58.20	4.58	55.74	4.05	2.00	1585
RW-KF	10.86	18.85	8.55	18.85	7.25	5.70	1292
RW-RTSS	6.10	37.70	5.68	37.70	4.22	2.88	1235
CRW-KF	7.35	36.07	6.24	35.25	5.59	2.85	1482
CRW-RTSS	6.43	39.34	6.00	36.89	4.76	2.75	1293
CTCRW-KF	7.12	36.07	5.94	35.25	5.12	3.11	1407
CTCRW-RTSS	6.13	40.98	5.78	38.52	4.46	2.60	1293

Table A.8: Overview of the tested outlier filters and their performance for test track '16200'.

	Excluded (%)	False neg. (%).	False pos. (%)	Avg. error (m)	95th perc. (m)
Unfiltered	0	0	40.41	5.80	24.77
HPE	28.77	17.81	29.45	5.57	24.86
Cluster	28.08	15.75	28.08	5.99	25.43
Speed	15.07	8.90	34.25	5.94	25.46
Two-stage	14.38	8.22	34.25	5.90	25.43
Three-Stage	16.44	9.59	33.56	5.66	24.95

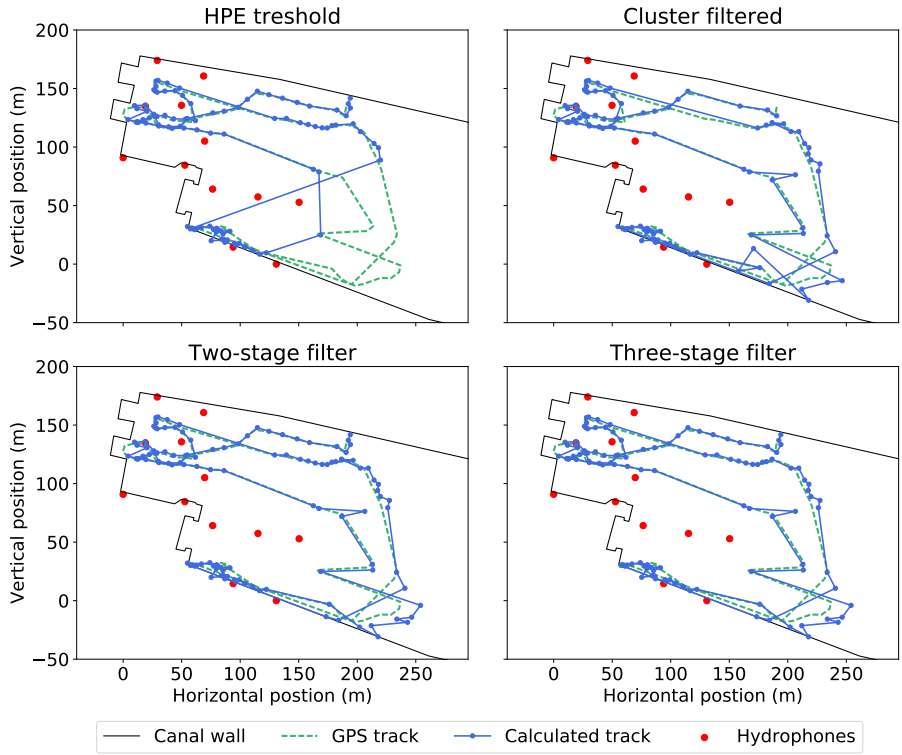

Figure A.6: Visualization of the tracks obtained by applying the outlier filters to unfiltered VPS data

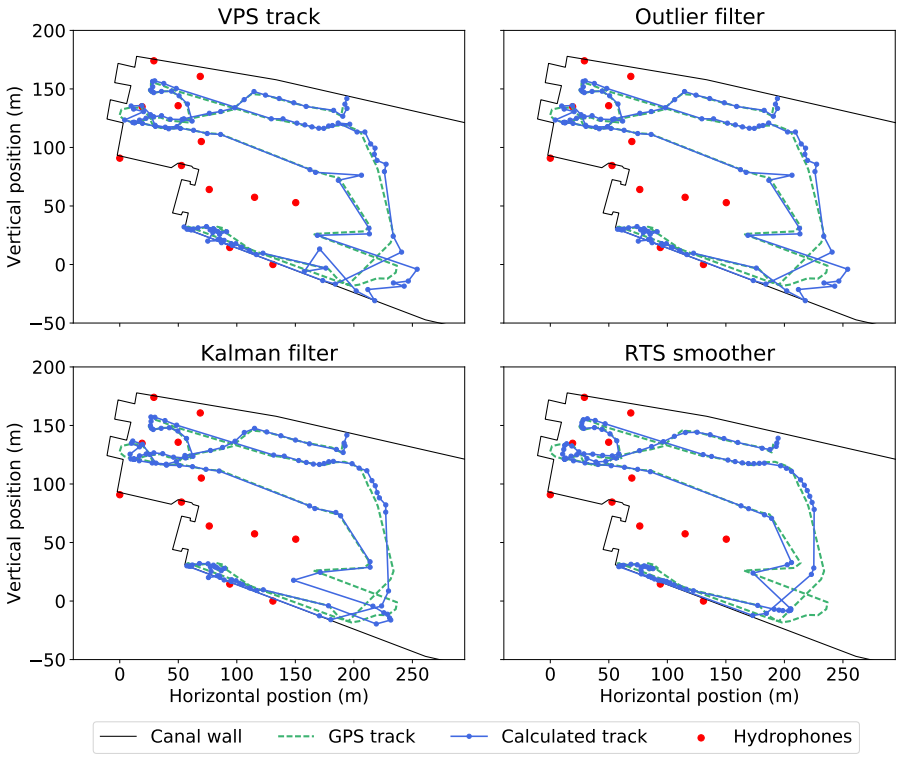

Figure A.7: Plot of the contribution of the different steps for the traditional aproach using the CTCRW model and the HPE as an error measure.

APPENDIX B

ADDITIONAL DATA FIGURES FOR TEST TRACK ’255’

B.1 Using the Ehrenberg error instead of HPE

Table B.1: Quantitative data for test track ’255’, with the Ehrenberg error as the measurement error. Should be compared to table 4.1. Underlined values are better than those obtained with the HPE.

	Total		**Local**				
	Error (m)	Correct (%)	Error (m (m)	Correct (%)	Range (°)	Bearing (m)	Length (m)
VPS	5.80	59.59	4.54	56.85	4.30	2.31	2194
RW-KF	9.52	28.77	7.50	28.08	6.26	4.08	1720
RW-RTSS	7.46	42.47	5.43	41.10	5.29	3.07	1545
CRW-KF	6.97	45.21	6.01	43.15	4.84	3.10	2063
CRW-RTSS	5.97	43.84	5.12	42.47	3.98	2.77	1713
CTCRW-KF	7.30	45.21	5.98	43.84	4.90	3.19	1897
CTCRW-RTSS	5.83	50.68	4.96	47.95	3.96	2.70	1704

B.2 Behaviour model performance

B.2.1 Without outlier filter

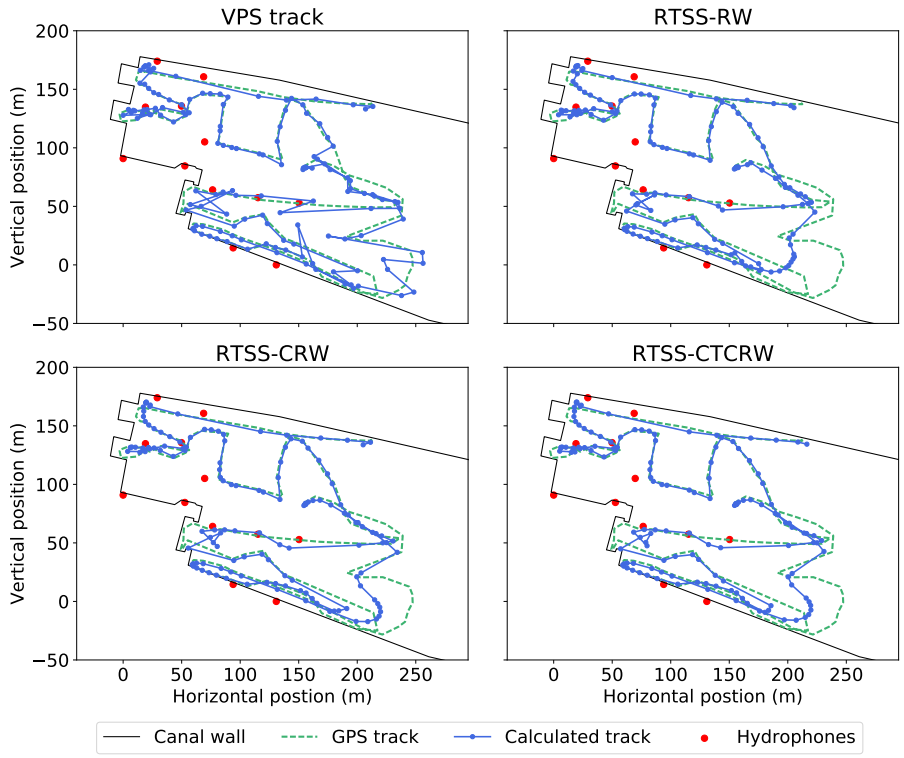

Figure B.1: The unfiltered VPS track and results of the RTSS for all three behaviour models. The KF and RTSS used the HPE as the measurement error and unfiltered VPS data as an input.

Table B.2: Performance of the subsequent filtering steps for test track '255'. Outliers, were filtered with the three-stage filter, and HPE was used as measurement error. For every performance indicator, the best behaviour model is underlined, both for the KF and RTSS.

	Total			**Local**				
	Error (m)	Correct (%)	Q3 (m)	Error (m)	Correct (%)	Range (°)	Bearing (m)	Length (m)
VPS	5.80	59.59	5.98	4.54	56.85	4.30	2.31	2194
Outl. filter	4.90	62.88	5.35	3.98	59.85	3.65	1.94	1958
RW-KF	7.99	40.15	8.11	4.97	40.15	5.51	3.12	1575
RW-RTSS	7.09	50.00	7.16	4.17	49.24	5.58	2.38	1425
CRW-KF	5.17	55.3	5.17	4.17	53.79	3.47	2.28	1807
CRW-RTSS	5.64	46.21	5.74	4.23	45.45	4.06	2.38	1532
CTCRW-KF	5.68	52.27	5.03	4.23	52.27	3.76	2.45	1733
CTCRW-RTSS	5.74	50.00	5.55	4.16	48.48	4.20	2.34	1502

B.2.2 With outlier filter

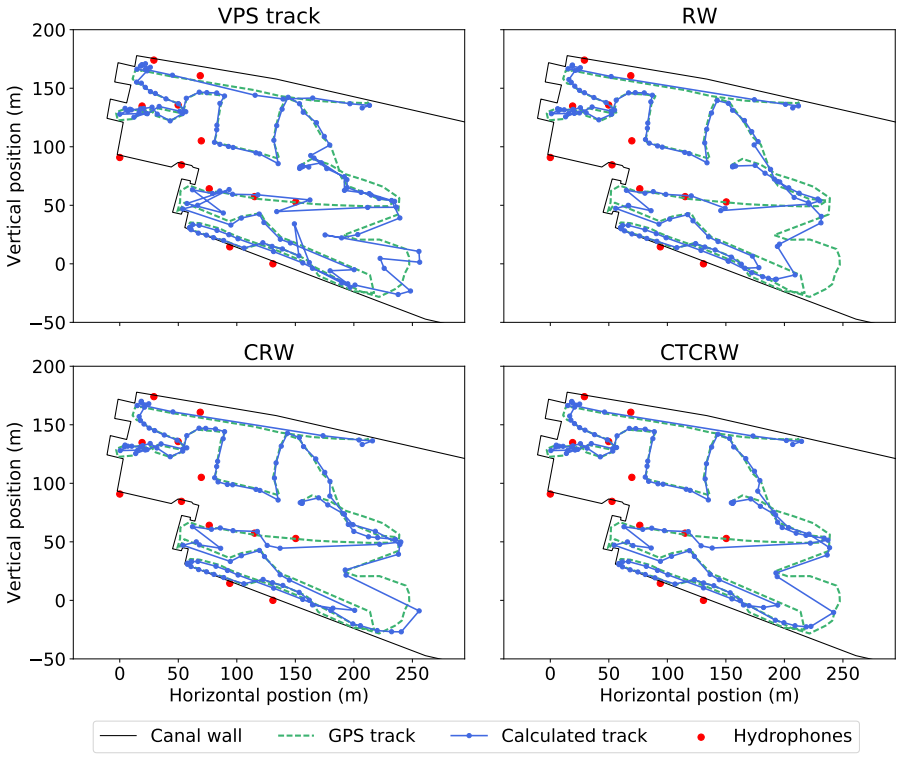

Figure B.2: The filtered VPS track and results of the KF for all three behaviour methods. The KF used the HPE as the measurement error and filtered data from the three-stage filter as an input.

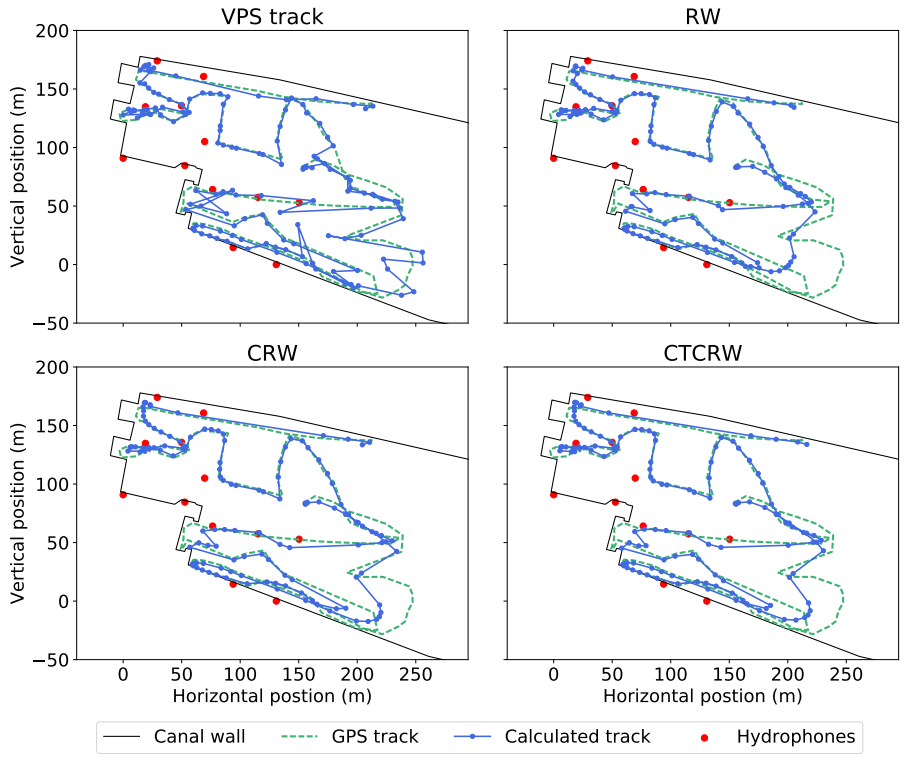

Figure B.3: The filtered VPS track and results of the RTSS for all three behaviour methods. The KF and RTSS used the HPE as the measurement error and filtered data from the three-stage filter as an input.

B.3 Best traditional approach used for LS positioned data

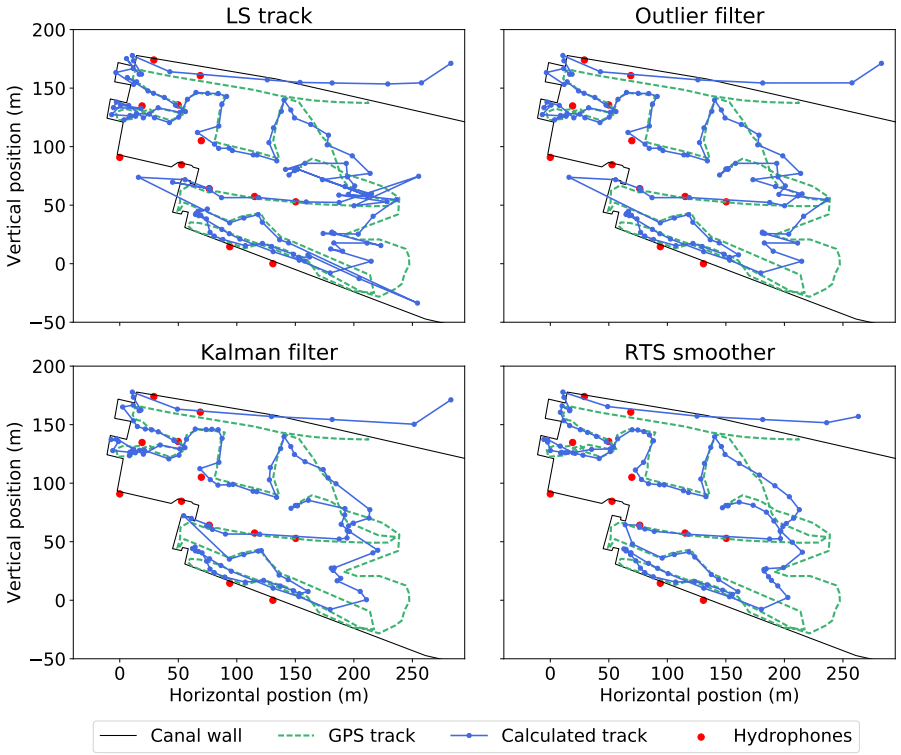

Figure B.4: Visualization of the tracks obtained after each filtering step for the LS positioned data, using the genetic algorithm. Outliers, were filtered with the three-stage filter, and the Ehrenberg error was used as measurement error.

Table B.3: Performance of the subsequent filtering steps for the LS positioning data. Outliers, were filtered with the three-stage filter, and the Ehrenberg error was used as measurement error.

	Total		**Local**				
	Error (m)	Correct (%)	Error (m)	Correct (%)	Range (°)	Bearing (m)	Length (m)
LS track	13.87	23.45	9.84	22.76	11.87	4.31	2711
Outlier	11.27	28.10	7.86	27.27	9.35	4.12	1933
KF	12.04	17.36	8.25	17.36	9.91	4.13	1681
RTSS	11.00	22.31	7.06	22.31	9.17	3.73	1522

B.4 Example of a failed YAPS run

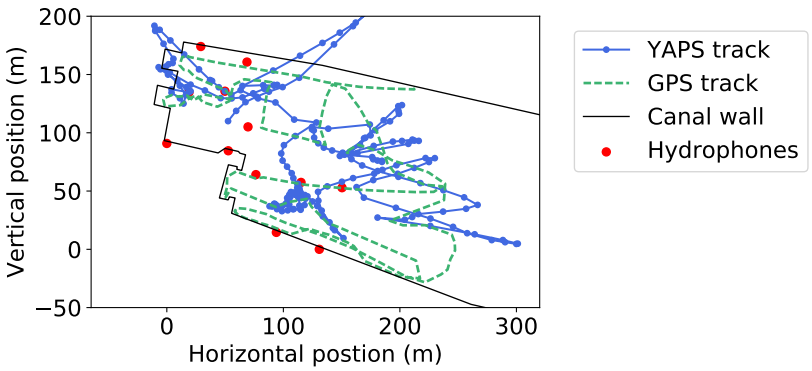

Figure B.5: Example of a result from the standard YAPS algorithm where it got stuck in a local optimum.

APPENDIX C

SIMULATION STUDY

C.1 Example of a simulated track

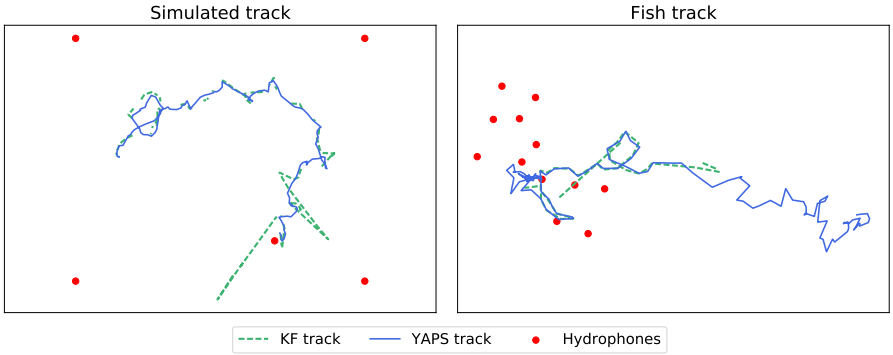

Figure C.1: Example of a simulated fish track (left) and an actual fish track (right). Both images show the results of Kalman filtering and YAPS. The fish track is from a European eel with tag number '103'. The TOA data was simulated under the worst conditions (p(NA) = 0.5, p(MP) = 0.15).

C.2 Additional quantitative figures

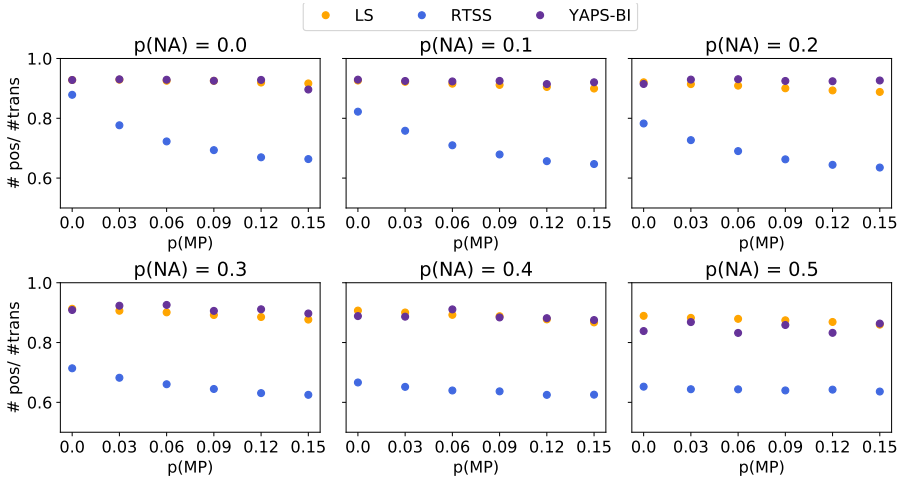

Figure C.2: Relative amount of calculated positions, calculated as the number of positions obtained, devided by the positions originally simulated. To illustrate the impact of crashes of the YAPS algorithm, we included the crashed tracks (which resulted in zero positions).

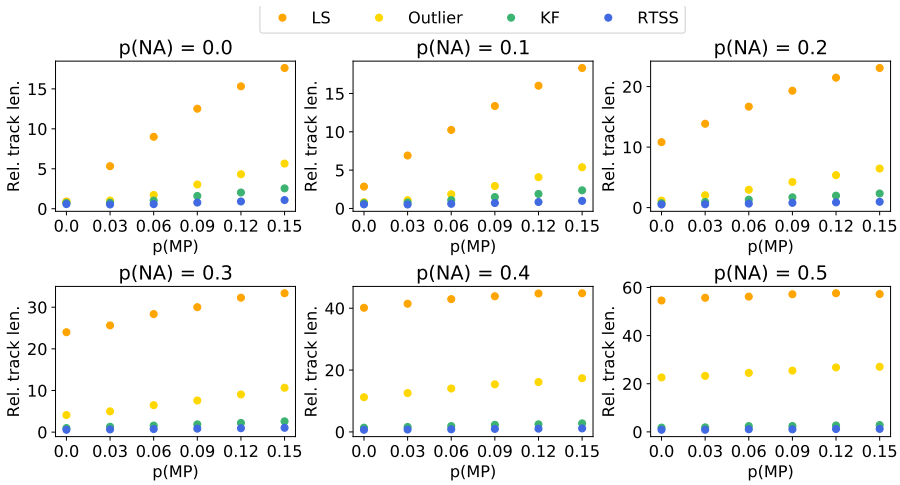

Figure C.3: Relative track lengths for all filtering steps of the traditional approach. Calculated by dividing the calculated track length by the true track length.

C.3 Error data for both methods separately

Table C.1: Average total error and its standard deviation for all simulated scenarios. This is the average for all 200 tracks an dall 250 positions per track.

p(NA)	p(MP)	**YAPS** mean (m)	std. (m)	**LS** mean (m)	std. (m)	**Outl.** mean (m)	std. (m)	**KF** mean (m)	std. (m)	**RTSS** mean (m)	std. (m)
0.0	0.00	0.58	0.37	0.62	0.38	0.62	0.38	3.41	3.03	2.09	1.78
	0.03	0.59	0.38	5.51	16.73	1.30	4.98	4.76	8.10	3.29	5.94
	0.06	0.64	0.66	9.91	22.36	3.08	10.03	7.39	12.67	5.84	10.07
	0.09	0.66	0.64	14.37	26.44	6.16	15.51	12.40	19.71	10.43	15.11
	0.12	0.66	0.58	18.34	29.06	9.62	19.48	17.14	24.15	14.73	18.03
	0.15	0.83	1.11	21.86	31.22	12.99	22.38	20.88	25.01	17.92	19.67
0.1	0.00	0.61	0.38	2.68	17.19	0.70	1.55	3.82	5.57	2.32	2.99
	0.03	0.62	0.41	7.34	24.42	1.50	6.36	5.40	10.40	3.57	6.95
	0.06	0.68	1.01	11.56	28.12	3.38	11.38	8.55	18.79	6.73	12.85
	0.09	0.67	0.54	15.68	31.57	6.17	16.79	12.49	20.87	10.52	16.25
	0.12	0.74	0.77	19.57	33.74	9.39	20.58	16.89	24.05	14.14	18.52
	0.15	0.83	1.03	23.24	35.75	12.98	23.71	21.23	28.01	18.02	20.46
0.2	0.00	0.69	0.81	11.51	40.32	1.54	9.52	4.78	9.27	3.06	8.47
	0.03	0.67	0.46	15.53	42.01	3.74	17.25	7.34	14.93	5.41	11.40
	0.06	0.70	0.54	19.27	43.94	6.06	20.93	11.43	23.48	9.03	17.15
	0.09	0.72	0.57	23.34	45.84	9.53	25.58	15.96	28.37	13.55	21.47
	0.12	0.87	1.03	26.81	46.94	12.76	28.60	19.66	28.72	16.53	21.56
	0.15	1.00	1.47	29.87	47.29	16.03	30.91	23.62	31.65	20.35	24.34
0.3	0.00	0.75	0.96	27.27	60.53	8.07	31.70	8.57	27.59	5.78	18.71
	0.03	0.73	0.57	30.33	60.64	10.72	34.75	12.57	33.70	9.41	22.21
	0.06	0.97	1.85	34.43	62.03	14.76	39.42	16.32	33.42	13.09	25.03
	0.09	0.95	1.35	37.82	62.51	18.42	41.98	20.15	35.64	16.41	25.63
	0.12	0.91	1.02	41.87	63.63	22.62	45.09	24.69	35.18	20.56	26.46
	0.15	1.39	2.36	44.87	63.60	27.06	47.62	29.19	39.57	24.32	28.40
0.4	0.00	0.90	1.57	49.39	76.80	25.67	57.55	15.42	45.06	10.98	30.67
	0.03	0.90	1.10	52.31	76.27	29.70	59.33	18.80	43.39	14.24	30.81
	0.06	0.94	1.35	55.91	76.71	34.11	61.75	24.17	50.28	19.01	35.27
	0.09	1.13	2.09	58.03	75.83	37.71	62.62	27.43	50.84	22.38	39.43
	0.12	1.31	1.92	61.49	75.86	41.74	63.75	31.58	48.57	25.89	37.19
	0.15	1.78	2.99	64.27	75.73	45.96	65.00	35.08	51.15	28.57	41.08
0.5	0.00	0.90	0.66	74.73	85.76	55.00	77.56	24.65	66.59	17.34	42.56
	0.03	1.23	2.43	77.39	85.10	58.19	77.36	26.29	59.86	19.71	45.79
	0.06	1.20	1.49	79.57	84.04	61.62	77.15	33.51	70.19	25.48	50.56
	0.09	1.68	2.94	83.27	83.98	66.28	78.07	35.42	66.86	27.15	46.42
	0.12	2.25	3.76	85.33	83.24	69.47	77.71	39.79	66.34	31.29	49.77
	0.15	2.21	3.67	87.50	82.60	72.49	77.64	44.03	71.77	34.46	50.00

APPENDIX D

ADDITIONAL IMAGES OF REAL FISH TRACKS

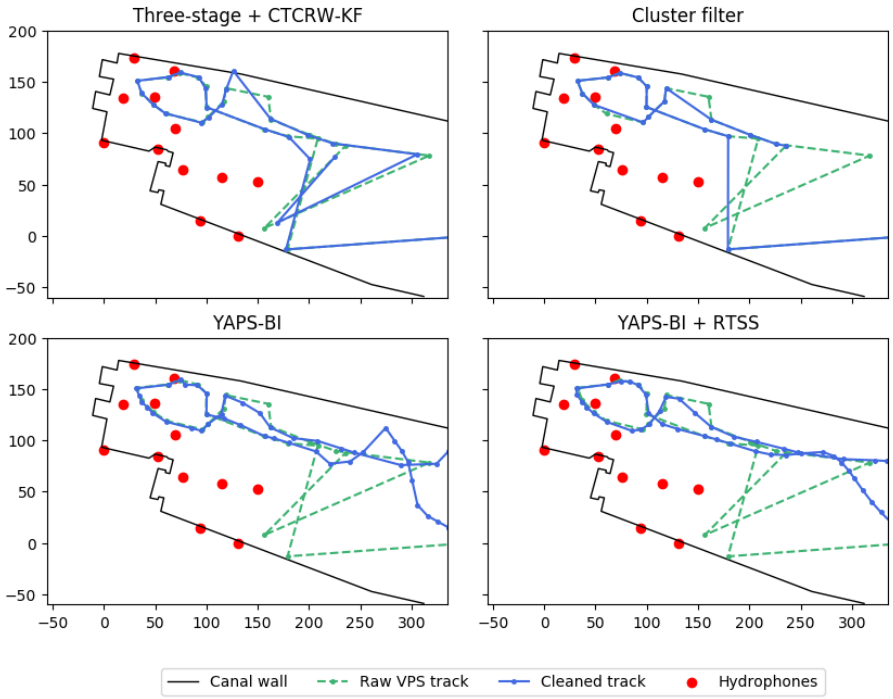

Figure D.1: Filtered tracks for a European eel with tag number ’38734’. The track was generated on 14/04/16 between 21:34 and 22:09.

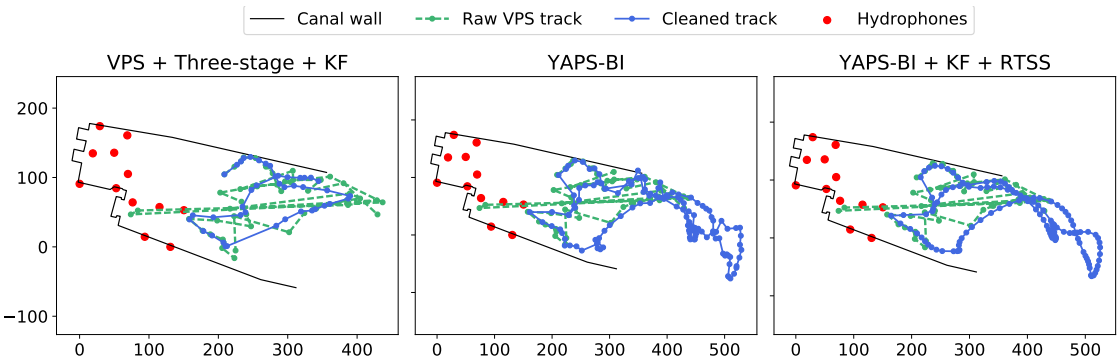

Figure D.2: Filtered tracks for a European eel with tag number '103'. The track was generated between on 25/05/16 between 21:33 and 22:33. This is an example of a track that YAPS can calculate far outside the array.

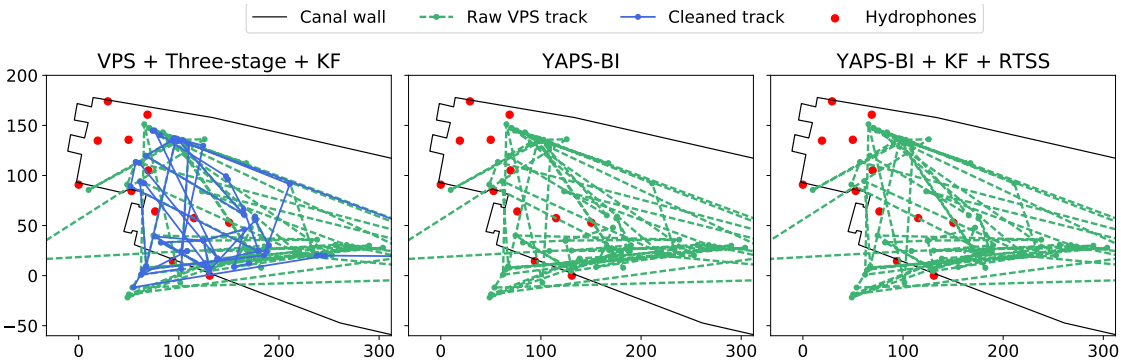

Figure D.3: Filtered tracks for a European eel with tag number '103'. This is an example of a track that is was too noisy to be positioned by YAPS.

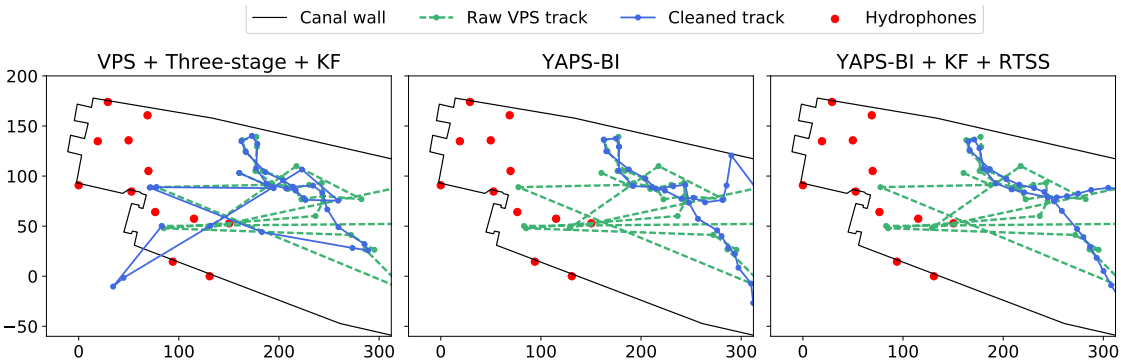

Figure D.4: Filtered tracks for a European eel with tag number '103'. This track was generated on 26/05/2016 between 22:00 and 22:34. YAPS results contain an unnatural jump at the right side of the track, which is effectively removed by the KF.